

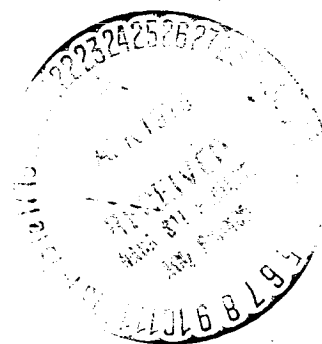
SATURN V MODEL
BASE HEATING
TEST ANALYSIS
(S-IC STAGE)
VOLUME 1

(NASA-CR-147085) SATURN V MODEL BASE
HEATING TEST ANALYSIS (S-IC STAGE), VOLUME 1
(Boeing Co., Seattle, Wash.) 127 p

N76-73540

00/98 Unclass
25913

AUGUST 25, 1966



ABSTRACT AND LIST OF KEY WORDS

This report contains the analysis of the Saturn S-IC Model Base Heating Test Program (X - 8). Four separate test facilities were used: Cornell 8-by 8-foot Transonic Wind Tunnel, Lewis 8-by 6-foot Transonic Wind Tunnel, Lewis 10-by 10-foot Supersonic Wind Tunnel and the Cornell High Altitude Chamber. The test conditions are from Mach 0.5 to 3.5 and altitudes from sea level to 205,000 feet.

Convection, radiation, and pressure data are shown for various points on the base heat shield, base of the engine fairing and fins, and on the engines. The data are compared with theoretical calculations where possible.

The test model employed a short-duration test technique developed by Cornell Aeronautical Laboratories. Engine combustion is simulated by gaseous oxygen and ethylene. Model geometry changes tested are engine fairing length, scoop and flow deflector size, engine gimbal patterns, engine-out and turbine exhaust simulation. The heating and pressure data provide information from a parametric standpoint, but the absolute magnitude may not be directly applicable to the prototype design.

Although the data presented herein were obtained in the CAL and NASA Lewis test facilities, the data, analysis, and conclusions do not necessarily reflect the endorsement of the Cornell Aeronautical Laboratories or the Lewis Research Center.

Base Heating
Base Environment
Convection, Base
Radiation, Base
Pressure, Base
Short Duration

CONTENTS

VOLUME 1 OF 2

	Page
ABSTRACT AND LIST OF KEY WORDS	i
CONTENTS	ii
ILLUSTRATIONS	v
TABLES	vii
PREFACE	viii
SUMMARY	ix

VOLUME 1

SECTION 1 - GENERAL TEST INFORMATION

1.0	INTRODUCTION	1
1.1	MODEL	1
1.1.1	FOREBODY	1
1.1.2	ENGINE	7
1.1.3	ENGINE FAIRINGS	7
1.1.4	FLOW DEFLECTORS AND ENGINE FAIRING SCOOPS	7
1.1.5	BASE PLATES	11
1.2	MODEL OPERATION	11
1.2.1	COMBUSTOR HARDWARE	11
1.2.2	TURBINE EXHAUST	14
1.3	TEST CONDITIONS	15
1.3.1	FACILITIES	15
1.3.2	ENGINE	19
1.3.3	HEATED BASE PLATE	19
1.3.4	CONFIGURATIONS	20
1.4	INSTRUMENTATION	21
1.4.1	HEAT TRANSFER	21
1.4.2	PRESSURE	23
1.4.3	BOUNDARY LAYER	24
1.4.4	MODEL PERFORMANCE	24
1.4.5	DATA RECORDING	24
1.4.6	CALIBRATION	24
1.4.7	INSTRUMENTATION LOCATIONS	28
1.5	DATA REDUCTION	28
1.5.1	PRESSURE	28
1.5.2	HEAT TRANSFER	39

SECTION 2 - OVERALL ANALYSIS

2.0	INTRODUCTION	40
2.1	BOUNDARY LAYER	41
2.2	RADIATION	42
2.2.1	RADIATION TO BASE	44

CONTENTS (Continued)

	Page
2.2.2 RADIATION TO FIN	44
2.2.3 RADIATION TO ENGINE FAIRING	51
2.2.4 RADIATION TO ENGINE (EXTERNAL)	51
2.2.5 RADIATION TO ENGINE (ENGINE OUT - INTERNAL)	51
2.2.6 COMPARISON WITH RADIATION THEORY	51
2.3 CONVECTION	55
2.3.1 CONVECTION TO BASE	57
2.3.2 CONVECTION TO FIN BASE	61
2.3.3 CONVECTION TO ENGINE FAIRING	61
2.3.4 CONVECTION TO ENGINE	64
2.3.5 COMPARISON WITH CONVECTIVE THEORY	71
2.4 BASE PRESSURE	74
2.4.1 COMPARISON WITH PRESSURE THEORY	79
2.5 CONCLUSIONS	85
APPENDIX A - THEORETICAL RADIATION	86
APPENDIX B - THEORETICAL CONVECTIVE HEATING	94
APPENDIX C - THEORETICAL BASE PRESSURE	102
REFERENCES	112
NOMENCLATURE	114
REVISIONS	117

VOLUME 2

SECTION 3 - ANALYSIS OF CORNELL AERONAUTICAL
LABORATORY (CAL 8 BY 8 FOOT TRANSONIC
TUNNEL TEST)

3.0	INTRODUCTION
3.1	BOUNDARY LAYER
3.2	RADIATION
3.3	CONVECTION
3.4	BASE PRESSURE
3.5	DATA ACCURACY
3.6	CONCLUSIONS

CONTENTS (Continued)

SECTION 4 - ANALYSIS OF LEWIS RESEARCH CENTER (LRC)
8 BY 6 FOOT TRANSONIC TUNNEL TEST

- 4.0 INTRODUCTION
- 4.1 BOUNDARY LAYER
- 4.2 RADIATION
- 4.3 CONVECTION
- 4.4 BASE PRESSURE
- 4.5 DATA ACCURACY
- 4.6 HEATED BASE PLATE
- 4.7 CONCLUSIONS

SECTION 5 - ANALYSIS OF LEWIS RESEARCH CENTER (LRC)
10 BY 10 FOOT SUPERSONIC TUNNEL TEST

- 5.0 INTRODUCTION
- 5.1 BOUNDARY LAYER
- 5.2 RADIATION
- 5.3 CONVECTION
- 5.4 BASE PRESSURE
- 5.5 DATA ACCURACY
- 5.6 CONCLUSIONS

SECTION 6 - ANALYSIS OF CORNELL AERONAUTICAL LABORATORY
(CAL) ALTITUDE CHAMBER TEST

- 6.0 INTRODUCTION
- 6.1 RADIATION
- 6.2 CONVECTION
- 6.3 BASE PRESSURE
- 6.4 DATA ACCURACY
- 6.5 HEATED BASE PLATE
- 6.6 CONCLUSIONS

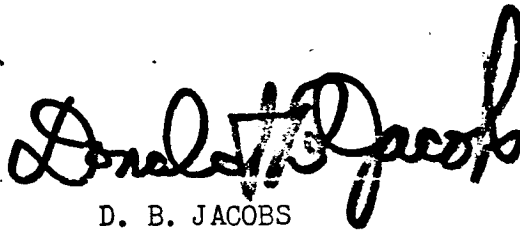
DOCUMENT NO. D5-15615

TITLE SATURN V MODEL BASE HEATING TEST ANALYSIS
(S-IC STAGE) VOLUME 1 OF 2

MODEL NO. SATURN V CONTRACT NO. NAS8-4608

THERMAL ANALYSIS GROUP

August 25, 1966

A large, stylized handwritten signature in black ink, reading "Donald B. Jacobs". The signature is written in a cursive, flowing style with prominent loops and flourishes.

D. B. JACOBS
CHIEF ENGINEER

ISSUE NO.

ISSUED TO

ILLUSTRATIONS

	Page
FIGURE 1 Model Combustion System	2
FIGURE 2 Model Base Geometry	3
FIGURE 3 Gimbal Patterns	4
FIGURE 4 Gimbal Patterns	5
FIGURE 5 Gimbal Patterns	6
FIGURE 6 Engine Fairing Configuration	8
FIGURE 7 Engine Fairing Scoop Configuration	9
FIGURE 8 Flow Deflector Configuration	10
FIGURE 9 S-IC Ethylene Mass Flow	12
FIGURE 10 S-IC Oxygen Mass Flow	13
FIGURE 11 H ₂ Turbine Exhaust Mass Flow - 5 Engines	16
FIGURE 12 C ₂ H ₄ Turbine Exhaust Mass Flow - 5 Engines	17
FIGURE 13 Facility Test Conditions	18
FIGURE 14 Oscilloscope Traces (Typical)	22
FIGURE 15 Boundary Layer Rake - CAL 8-by 8-Foot Tunnel	25
FIGURE 16 Boundary Layer Rake - Lewis 8-by 6 and 10-by 10 Tunnels	26
FIGURE 17 Variation of Heat Transfer Gage Sensitivity with Temperature	27
FIGURE 18 Variation of $(\rho ck)^{\frac{1}{2}}$ with Temperature (7740 Pyrox)	29
FIGURE 19 Pressure and Heat Transfer Base Plate - PL ₁	30
FIGURE 20 Pressure Base Plate - PL ₂	31
FIGURE 21 Heated Base Plate - PL ₃	32
FIGURE 22 Engine Instrumentation - External	33
FIGURE 23 Engine Instrumentation - External	34
FIGURE 24 Engine Out Instrumentation - Internal	35
FIGURE 25 Engine Out Instrumentation - Internal	36
FIGURE 26 Fin Instrumentation	37
FIGURE 27 Engine Fairing Instrumentation	38
FIGURE 28 Model Boundary Layer Thickness Versus Theory	43
FIGURE 29 Base Heating - Radiation	45
FIGURE 30 Base Heating - Radiation	46
FIGURE 31 Base Heating - Radiation	47
FIGURE 32 Base Heating - Radiation	48
FIGURE 33 Base Heating - Radiation	49
FIGURE 34 Fin Heating - Radiation	50
FIGURE 35 Engine Fairing Heating - Radiation	52
FIGURE 36 Engine Heating - Radiation (External)	53
FIGURE 37 Engine Heating - Radiation (Engine Out)	54
FIGURE 38 Base Heating - Radiation versus Theory	56
FIGURE 39 Base Heating - Convection	58
FIGURE 40 Base Heating - Convection	59
FIGURE 41 Base Heating - Convection	60
FIGURE 42 Base Heating - Convection	62

ILLUSTRATIONS (Continued)

	Page
FIGURE 43 Base Heating - Convection	63
FIGURE 44 Base Heating - Convection	65
FIGURE 45 Fin Heating - Convection	66
FIGURE 46 Engine Fairing Heating - Convection	67
FIGURE 47 Engine Heating Convection - (External)	68
FIGURE 48 Engine Heating - Convection (External)	69
FIGURE 49 Engine Heating - Convection (External)	70
FIGURE 50 Base Gas Temperature - Comparison with Theory	72
FIGURE 51 Convective Heating - Comparison with Theory	73
FIGURE 52 Base Pressure	75
FIGURE 53 Base Pressure	76
FIGURE 54 Base Pressure - Turbine Exhaust Effect	77
FIGURE 55 Base Pressure - Scoop and Deflector Effect	78
FIGURE 56 Base Pressure - Engine Fairing Length Effect	80
FIGURE 57 Base Pressure - Engine Fairing Length Effect	81
FIGURE 58 Base Pressure - Engine Out Effect	82
FIGURE 59 Engines Off Base Pressure Comparison	83
FIGURE 60 Base Pressure Comparison with Theory	84

TABLES

		Page
TABLE I	Model Forebody	7
TABLE II	Facility Test Conditions	15
TABLE III	Combustion Parameters	19
TABLE IV	Heated Base Plate Temperatures	19
TABLE V	Configurations Tested	20

PREFACE

The Saturn S-IC model base heating test program (X - 8) includes tests conducted at four separate test facilities. Testing began in February 1963 and extended through August 1965.

Data reports and informal analysis reports were submitted to MSFC at the conclusion of each phase of testing. This document incorporates the analysis reports into a single two-volume formal document.

The first volume includes Sections 1 and 2. Section 1 is a general description of the model, instrumentation, and test conditions in the various facilities. A general analysis of the overall test results is presented in Section 2. Sections 3, 4, 5, and 6 contained in Volume II, are detailed analyses of the data obtained at each test facility. Information contained in Paragraphs 1.2, 1.4.1, 1.4.2, 1.4.6, and 1.5 was taken essentially intact from Reference 1 which was prepared by E. A. Czeck at Cornell Aeronautical Laboratory.

This report was prepared by Jack A. McEntire, Charles R. Mullen, and Joseph D. Fowler, Jr.

D5-15615 is deliverable under Contract NAS8-5608, Schedule II, Article I, Exhibit AA, Part I, Paragraph 8.1.2.

SUMMARY

The reported model test results provide Saturn V S-IC stage base heating and pressure wind tunnel data through the first 100,000 feet of flight and trajectory altitude chamber data from 125,000 through 205,000 feet. In general, the data trends compare favorably with predicted criteria.

The magnitude of the model radiation heating rates is believed to be approximately one-third that which will occur on the prototype. Configuration changes in flow deflector and engine fairing size will not materially affect the radiation heating rates.

Model convection heating rates are believed to reflect the prototype values. The data indicate that heating due to convection will be essentially negligible through the first 125,000 feet unless base burning occurs. Base burning is less likely to occur and is considerably less severe with flow deflectors installed. Convection data obtained in a static chamber are higher than data at the same altitude in a wind tunnel.

Model pressure data appear valid and are believed to reflect prototype values. Configuration changes cause relatively slight base pressure variations.

These tests have shown that the design values for Saturn V base heating are adequate. They have proved invaluable in providing a better understanding of the flow patterns for a five engine configuration through a wide range of altitudes. Although additional development is desirable, the basic philosophy of short duration testing has proved to be an advance in the state of the hot flow testing art.

SECTION 1 - GENERAL TEST INFORMATION

1.0 INTRODUCTION

Prior to S-IC model tests, a study was conducted to determine whether the model should be prepared for long-duration motor runs or whether a relatively new short-duration technique developed by Cornell Aeronautical Laboratory (Reference 2) should be used. On the strength of data available from Saturn I short-duration tests that compared favorably with earlier long-duration data, it was decided to test using the new technique. Instrumentation similar to that used in shock tunnels was developed by CAL to obtain pressure, convection, and radiation data.

The same general model was used throughout the test program with major modifications on the combustor from one test sequence to the next. A pressure base plate was constructed and two new gimbal arrangements were used during the final tests in the Lewis Research Center 8-by 6-foot Transonic Tunnel.

Model description, test conditions, and instrumentation details are described in the following paragraphs.

1.1 MODEL

The 2.22 percent scale test model of the Saturn S-IC stage was designed by Cornell Aeronautical Laboratory (CAL) and fabricated by Marshall Space Flight Center, NASA. The model consists of two charge tubes, a quick-acting valve, mixer plate, combustion chamber, spark plug, and five nozzles depicted schematically in Figure 1. The internal parts are contained in a cone-cylinder forebody with the basic stage base attached. Scaled engine fairings and fins are attached to the model forebody (Figure 2). The scoops and deflectors (not shown) are not geometrically similar to the prototype, but do represent equivalent areas of the prototype as well as area variations.

Nozzle adapters are used to gimbal the engines to the gimbal patterns shown in Figures 3, 4, and 5. The gimbal patterns in Figure 3 are the maximums that can physically occur. The patterns in Figure 4 represent a nominal prototype flight condition while the one in Figure 5 simulates an outboard engine out. The center-engine-out case is also tested with a plugged and instrumented nozzle.

1.1.1 Forebody

The basic forebody of the 1/45 scale model is 8.875 inches in diameter. The forebody length from nose to nozzle exit plane varied depending on the test facility. Table I on the following page indicates the length of the various forebodies.

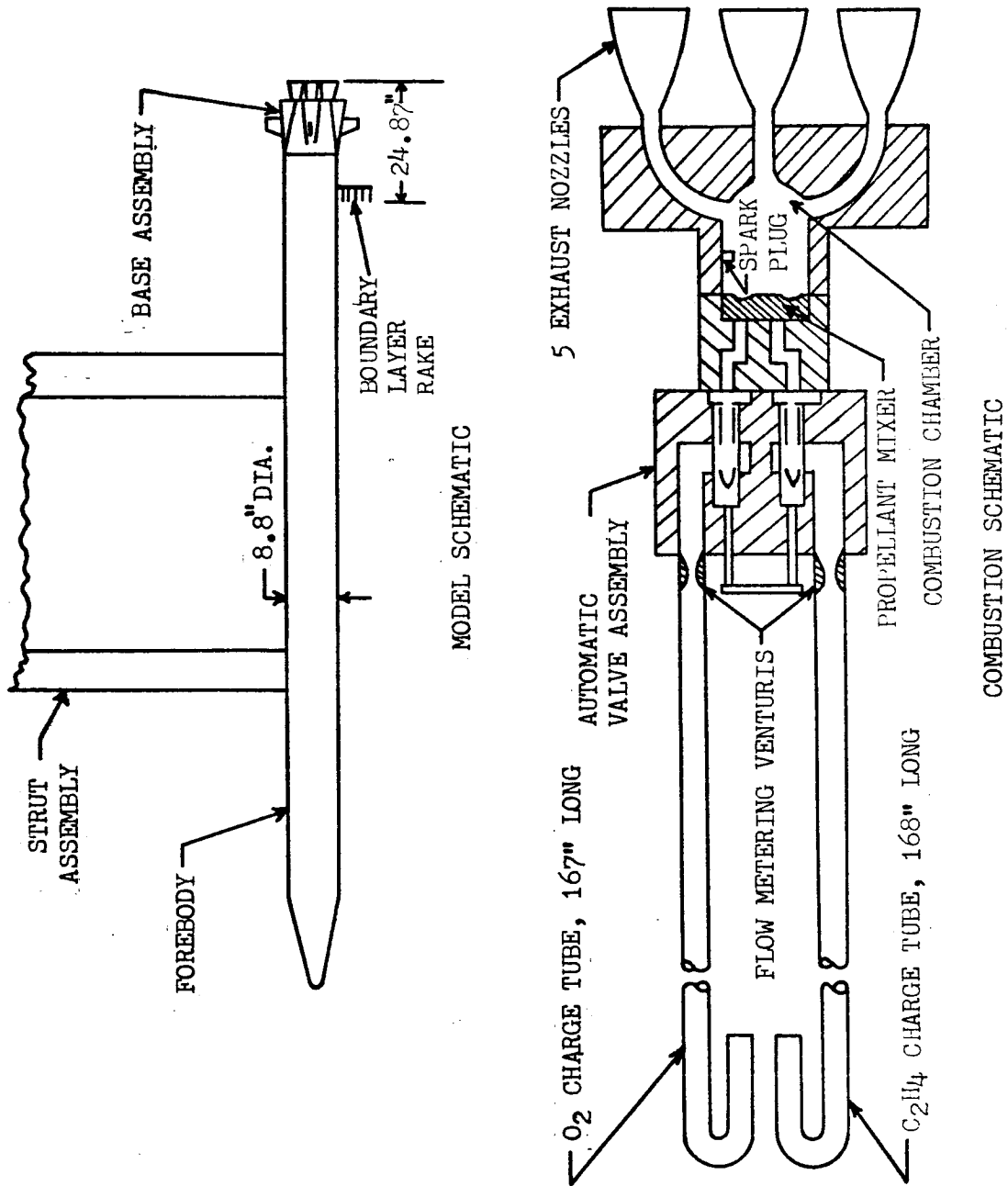


FIGURE 1 Model Combustion System

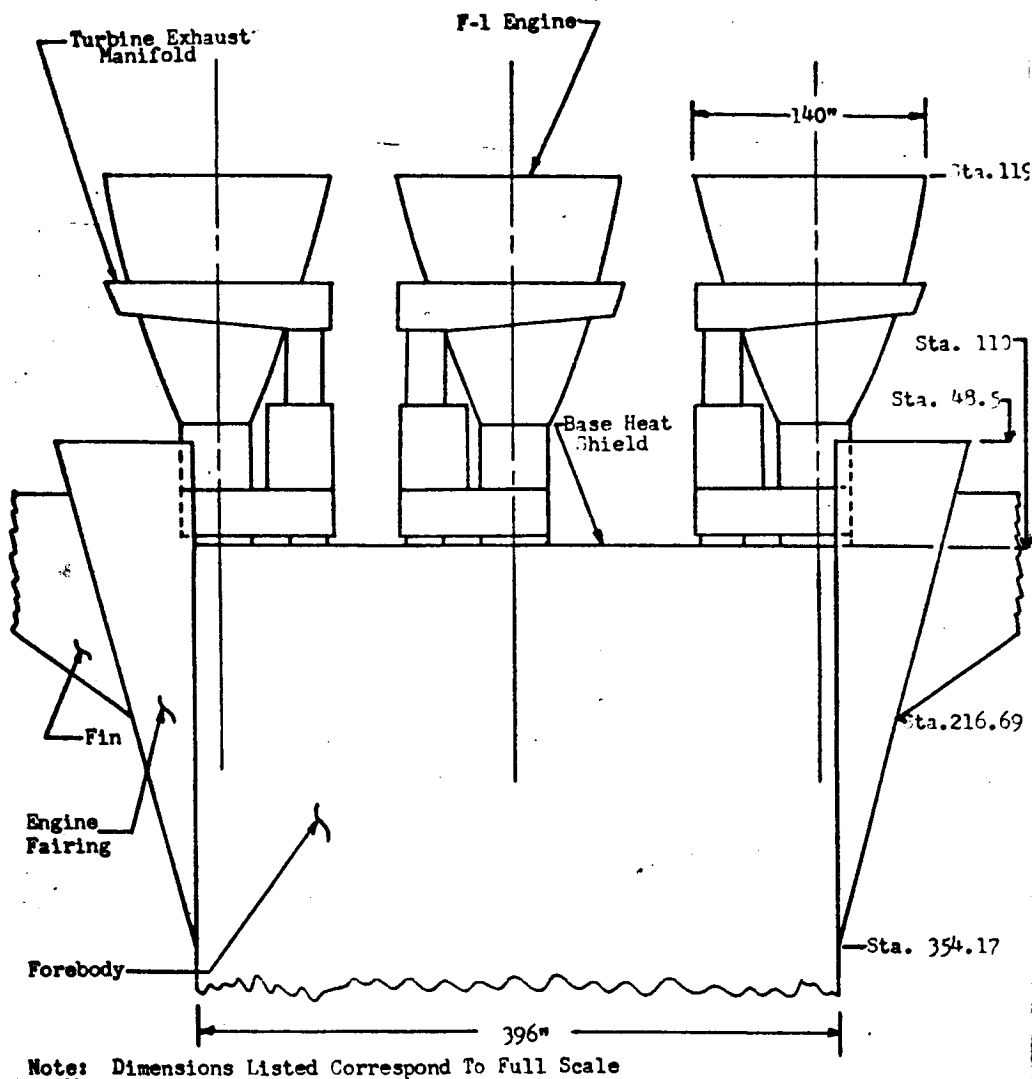
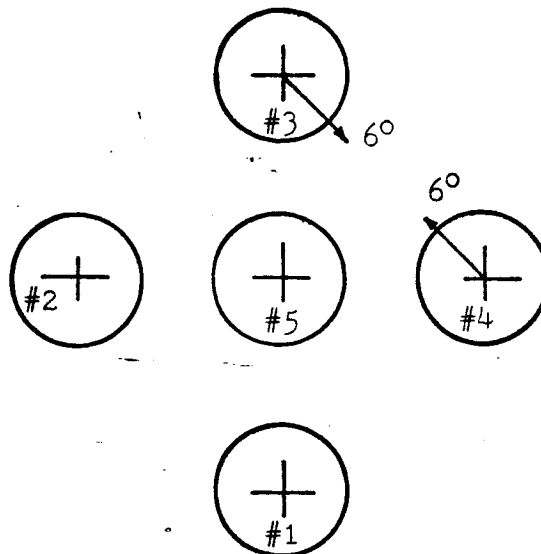
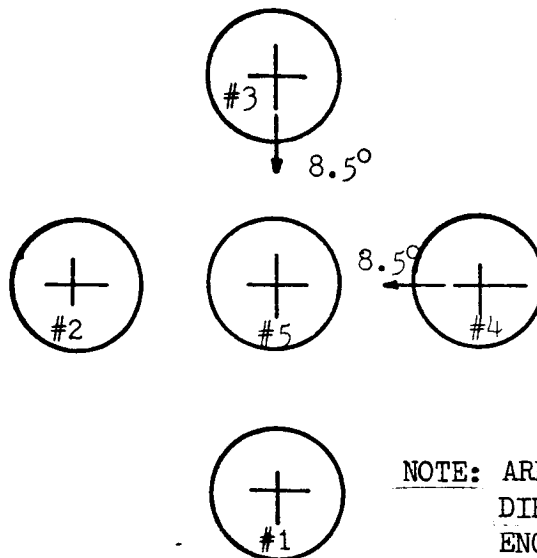


FIGURE 2 Model Base Geometry



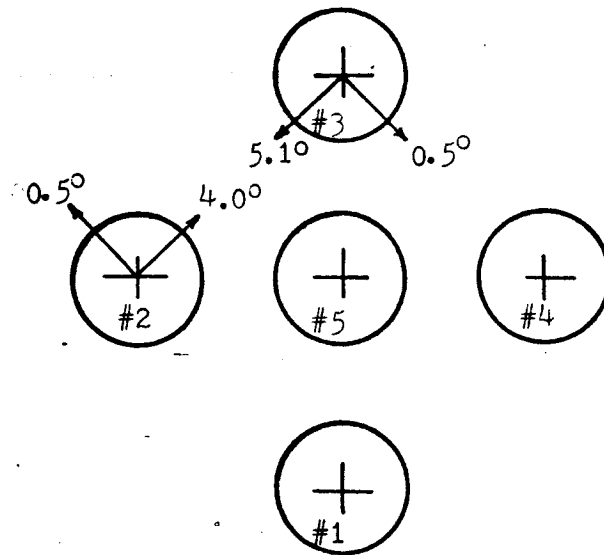
GIMBAL PATTERN #1 ($N_{G_3} N_{G_4}$)



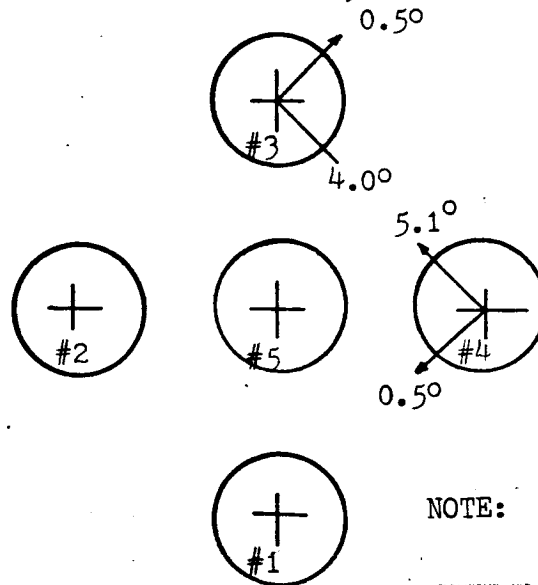
NOTE: ARROWS INDICATE
DIRECTION OF
ENGINE GIMBAL

GIMBAL PATTERN #2 ($N_{G_5} N_{G_6}$)

FIGURE 3 Gimbal Patterns



GIMBAL PATTERN #4 (N_{G9} N_{G10})

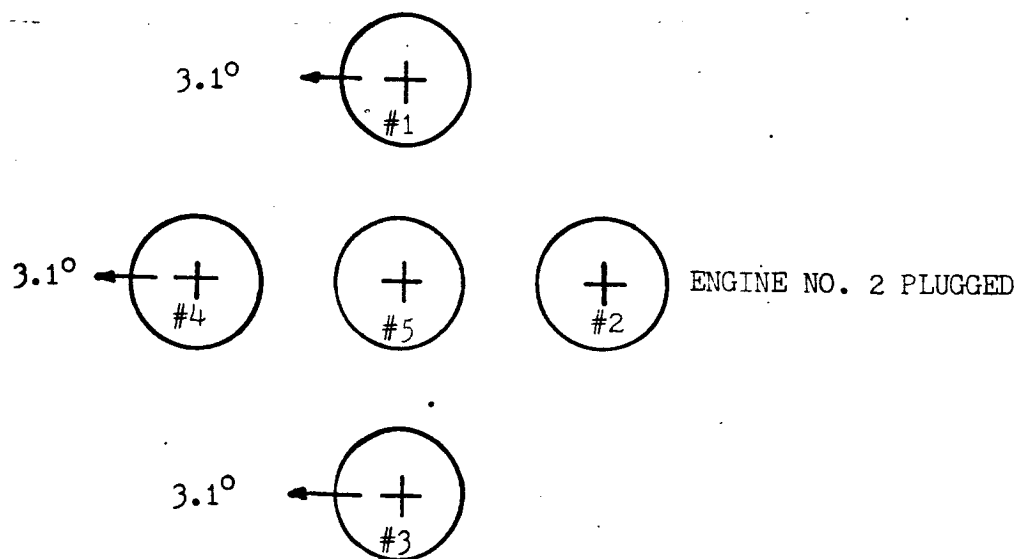


NOTE: ARROWS INDICATE
DIRECTION OF
ENGINE GIMBAL

GIMBAL PATTERN #3 (N_{G7} N_{G8})

FIGURE 4 Gimbal Patterns

NOTE: N₇ AND N₁₀ INDICATE PLUGGED
AND INSTRUMENTED ENGINE LOCATED
AT ENGINE POSITIONS 5 AND 2
RESPECTIVELY (SEE NOMENCLATURE)



NOTE: ARROWS INDICATE
DIRECTION OF
ENGINE GIMBAL

GIMBAL PATTERN #5 (N_{G11} N_{G12} N_{G13})

FIGURE 5 Gimbal Patterns

1.1.1 (Continued)

TABLE I Model Forebody

<u>Designation</u>	<u>Length - Inches</u>	<u>Tunnel</u>
B ₁	126.8	CAL 8 by 8
B ₃	132.772	Lewis 10 by 10
B ₄	148.77	Lewis 8 by 6

The forebody length changed between the CAL 8 by 8 foot tunnel test and the Lewis 10 by 10 foot tunnel test because of a charge tube redesign. The length was again changed in the Lewis 8 by 6 foot tunnel test to relocate the reflected model bow shock.*

A 15 degree half angle nose cone is capped with a 0.75 inch hemisphere and attached to the cylindrical body.

1.1.2 Engine

The nozzle internal contour, scaled from the proposed F-1 engine, has an area ratio of 16:1 and an exit divergence angle of 9.5 degrees. A turbine exhaust plenum is located on each of the nozzles at the 10 to 1 ratio. Two rows of fifty-two, 0.0595-inch diameter holes, spaced on 0.0714-inch staggered centers drilled normal to the surface may be used to simulate the turbine exhaust flow.

1.1.3 Engine Fairings

Each of the outboard engines has an engine fairing to reduce aerodynamic loads on the nozzle. Three different engine fairing lengths were tested. The basic design, S₁, ends at Station 48.5 full scale, and the S₄ engine fairing ends at Station 100, i.e., the base heat-shield position, S₂ is an intermediate length fairing located at Station 80. Figure 6 illustrates the engine fairing positions.

1.1.4 Flow Deflectors and Engine Fairing Scoops

Flow deflectors and engine fairing scoops are used to scavenge the base region of exhaust products. Eight deflectors, two between each fairing, are located on the periphery of the base region. Various combinations of scoop and deflector sizes enable testing with scooping area to base area varying from 10.0 percent to 19.8 percent.

The two scoop and three flow deflector sizes are shown in Figures 7 and 8.

* Test facilities are noted in the remainder of the report without reference to dimensions or tunnel, i.e., CAL 8 by 8 foot tunnel may be noted CAL 8 by 8.

ENGINE FAIRING CONFIGURATIONS

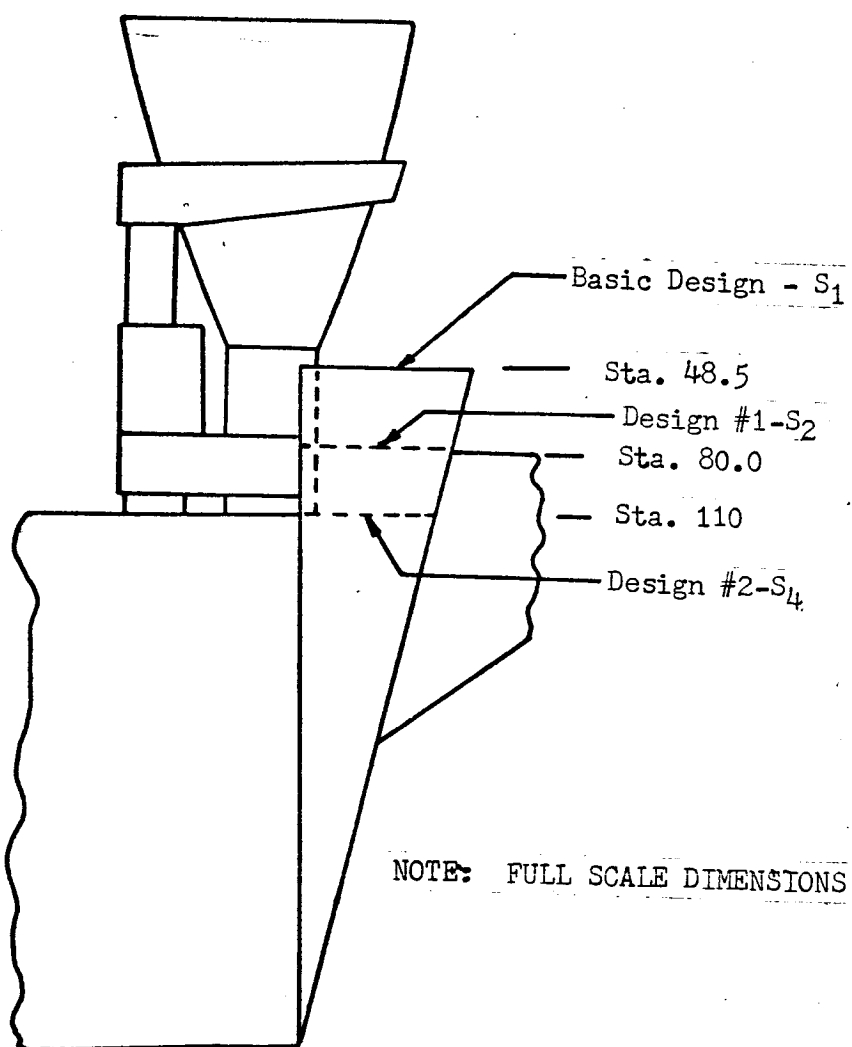
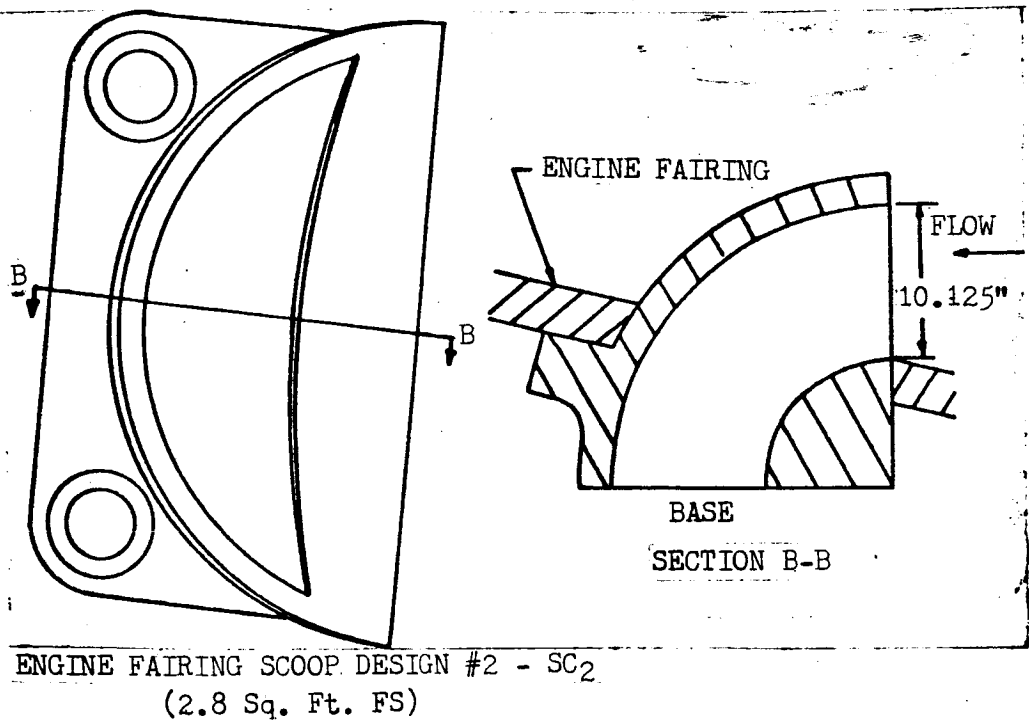
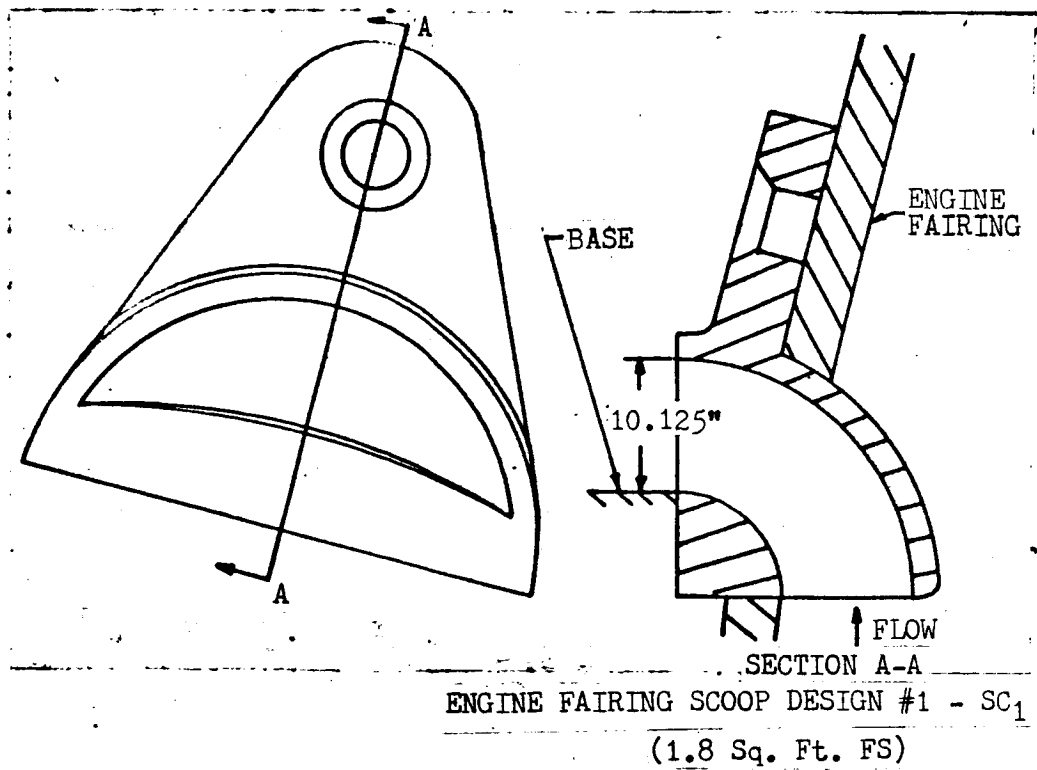


FIGURE 6 Engine Fairing Configuration



NOTE: FULL SCALE DIMENSIONS

FIGURE 7 Engine Fairing Scoop Configurations

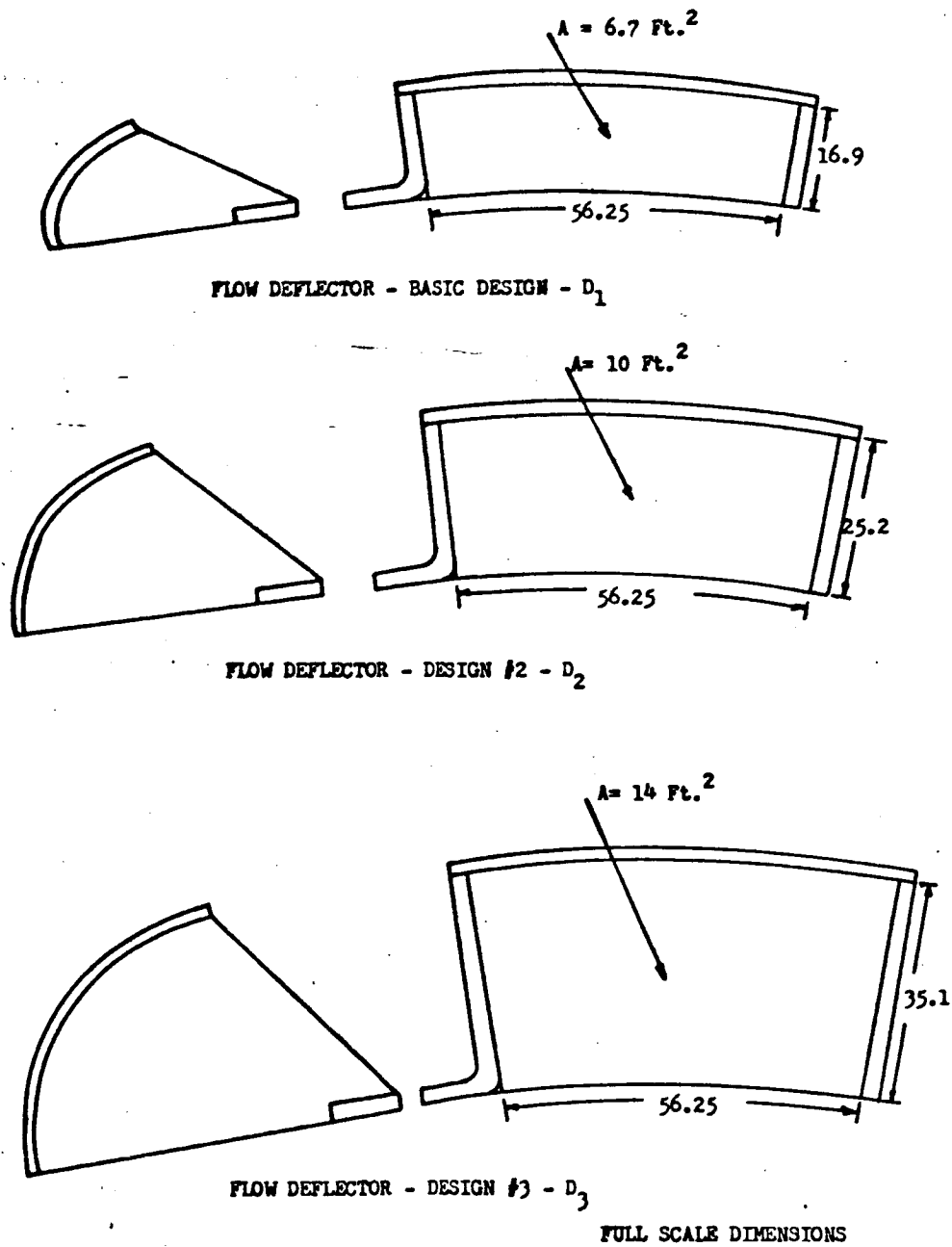


FIGURE 8 Flow Deflector Configurations

1.1.5 Base Plates

Three instrumented base configurations, identified as PL₁, PL₂, and PL₃, are used. The PL₁ base is instrumented for both pressures and heating rates, while the PL₂ base is instrumented only for pressures. Copper tubes are embedded in both the PL₁ and PL₂ bases to allow for circulation of cooling water in order to maintain the base temperature below 120°F. Cooling is necessary to minimize temperature effects on the pressure transducers in the high-temperature environment of the wind tunnels (tunnel total temperatures up to 175°F are experienced). The PL₃ base is instrumented only for heat transfer with special high-temperature gages and is used in an attempt to determine base recovery temperatures by means of a "hot base" technique described in Paragraphs 4.6 and 6.5. Resistance heaters are embedded in this base for heating and temperature control. Power was applied to the heaters through variable transformers and controlled by "West" recorders sensing thermocouples placed in the base.

1.2 MODEL OPERATION

A schematic of the model propulsion system is shown in Figure 1. The system includes separate propellant supply tubes containing gaseous oxygen and gaseous ethylene at high pressure. A quick-opening valve is installed downstream of the fuel and oxidizer flow metering venturis sealing and isolating the individual charge tubes. When the ends of the tubes are suddenly opened flow commencing from the tubes is mixed and burned in the combustion chamber and passed out of the exhaust nozzles. The period of steady combustion pressure is determined by the time required for expansion waves to travel the length of the gas supply tubes and return to the combustor.

1.2.1 Combustor Hardware

To assure proper metering of propellants, sonic venturis were installed in each charge tube prior to testing in the Lewis 10 by 10 foot super-sonic tunnel. (Prior to this orifices were used but proved unsatisfactory.) The application of venturis to the metering of propellants in the presence of nonsteady expansion waves is discussed in detail in Reference 3. Calculated propellant mass flow rates as a function of initial charge tube pressures are presented in Figures 9 and 10. During the Lewis 8 by 6 foot tunnel tests the charge tubes and quick-opening valve were electrically heated to 200°F to preclude the possibility of condensation of the ethylene during the rapid expansion through the valve and at the venturi throat.

The quick-opening valve as designed by CAL satisfies the following operating requirements:

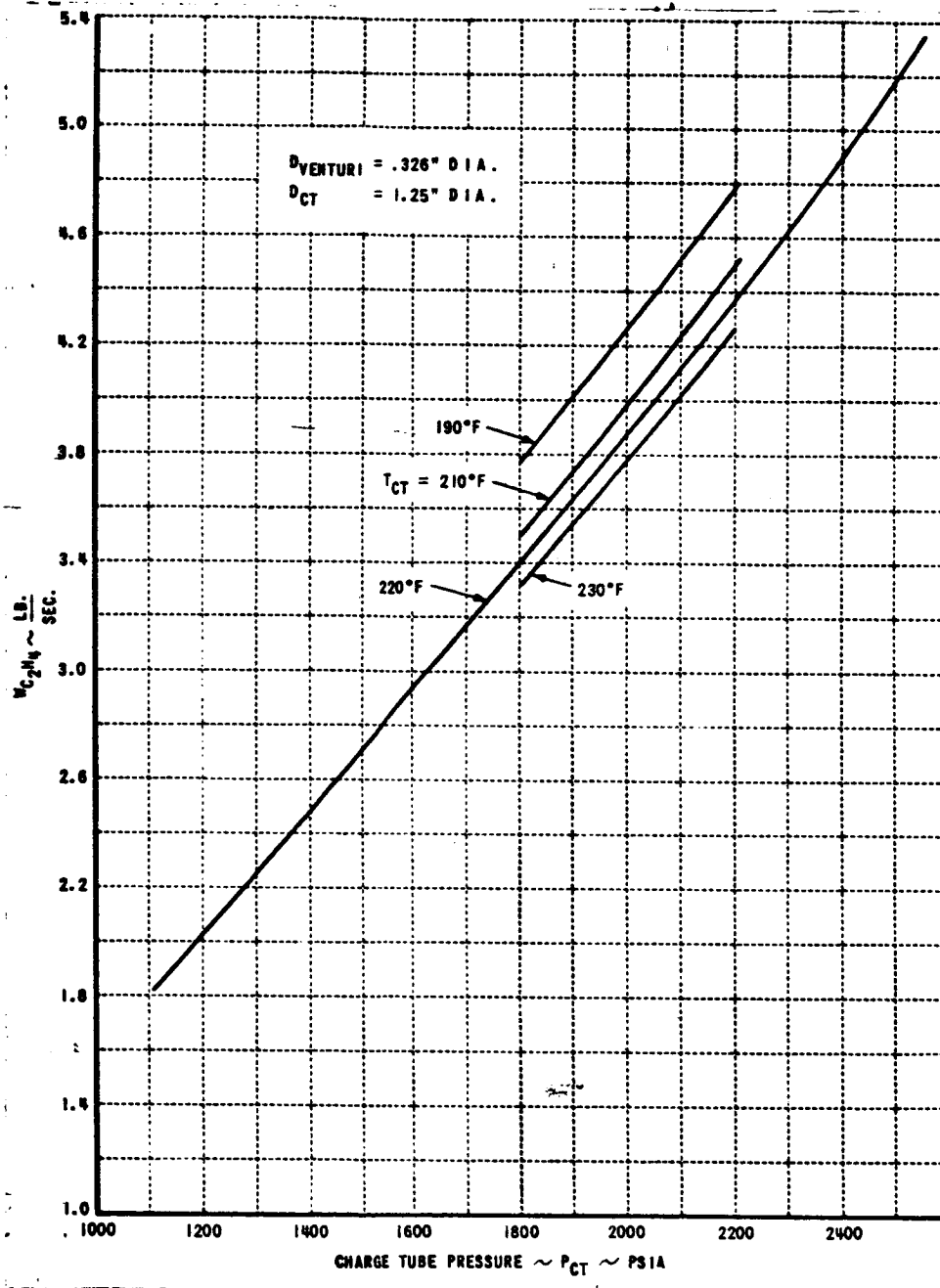


FIGURE 9 S-IC Ethylene Mass Flow

D5-15615

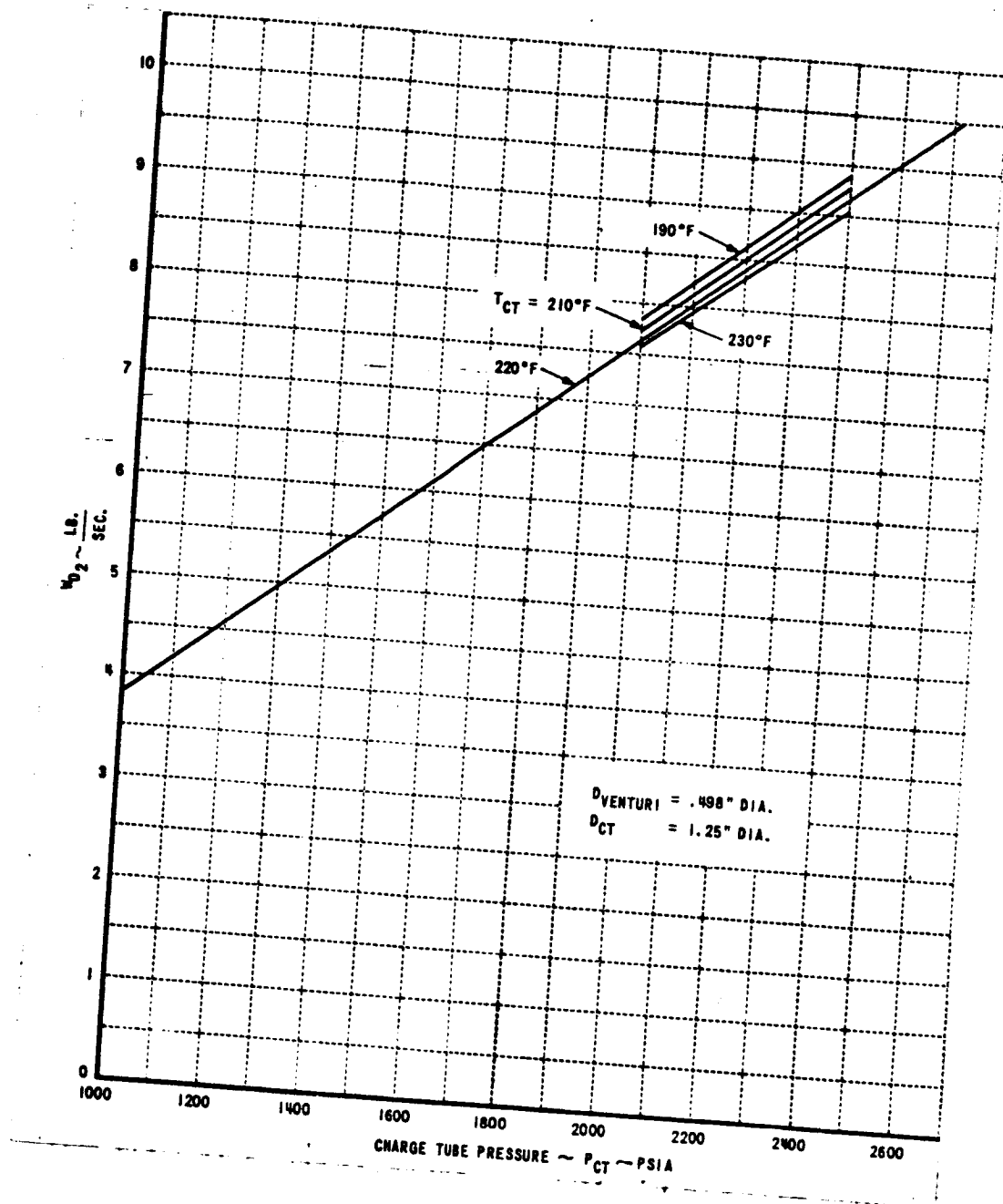


FIGURE 10 S-IC Oxygen Mass Flow

1.2.1 (Continued)

- a) Opens in 3 to 4 milliseconds.
- b) Discharges high-pressure gases from two separate propellant supply tubes simultaneously.
- c) Closes quickly, after remaining open 20 to 30 milliseconds, to minimize the combustion duration after the required test time.
- d) Remotely operable.

The valve housing is machined from a forged steel billet. The major components of the valve consists of a hydraulic actuator, an opening pressure chamber, a holding-closing pressure chamber, two aluminum pistons secured to a yoke and two ported plugs. A hydraulic system initiates the valve opening and the remaining operations are performed pneumatically.

A high-efficiency impinging doublet-type injector is located downstream of the quick-opening valve to provide mixing of the propellants in the combustion chamber. Fuel orifices located near the combustor wall provide a fuel-rich zone which protects the wall against excessive heating.

A single combustion chamber is used to contain the products of combustion and to channel them to the nozzles. The combustion chamber characteristic length ($L^* = \text{chamber volume} / \text{nozzle throat areas}$) which varied during the tests was 20 inches for the two Lewis tests. A spark plug located in the combustion chamber is timed to discharge when the cold flow chamber pressure is less than 100 psia. High overpressures could occur if significantly higher cold flow propellant pressures were present before discharging the spark plug.

1.2.2 Turbine Exhaust

The hydrogen turbine exhaust is injected into the nozzles simultaneously with the initiation of chamber combustion. When ethylene turbine exhaust is used, however, it is necessary to initiate the turbine-exhaust flow approximately 35 milliseconds prior to main combustion. This lead time is necessary to establish a steady level of turbine exhaust flow during the combustion event. Ethylene would more nearly simulate the actual gas conditions on the prototype but with the small model the base gas dwell time may be insufficient to let combustion occur. Ethylene was used for a few low altitude runs and was found to burn but it coated the heating gages so badly with soot that it was impractical to use. Hydrogen gas is preferred for simulating turbine exhaust since it has a wide flammability limit (4 percent - 74 percent) which would allow it to burn if the conditions for combustion exist.

1.2.2 (Continued)

A 1/8" diameter orifice is installed in each of the five supply lines between the common turbine exhaust manifold and individual engine plenums to meter the turbine exhaust flow. The manifold pressure necessary to maintain the required mass flow through the five orifices is computed as shown in Figures 11 and 12. During the pretest checkout of the model, a calibration was made to determine the manifold pressure corresponding to several supply pressures. This calibration is used to set the proper turbine exhaust supply pressure during the test. Hydrogen is injected at a rate that simulates the caloric content of the unburned fuel in the prototype turbine exhaust, while the ethylene mass flow rate simulates the scaled prototype turbine exhaust mass flow.

1.3 TEST CONDITIONS

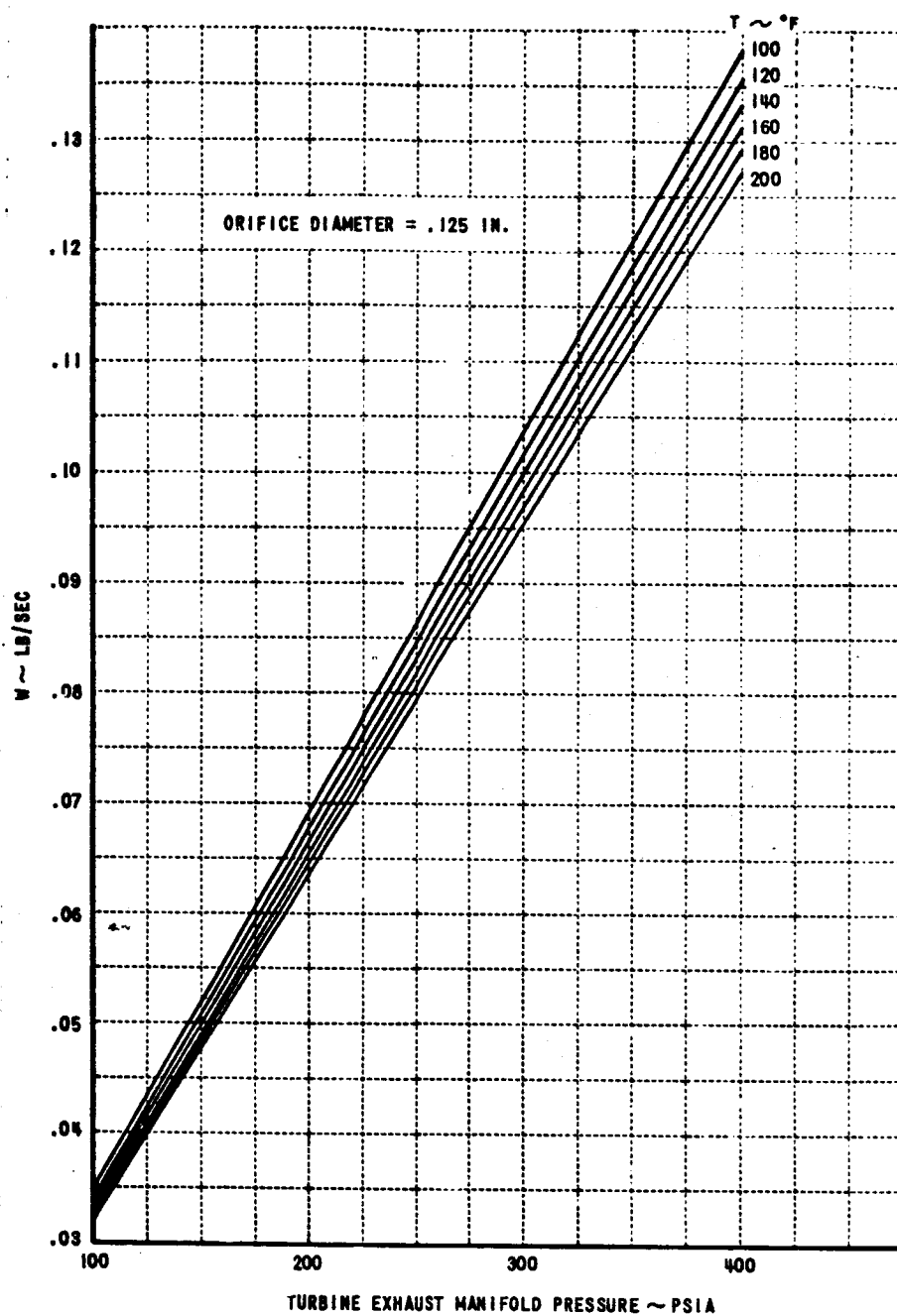
The facilities, engine operating parameters, heated base plate conditions and the configurations tested are discussed in the following paragraphs.

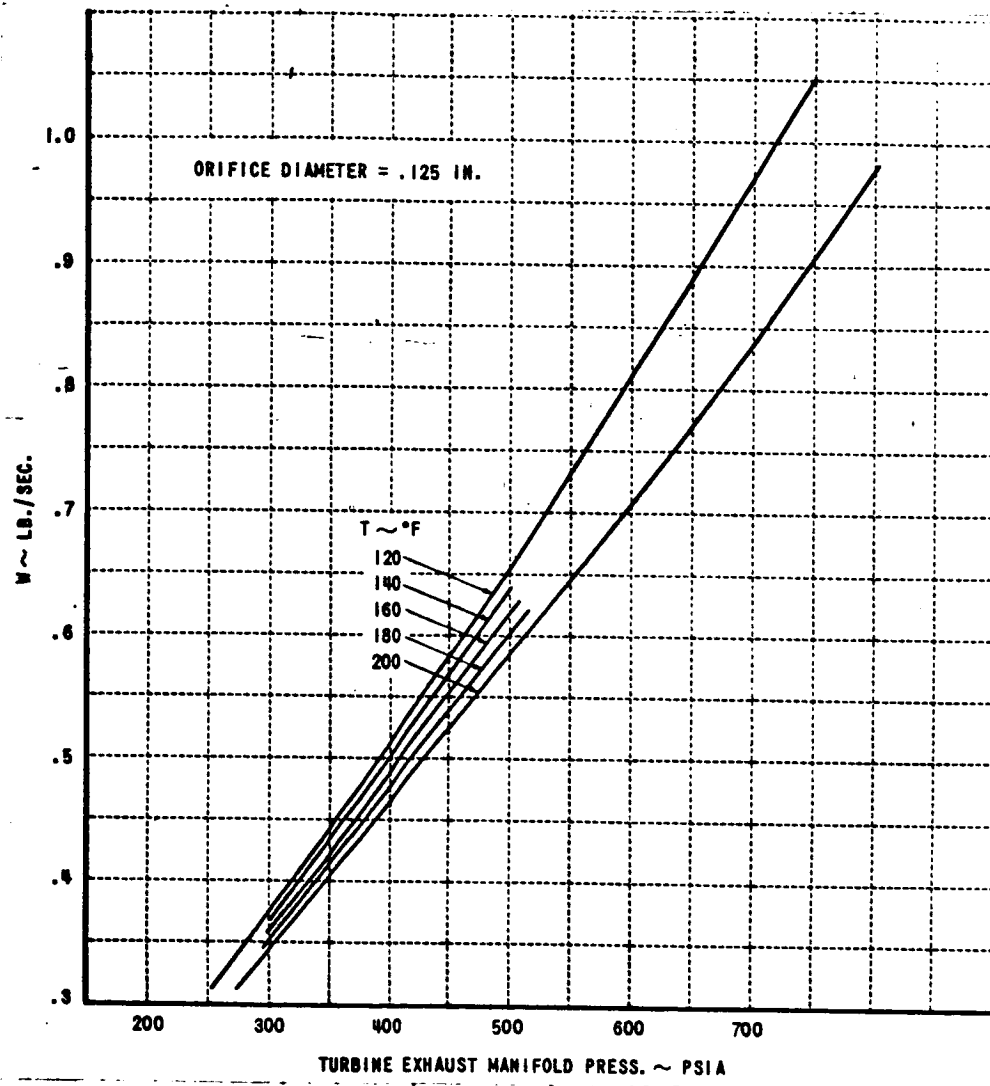
1.3.1 Facilities

Table II lists the test conditions for the four facilities used in this program. Test and trajectory total-temperature and altitude comparisons are plotted in Figure 13.

TABLE II Facility Test Conditions

<u>Facility</u>	<u>Mach</u>	<u>Test Altitude (Feet)</u>	<u>Trajectory (Feet)</u>
Lewis 8 by 6	0.55	1,600	12,000
	0.80	7,400	18,000
	1.00	13,400	26,000
	1.35	22,600	35,000
	1.66	29,400	43,000
	1.95	35,200	50,000
Lewis 10 by 10	2.00	51,000	51,000
	2.50	66,000	66,000
	3.00	81,000	81,000
	3.50	96,000	96,000
	3.50	150,000	96,000
CAL 8 by 8	0.60	13,000	13,000
	0.80	18,000	18,000
	1.00	26,000	26,000
	1.20	34,000	34,000

FIGURE 11 H₂ Turbine Exhaust Mass Flow - 5 Engines

FIGURE 12 C₂H₄ Turbine Exhaust Mass Flow - 5 Engines

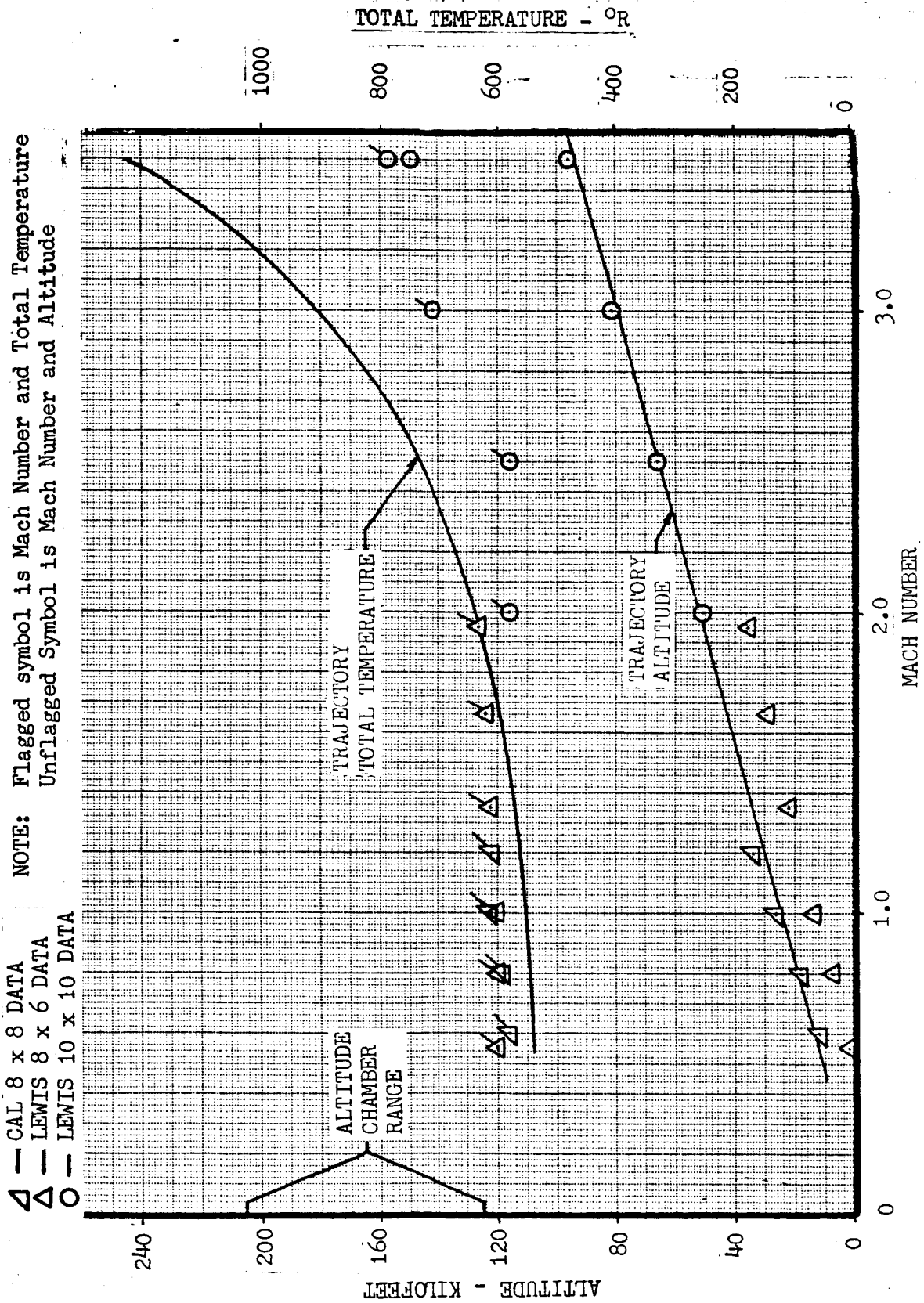


FIGURE 13 Facility Test Conditions

1.3.1 (Continued)

<u>Facility</u>	<u>Mach</u>	<u>Test Altitude (Feet)</u>	<u>Trajectory (Feet)</u>
CAL Altitude Chamber	No	125,000	125,000
	External Flow	135,000	135,000
		145,000	145,000
		155,000	155,000
		165,000	165,000
		175,000	175,000
		185,000	185,000
		195,000	195,000
		205,000	205,000

1.3.2 Engine

Model propellants are gaseous oxygen and ethylene. Combustion conditions of the model are compared with the LOX RP-I propellants, used by the prototype, in Table III.

TABLE III Combustion Parameters

<u>Parameter</u>	<u>GOX-Ethylene</u>	<u>LOX RP-I</u>
O/F	2.20 - 2.30	2.25
T _c	6830 - 6870°R	6400°R
P _c	1030 - 1100 PSIA	1050 PSIA
Y	1.22 - 1.206	1.223
R	73.6 - 72.5	70

1.3.3 Heated Base Plate

Convective heating rates are obtained with the base plate heated to the values in Table IV.

TABLE IV Heated Base Plate Temperatures

<u>Facility</u>	<u>Temperatures</u>
Lewis 8 by 6	200, 350 °F
CAL Altitude Chamber	400, 700, 900 °F

1.3.4 Configurations

Table V is a compilation of the various configurations tested in each of the facilities. Each configuration is described by groups of letters and numbers which indicate the variables described in Paragraph 1.1.

- | | |
|------------------------------|----|
| a) Forebody | B |
| b) Engine fairing length | FS |
| c) Deflector size | D |
| d) Engine fairing scoop size | SC |
| e) Engines | N |
| f) Base Plate | PL |

Numbered subscripts indicate a particular size or geometry. For example:

$$B_1FS_1D_1SC_1N_3N_4PL_1-$$

describes a configuration using the original cone cylinder forebody with a standard length engine fairing, deflectors with the smallest inlet area, engine fairing scoops with the smallest inlet area, engines 3 and 4 gimbaled toward each other at 6-degrees and the base plate which is instrumented with both heating and pressure gages. Additional definition is provided in Figures 3, 4, 5, 6, 7, and 8, Paragraphs 1.1.1 and 1.1.5 and the nomenclature.

TABLE V Configurations Tested

Facility	CAL 8 x 8	Lewis 8 x 6	Lewis 10 x 10	CAL Altitude
Forebody	B ₁	B ₄	B ₃	B ₁
	Base Plate	Base Plate	Base Plate	Base Plate
FS ₁ N ₁₋₅	PL ₁	PL ₁ , PL ₃	PL ₁	PL ₁ , PL ₃
FS ₄ N ₁₋₅		PL ₁	PL ₁	
FS ₁ D ₂ N ₁₋₅		PL ₁ , PL ₂		
FS ₄ D ₂ N ₁₋₅		PL ₁		
FS ₄ SC ₁ N ₁₋₅				PL ₁
FS ₁ D ₁ SC ₁ N ₁₋₅	PL ₁		PL ₁	
FS ₁ D ₁ SC ₂ N ₁₋₅		PL ₁ , PL ₂		
FS ₂ SC ₁ N ₁₋₅	PL ₁			
FS ₄ D ₁ SC ₁ N ₁₋₅	PL ₁			
FS ₁ D ₃ SC ₁ N ₁₋₅	PL ₁			
FS ₁ D ₃ SC ₂ N ₁₋₅			PL ₁	

1.3.4 (Continued)

TABLE V (Continued)

Facility	CAL 8 x 8	Lewis 8 x 6	Lewis 10 x 10	CAL Altitude
Forebody	B ₁	B ₄	B ₃	B ₁
	Base Plate	Base Plate	Base Plate	Base Plate
FS ₁ N ₇			PL ₁	PL ₁
FS ₁ D ₁ N ₇		PL ₁		
FS ₁ D ₂ N ₇		PL ₁		
FS ₁ NG ₃ NG ₄			PL ₁	PL ₁
FS ₁ NG ₅ NG ₆			PL ₁	PL ₁
FS ₁ D ₂ NG ₇ NG ₈		PL ₁ , PL ₂		
FS ₁ D ₁ SC ₂ NG ₇ NG ₈		PL ₁		
FS ₁ D ₂ NG ₁₀ NG ₁₁ NG ₁₂		PL ₁ , PL ₂		

1.4 INSTRUMENTATION

The short-duration instrumentation provided by CAL, used in the operation of the model and to record engine-on data, is described below. The steady-state instrumentation supplied and used by NASA to monitor tunnel operation and to record the continuous external flow data is not discussed.

1.4.1 Heat Transfer

Thin-film heat-transfer gages were employed for the measurement of short-duration heating. The thin-film heat-transfer gages operate on the principle of sensing the transient surface temperature of the model. The sensing element is a thin (0.1 micron) platinum strip fused on the front surface of a pyrex glass substrate which conforms to the local surface contour of the model. Since the heat capacity of the platinum strip is negligible, the film temperature is equal to the instantaneous surface temperature of the pyrex substrate, which is related to the model heat transfer rate by the theory discussed in Reference 4. The output of the heat-transfer gage is fed through an analog network (Reference 5) which converts the signal from one representing temperature to a signal directly proportional to the instantaneous transfer rate. A typical analog circuit heating rate output is shown in Figure 14.

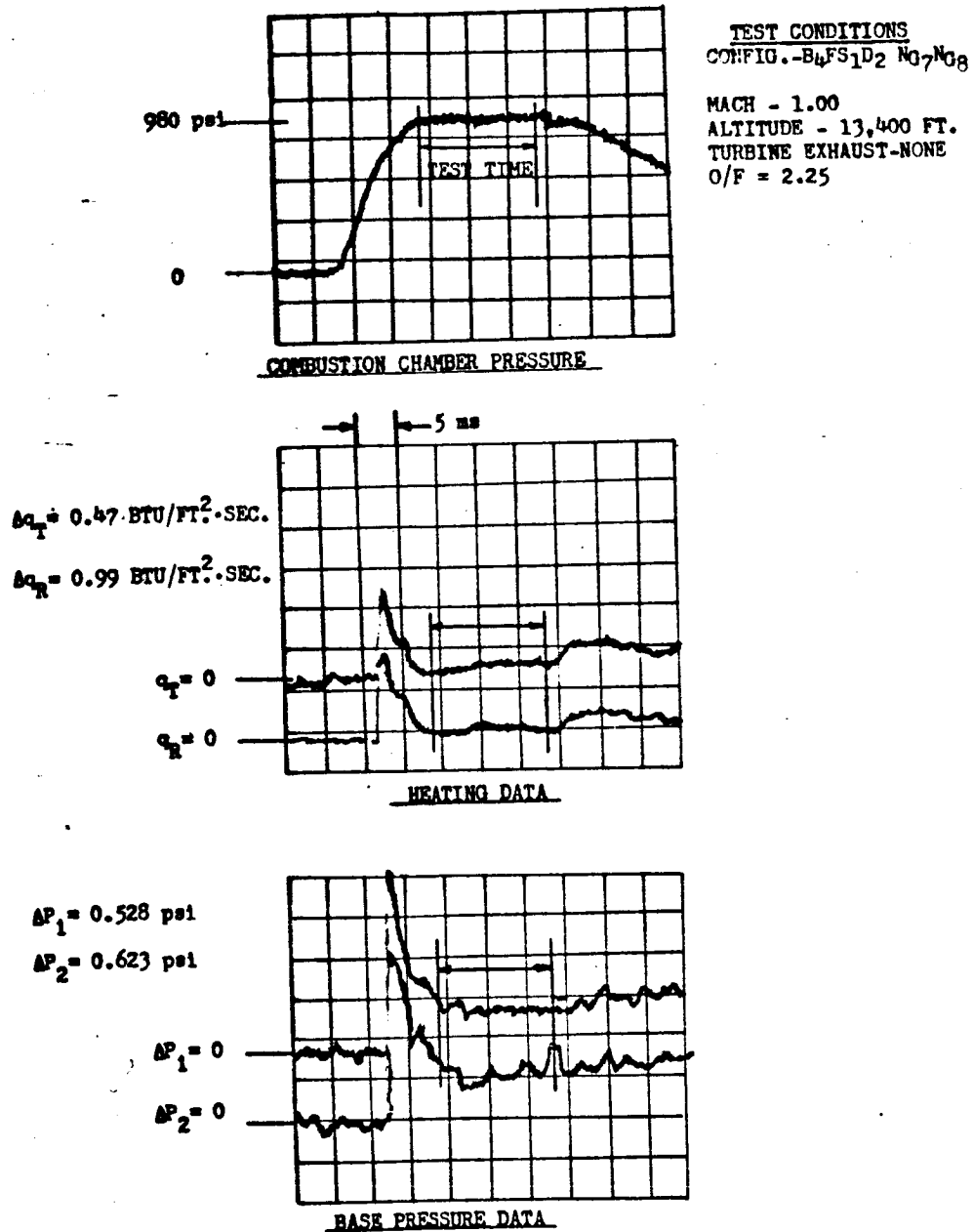


FIGURE 14 Oscilloscope Traces (Typical)

1.4.1 (Continued)

Heat-transfer gages constructed to allow measurement of radiant, and total heating rates are used. These gages contain a second platinum strip applied to the rear side of the substrate material. The two strips are perpendicular to one another, so as to minimize shadowing of the rear film by the front surface film. Also, because of its superior transmission characteristics, quartz is used as the substrate material, rather than pyrex. Ability of the gage to differentiate between radiative and convective heating is based on the concept that, during the short test time, the quartz substrate effectively acts as a thermal insulator for the rear gage such that only the radiative heating component is sensed by this element. Alternately, the front gage feels the total heating, both radiant and convective. A knowledge of the substrate absorption and transmission characteristics (discussed in Reference 6) then allows the convective and radiant heating rates to be separated.

Special high-temperature gages are used in the PL₃ heated base. These gages employ the same sensing technique as the standard gage described above, but are of somewhat different construction. The primary limitation of the standard gage for high-temperature work is the soldered connection between the gage lead-in wires and the thin-film terminals. For high-temperature gages, a fabrication process has been developed in which platinum lead-in wires are bonded directly to the platinum film, allowing gage temperatures up to 1000°F. (A maximum steady-state temperature limit of 1000°F is established because of the incipient softening of the pyrex substrate above that temperature.) Radiant heat-transfer gages for the PL₃ base are the same type of high-temperature units as described above, with the addition of a quartz window placed in front of the gage.

1.4.2 Pressure

Short-duration surface pressure measurements are made on the model base, using CAL-developed piezoelectric pressure transducers. These transducers are small in size and are linear to pressure levels well beyond those experienced in these tests. A dual element feature reduces acceleration sensitivity to an indicated pressure of .003 psi/g. Due to the very high model acceleration associated with the sudden initiation of flow from the rocket nozzles, however, the internal acceleration compensation has sometimes been found to be inadequate. To further reduce acceleration effects, the transducers were mounted on a spring-suspended seismic mass and connected to the model orifice with a soft rubber tube.

1.4.3 Boundary Layer

Measurement of the boundary layer total-pressure distribution forward of the model base is made with a pressure rake. The rake in Figure 15 is used in the CAL 8 by 8 test while the rake in Figure 16 is used in both Lewis tunnels.

1.4.4 Model Performance

Kistler piezoelectric crystal transducers were used to sense fuel and oxidizer venturi throat pressure, injector pressures, combustion pressures and turbine exhaust manifold pressures. Base temperatures, auto-valve temperatures and the initial turbine gas temperatures were measured with chromel-alumel thermocouples.

1.4.5 Data Recording

Polaroid pictures record the oscilloscope traces of the instrumentation outputs. Data are measured directly from the pictures. Typical test data are shown in Figure 14, including traces of combustion chamber pressure, heating rate, and base pressure. The test time, or segment of the trace which is marked for evaluation, is determined by the time during which combustion chamber pressure is a steady value.

1.4.6 Calibration

The CAL pressure transducers were calibrated after installation in the model. The Kistler transducers were installed in a special fixture and calibrated with a dead weight tester. The voltage variation (i.e., voltage output versus applied pressure) of the transducers is linear over the range of pressures normally encountered in testing. These calibrations, in conjunction with estimated values for the model pressures to be experienced during the actual test, also provide the basis for adjusting the gain of the data recording system to achieve maximum "readability" of the oscilloscope traces. The transducers were check-calibrated periodically throughout the program.

The wide range of temperatures over which the heat transfer gages were operated made it necessary to have an accurate knowledge of the gage resistance characteristics and the value of $(\rho c k)^{1/2}$ as functions of temperature. The resistance characteristics were determined from a calibration consisting of measuring gage resistance at two temperatures, approximately 70°F and 150°F. The appropriate value of $\Delta R/\Delta T$ for the existing ambient temperature was determined from this calibration and a correction given in graphical form in Figure 17. The correction curve of Figure 17 was obtained during the development of the heat-transfer gages by measuring gage resistance while in a well-regulated furnace. This information was then used to determine the value of a shunt resistor (dummy load resistor - DLR) that was chopped into the heat transfer gage circuitry to generate the same ΔV signal that would be

* See Paragraph 1.5.2 for definition

D5-15615

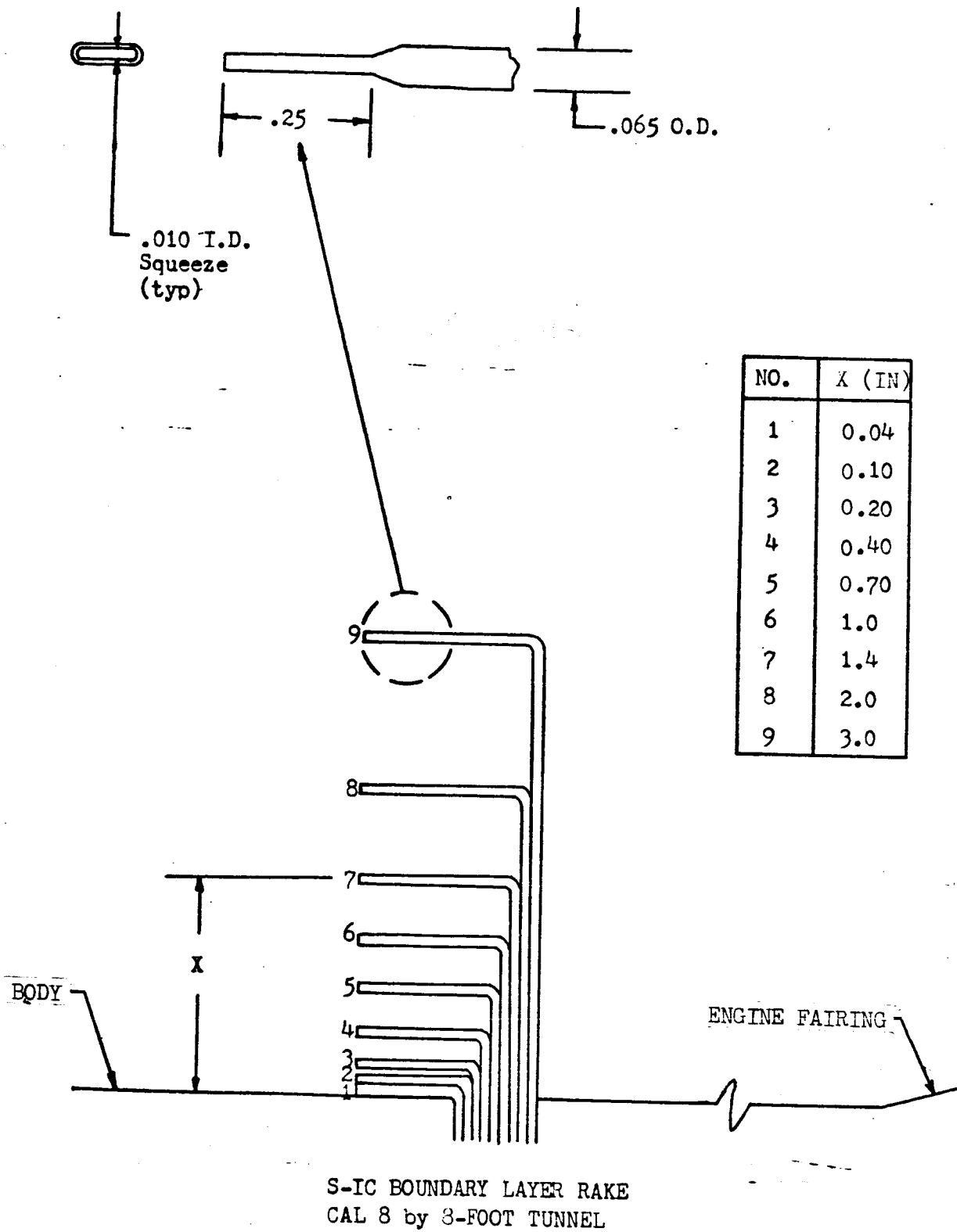
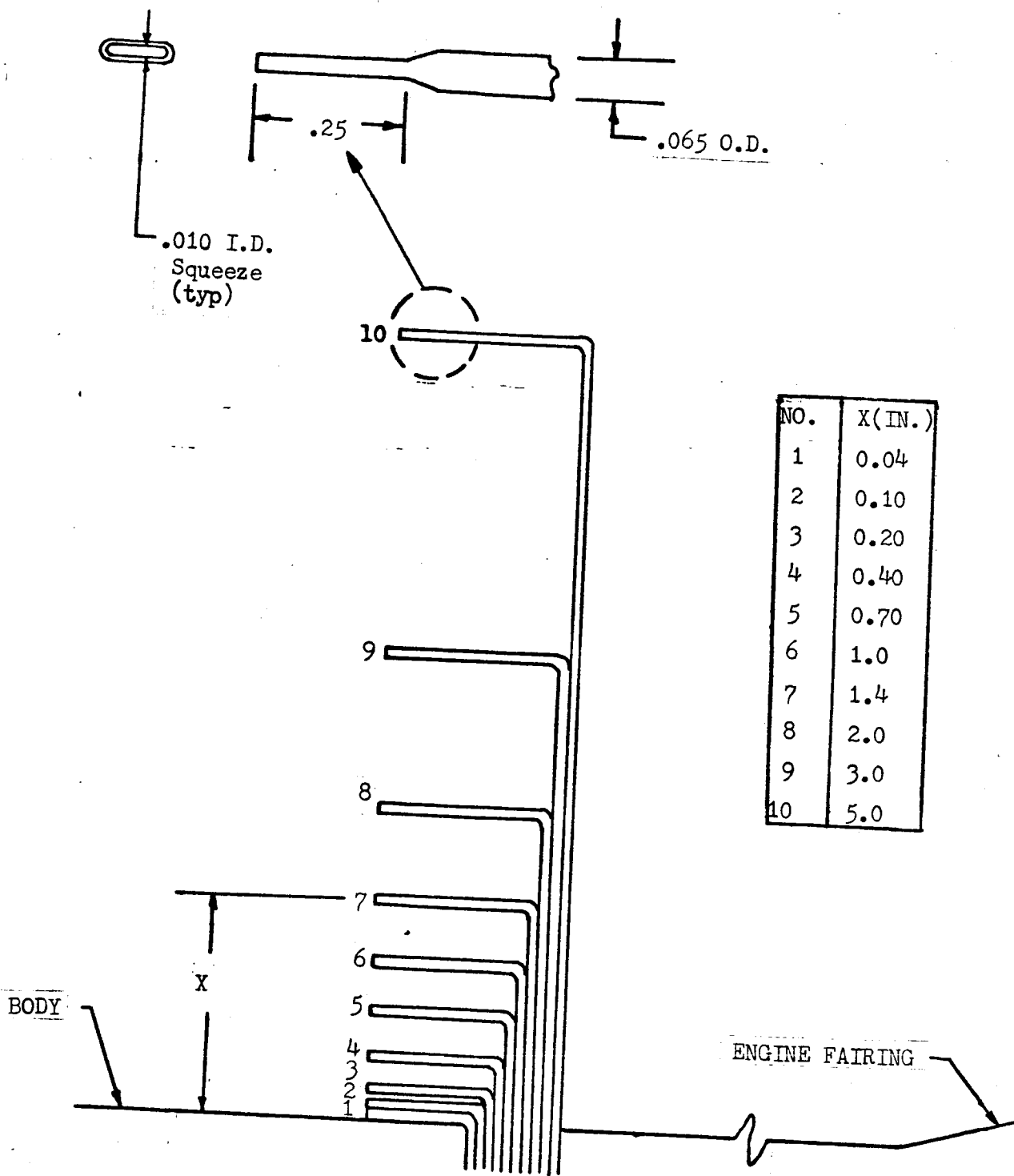


FIGURE 15 Boundary Layer Rake - CAL 8-BY 8-Foot Tunnel



S-IC BOUNDARY LAYER RAKE
LEWIS 8 by 6 AND 10 by 10 FOOT TUNNELS

FIGURE 16 Boundary Layer Rake - Lewis 8-by 6 and 10-by 10 Tunnels

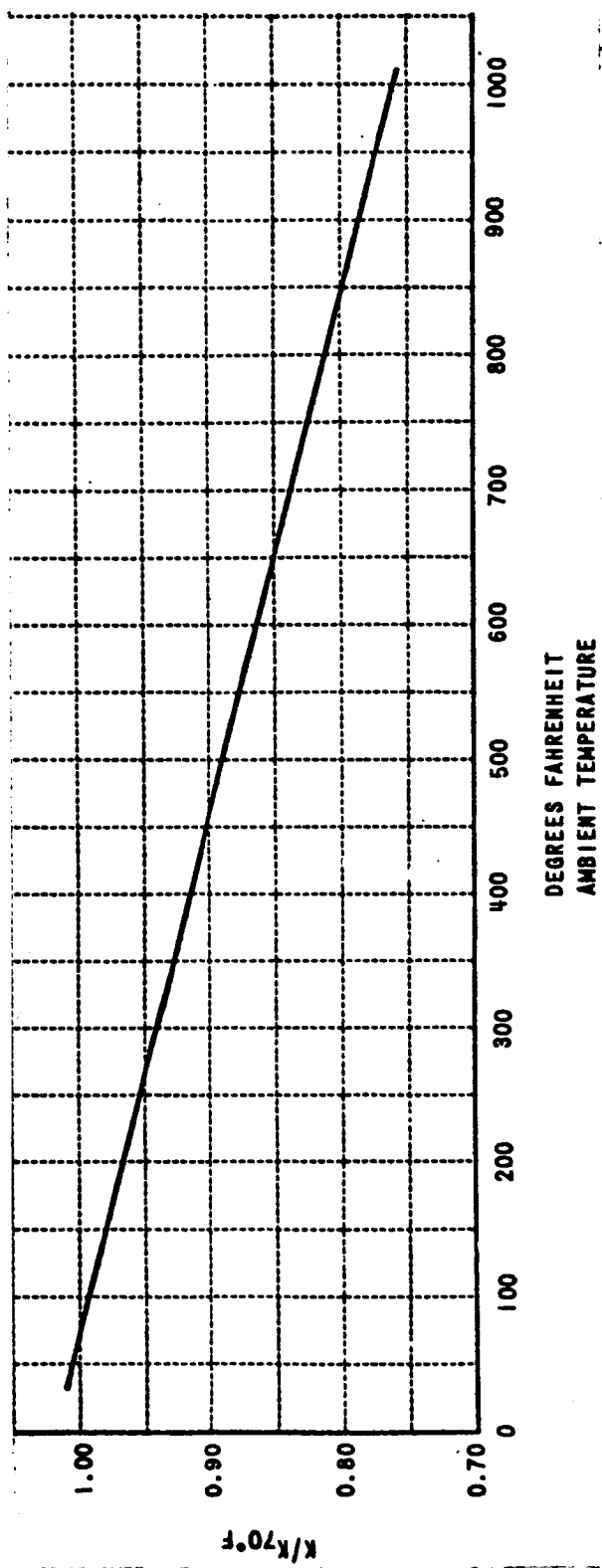


FIGURE 17 Variation of Heat Transfer Gage Sensitivity with Temperature

1.4.6 (Continued)

produced if the gage increased in resistance due to heating. Proper DLR values are given by

$$DLR = \frac{R_p^2}{K\Delta T} \left[\left(\frac{R_1 + R_g'}{R_1 + R_p} \right)^2 \right] - R_p$$

where: R_p - Precision resistor - 100Ω

K - $\frac{\text{Change in gage resistance} - \Delta R}{\text{Change in temperature} - \Delta T}$

R_1 - Series resistor - 1000Ω

R_g' - Gage resistance at temperature T

Details and techniques of the experimental procedure employed in determining the temperature characteristics of the parameter $(\rho ck)^{\frac{1}{2}}$ for gage substrates are discussed in References 7 and 8. The normalized variation of $(\rho ck)^{\frac{1}{2}}$ with temperature determined from test data is given in Figure 18.

1.4.7 Instrumentation Locations

Base instrumentation consists of total heating, radiation heating, and static pressure gages on the three base plates (see Paragraph 1.1.4). The instrumentation locations on each base plate are shown in Figures 19, 20 and 21. Figures 22 and 23 are composites of the external nozzle instrumentation and include heat-transfer gages on all nozzles. Nozzle instrumentation for the no-flow nozzle is shown in Figures 24 and 25. The base of the fin and the engine fairing are instrumented as shown in Figures 26 and 27, respectively.

1.5 DATA REDUCTION

1.5.1 Pressure

The CAL pressure transducers measure the difference between the initial steady state base pressure and the local pressure during model operation. The initial pressure (engine off) is added to the measured pressure difference to obtain the absolute model pressure (engine on).

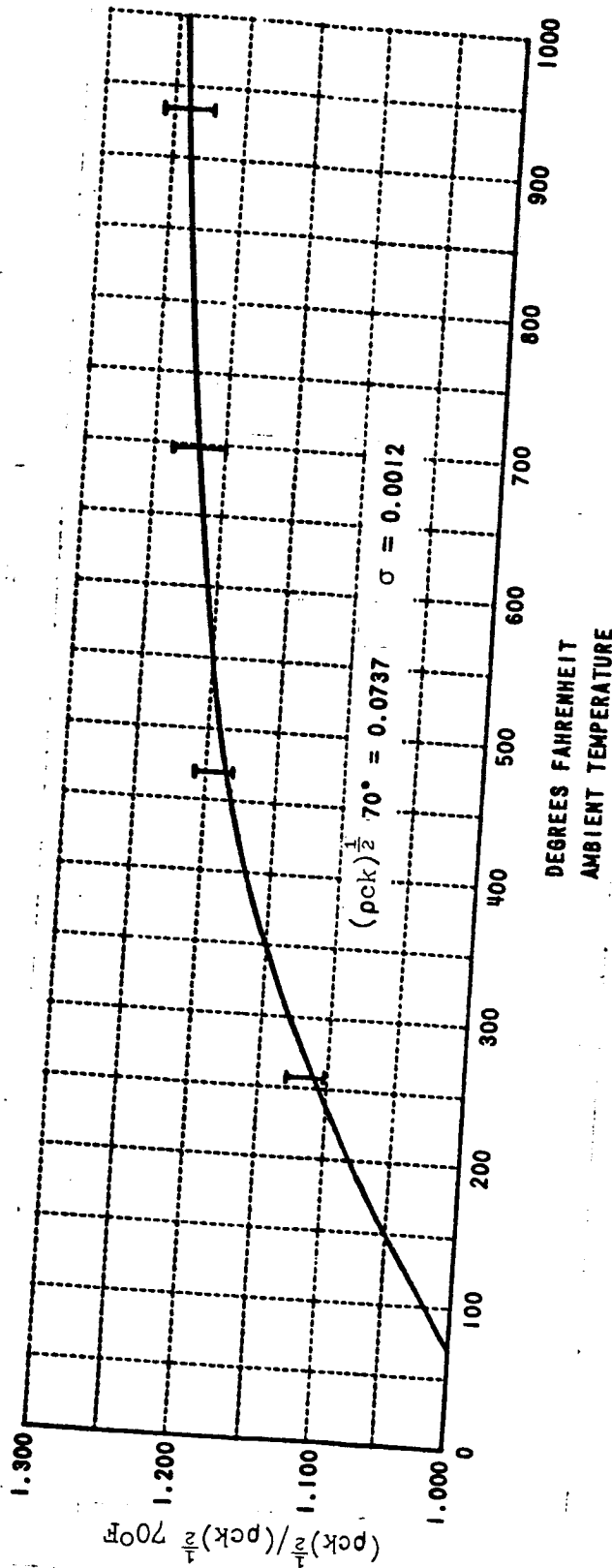
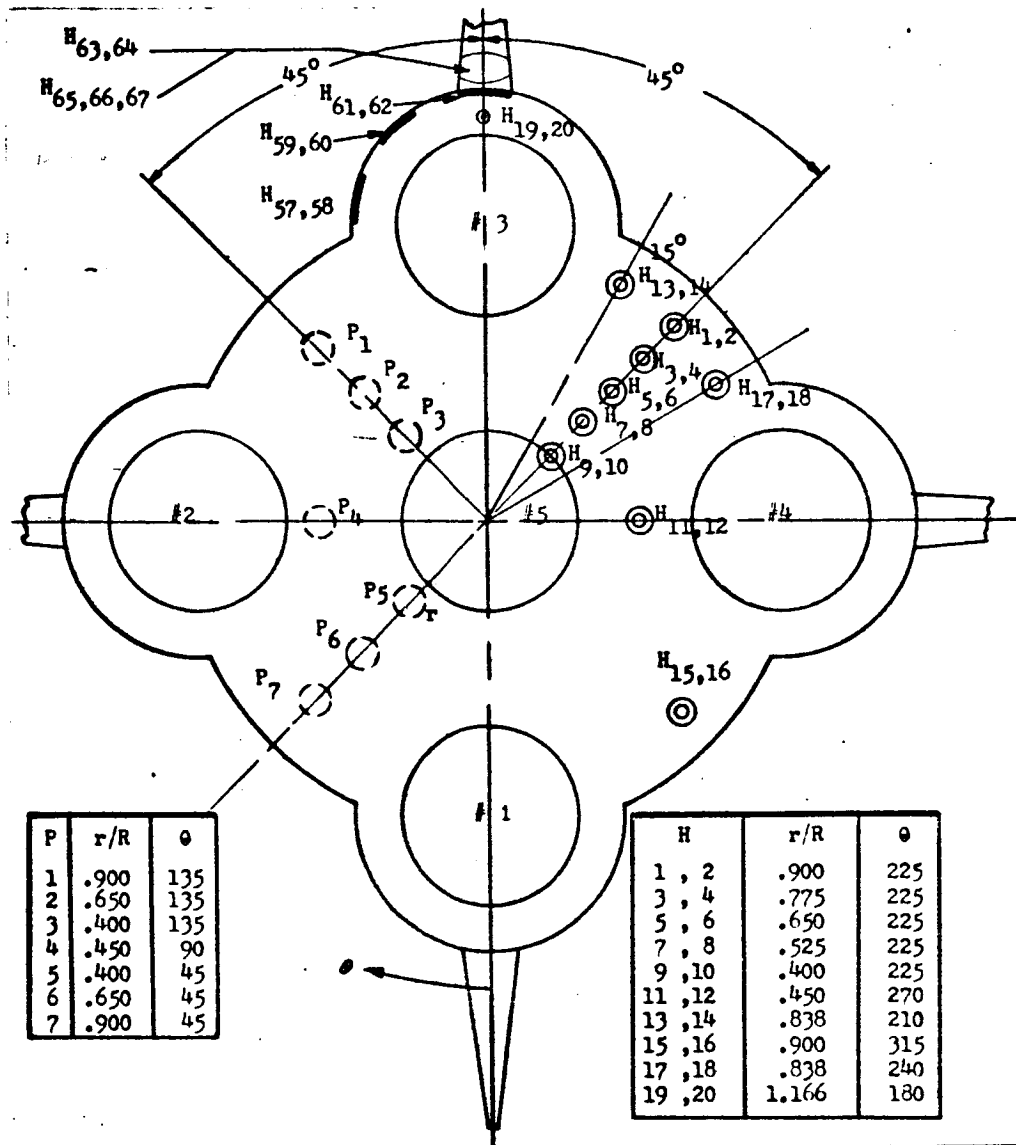
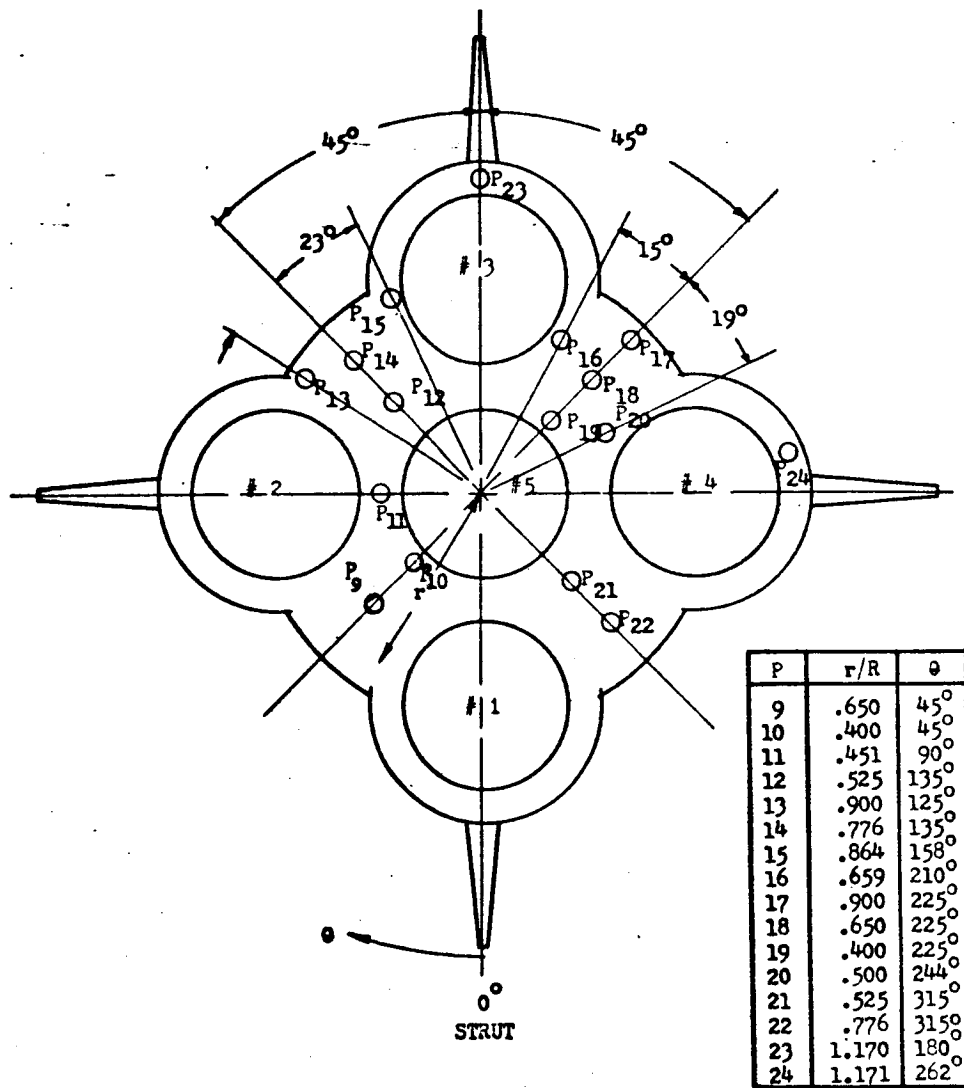
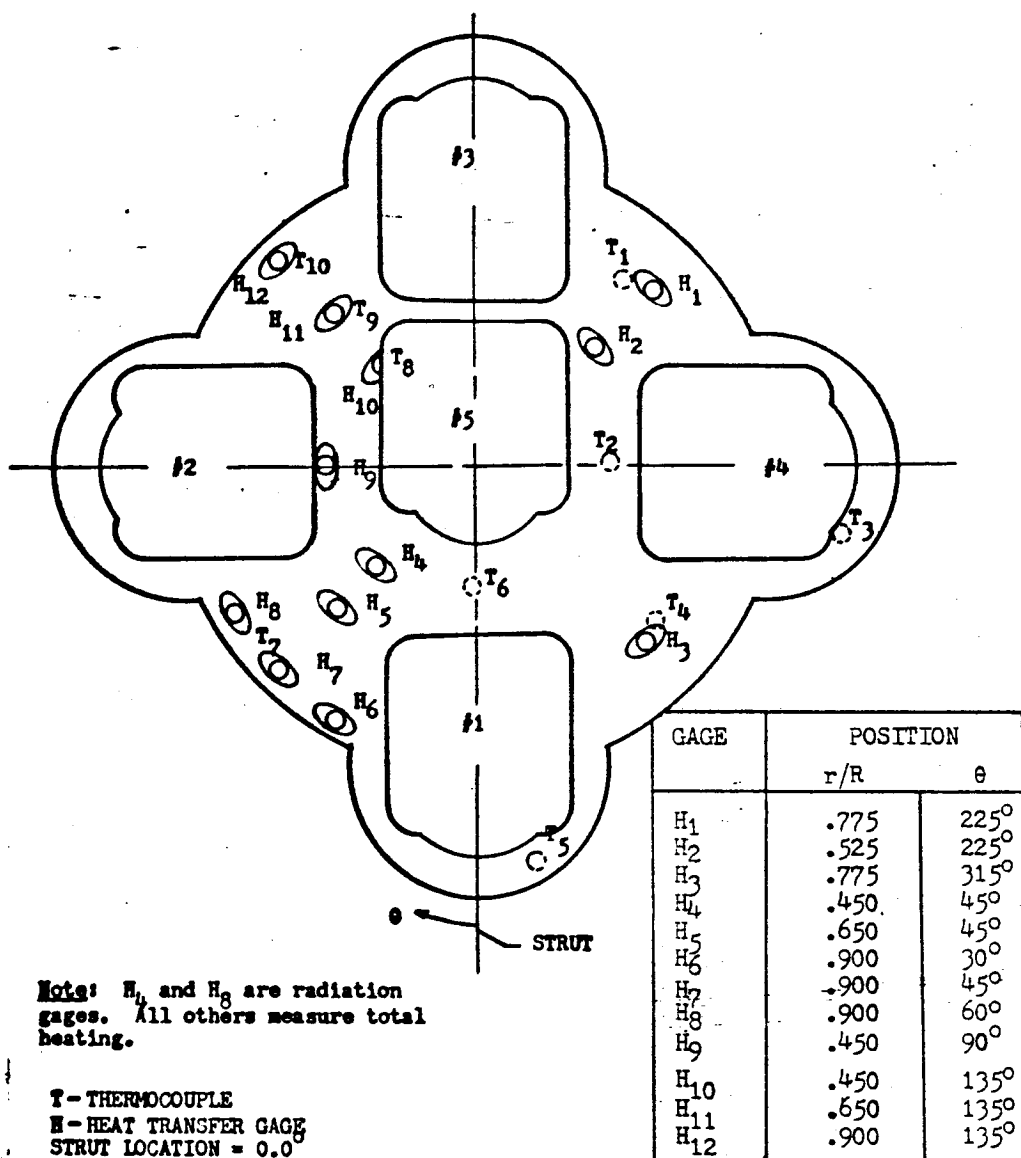


FIGURE 18 Variation of $(\rho_{ck})^{1/2}$ With Temperature (7740 Pyrex)

PRESSURE AND HEAT TRANSFER BASE PLATE - P_{L1} FIGURE 19 Pressure and Heat Transfer Base Plate - PL_1

PRESSURE BASE PLATE

PL₂FIGURE 20 Pressure Base Plate - PL₂

HOT BASE INSTRUMENTATION PLATE - PL₃FIGURE 21 Heated Base Plate - PL₃

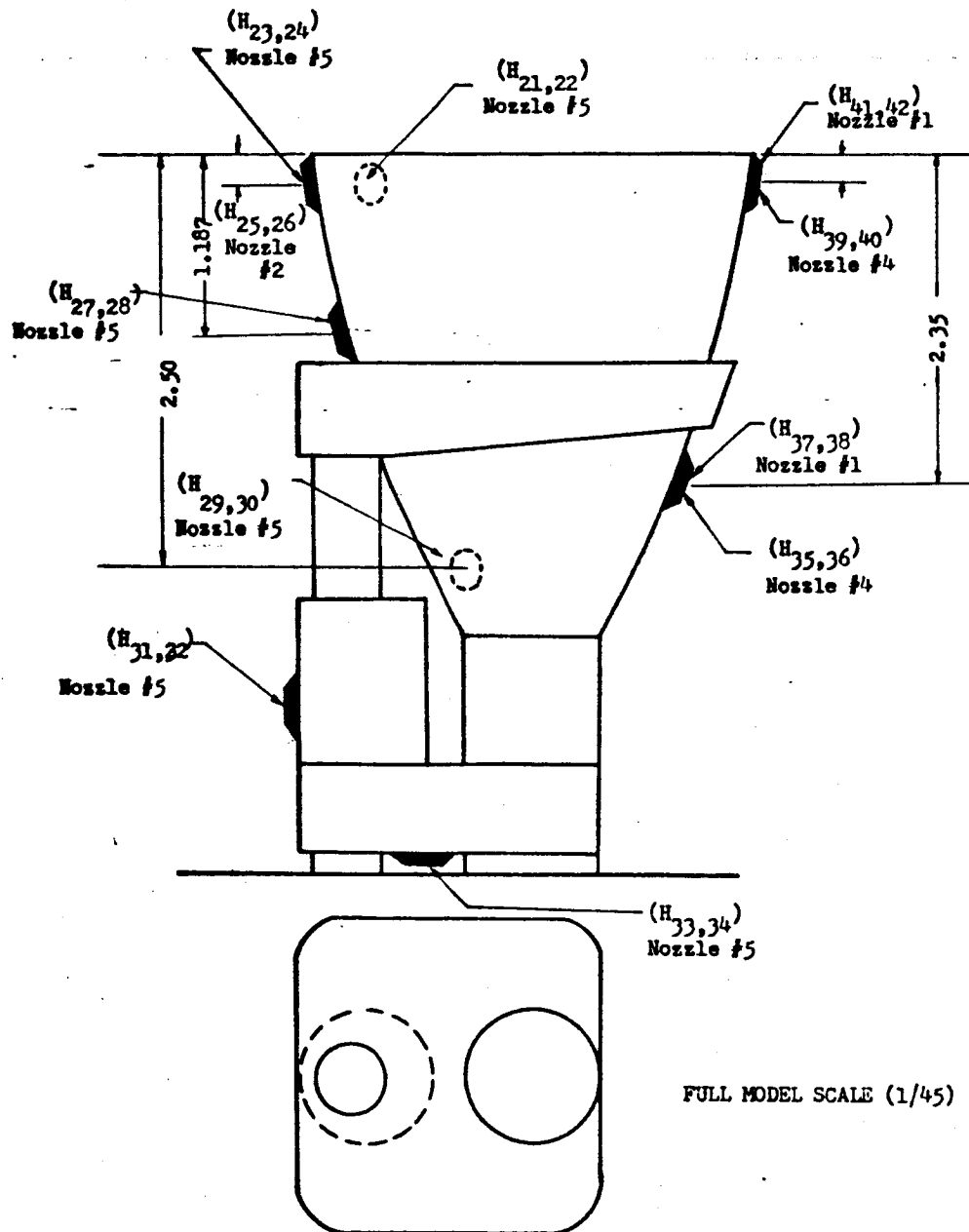


FIGURE 22 Engine Instrumentation - External

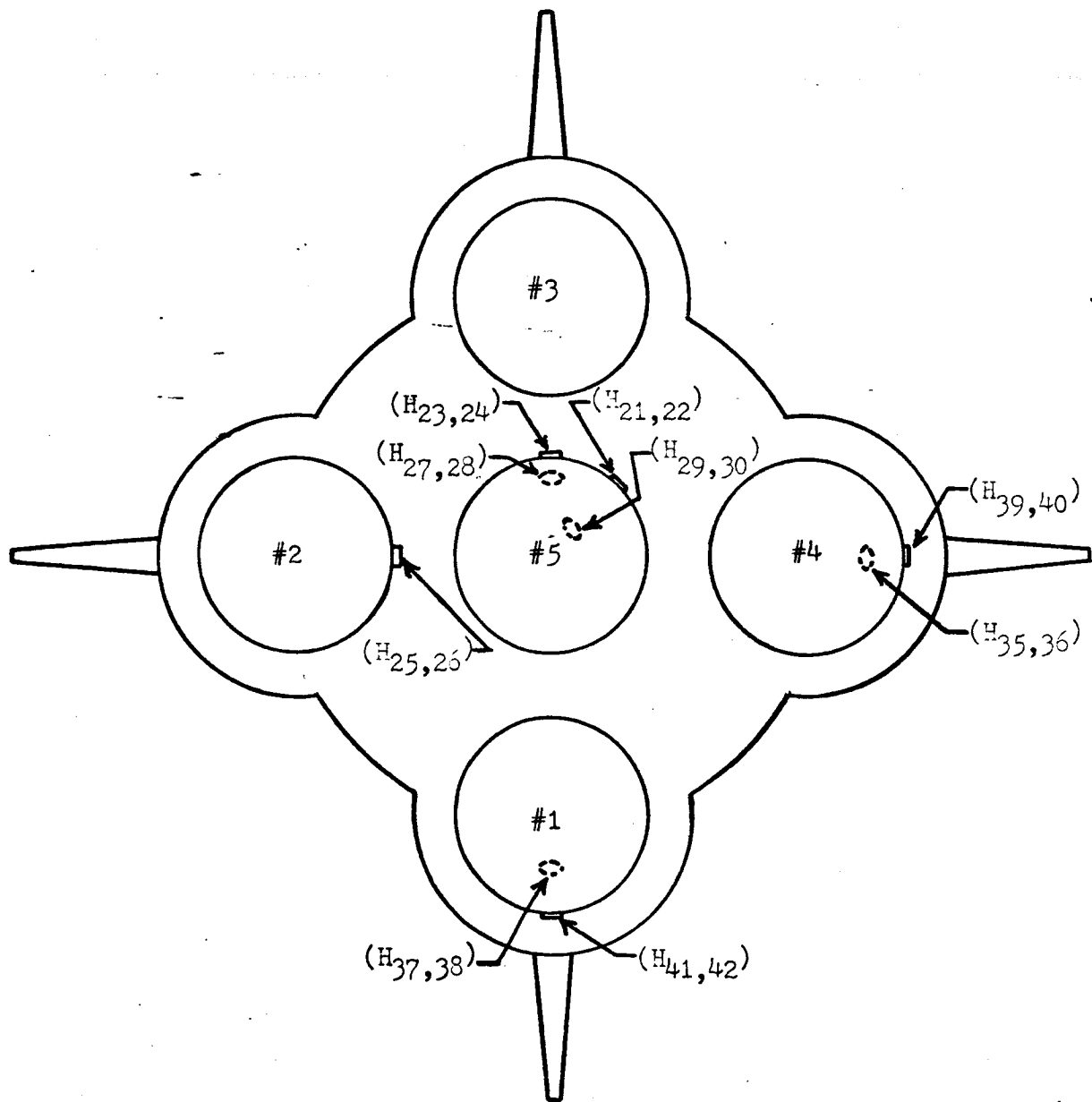


FIGURE 23 Engine Instrumentation (External)

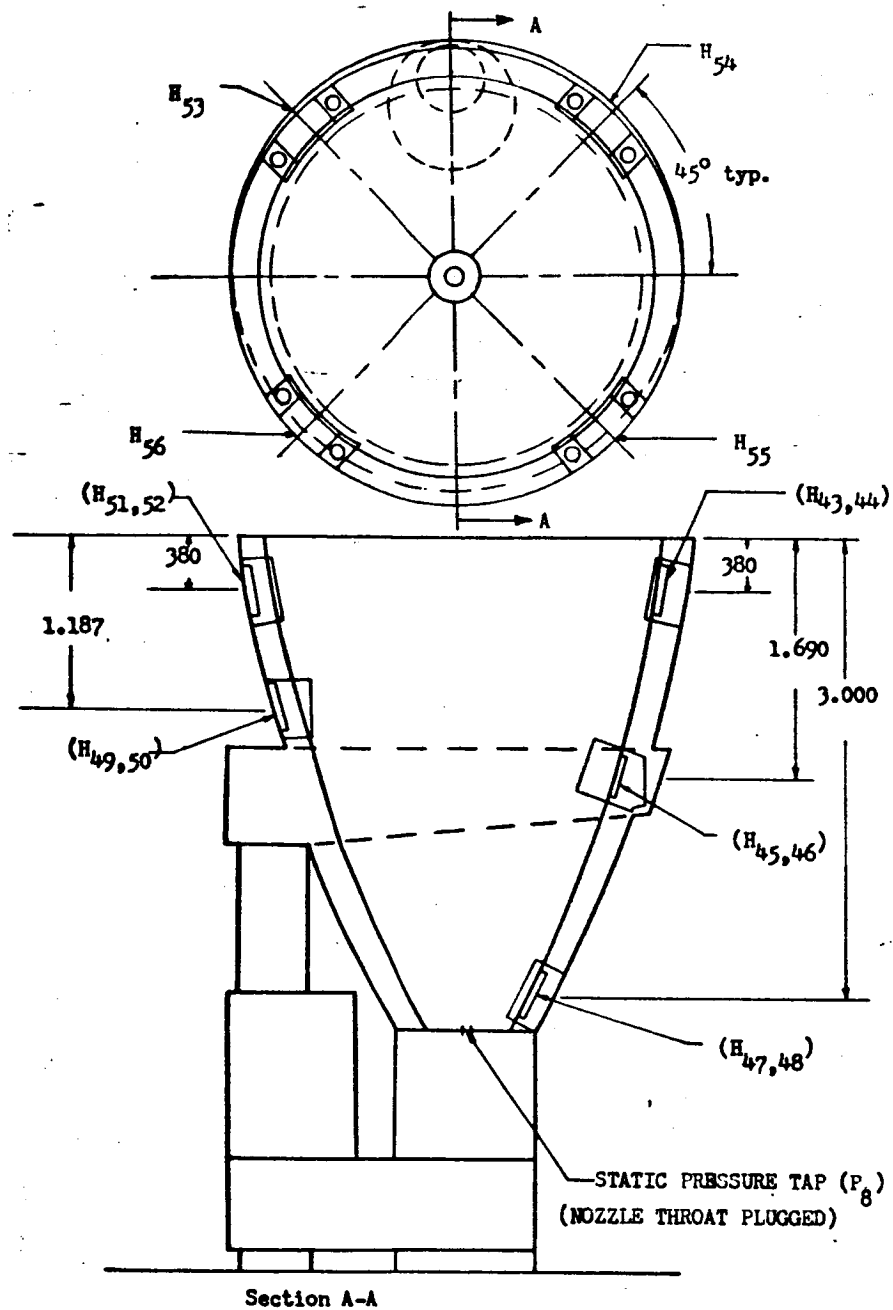


FIGURE 24 Engine Out Instrumentation - Internal

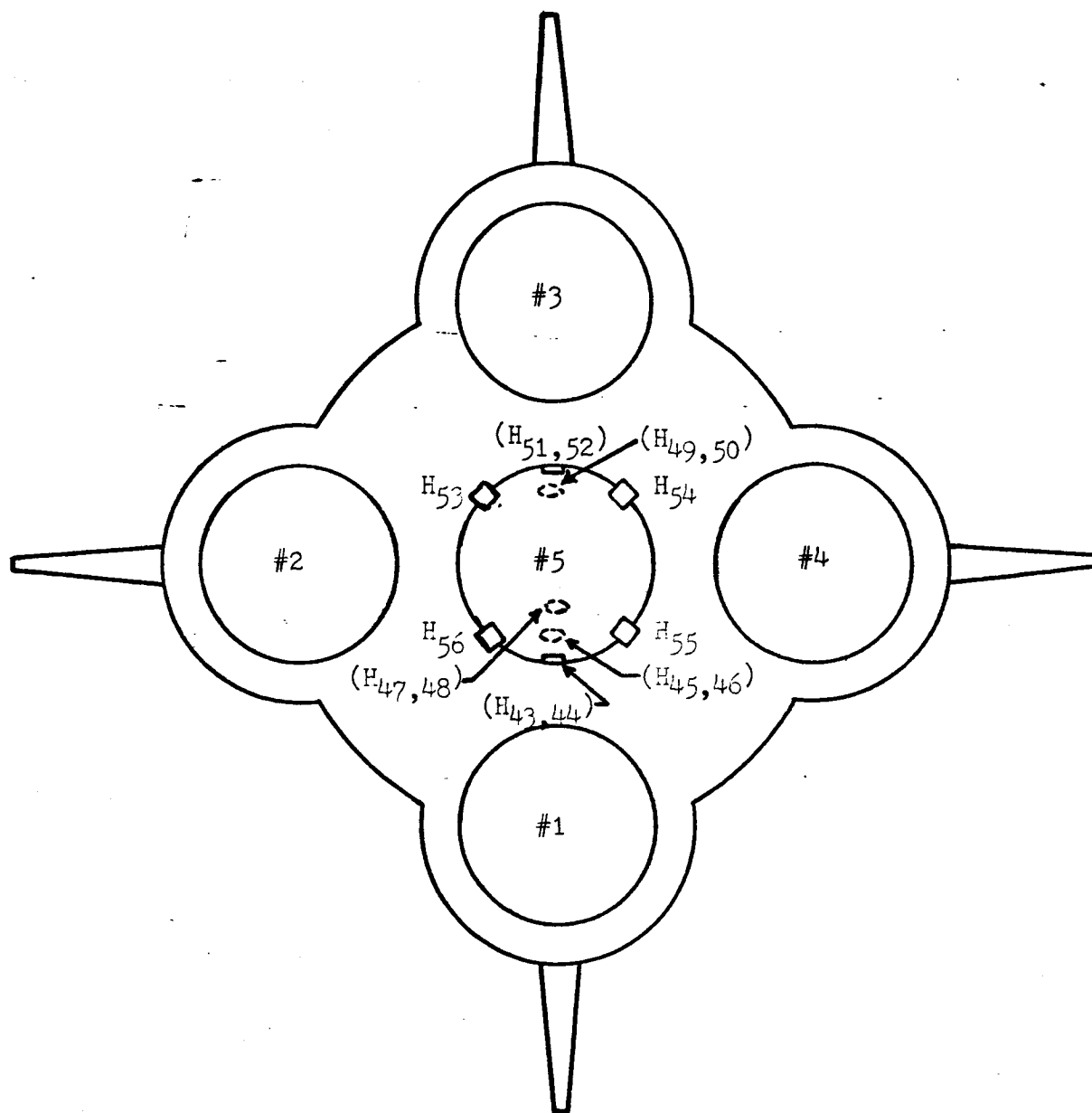


FIGURE 25 Engine Out Instrumentation - Internal

D5-15615

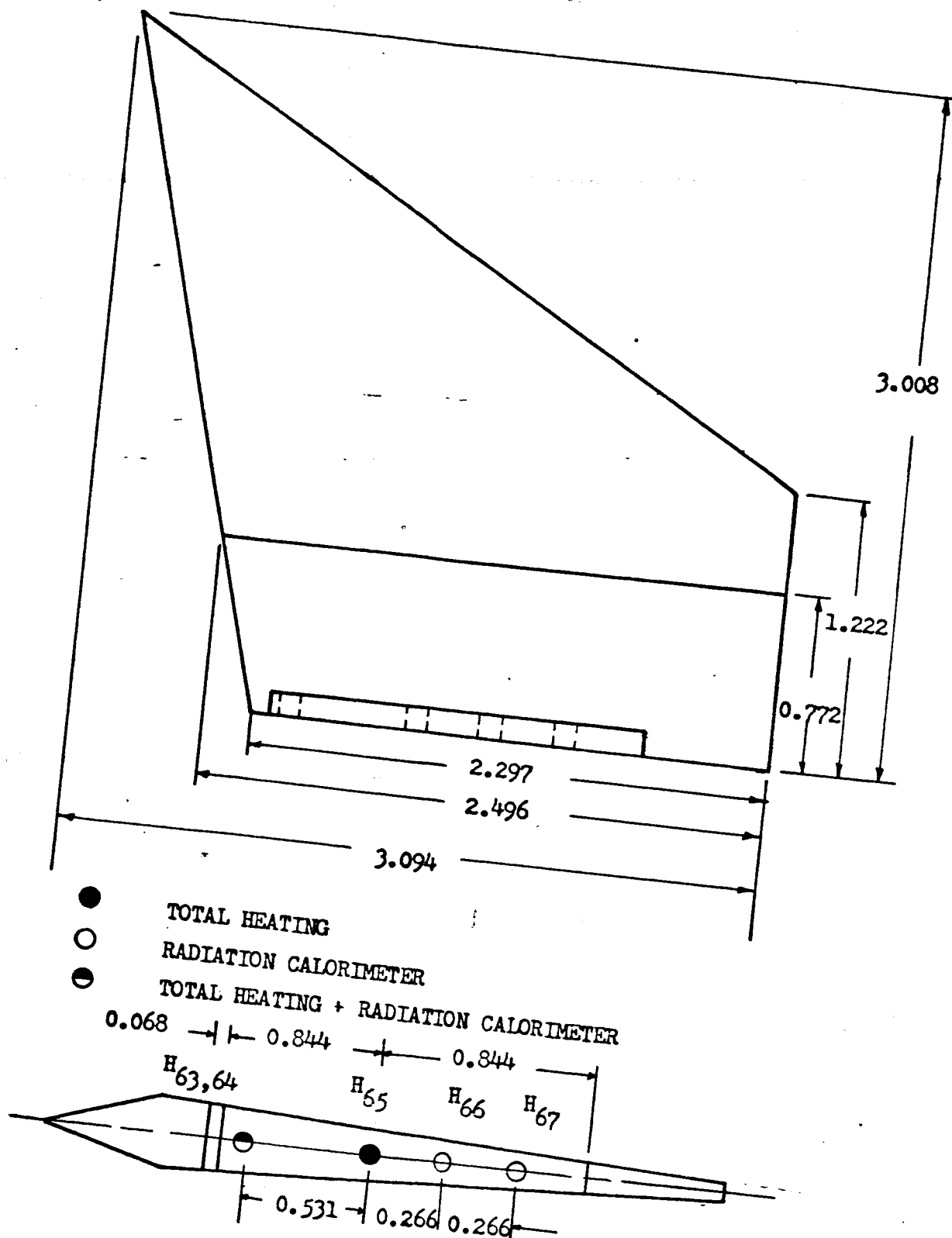


FIGURE 26 Fin Instrumentation

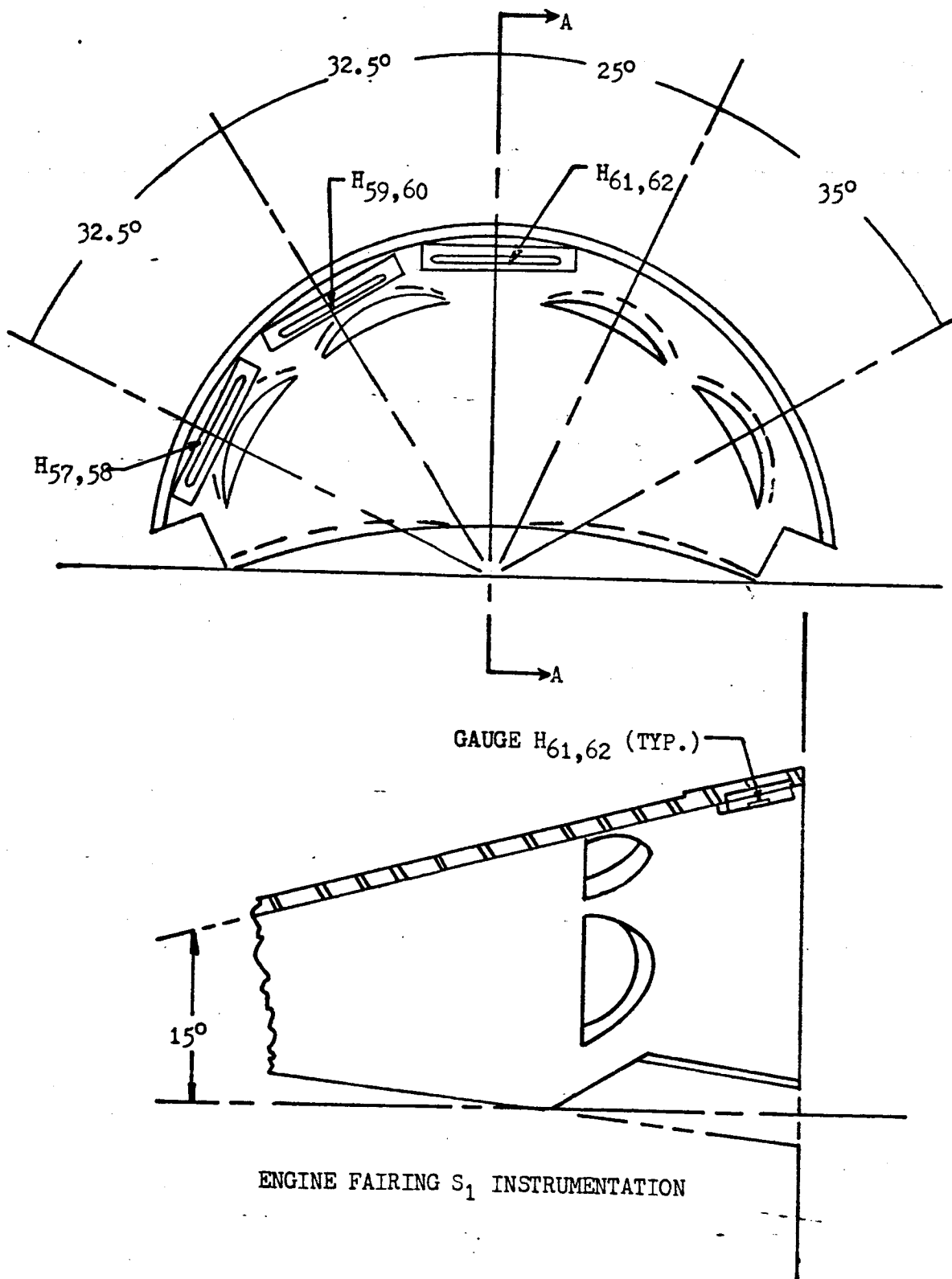


FIGURE 27 Engine Fairing Instrumentation

1.5.2 Heat Transfer

The thin-film gage is a resistance thermometer which reacts to the local surface temperature of the model. The theory of heat conduction in a homogeneous body is used to relate the surface temperature history to the rate of heat transfer: assuming that the temperature sensed by the element is the surface temperature and that a first order correction for element thickness will be adequate, the solution for the surface temperature as a function of time is:

$$\bar{T}(t) = \frac{1}{\sqrt{\pi c_2 \rho_2 k_2}} \int_0^t \frac{\dot{q}(\lambda) d\lambda}{\sqrt{t-\lambda}} - \dot{q}(t) \frac{L}{k_1} \left(\frac{c_1 \rho_1 k_1}{c_2 \rho_2 k_2} - 1 \right)$$

where k is thermal conductivity, c the specific heat, ρ the density, and L the film thickness; λ is a variable of integration; and subscripts 1 and 2 refer to the metal film and the pyrex substrate, respectively.

When the above equation is properly inverted to express the heat transfer rate as a function of temperature and time, it can be programmed into a digital computer for solution. However, considerable effort is involved in converting the raw temperature-time data into a form suitable for insertion into the computer program. To overcome this restriction, an analog network, referred to as a "q-meter", has been developed at CAL to convert the temperature signal directly into a heat flux in real time for presentation on the oscilloscope. All heat-transfer data for this study are obtained directly through the use of q-meters.

Three corrections must be applied to the recorded analog data to obtain a true heat transfer rate. These corrections are applied to the gage sensitivity factor K , the gage resistance R_g and the value of $(\rho ck)^{\frac{1}{2}}$. The corrections account for the fact that the gage temperature is actually at some value other than the temperature for which the calibration value of the dummy load resistor had originally been determined. The corrected values of K , R_g , and $(\rho ck)^{\frac{1}{2}}$ are used to determine the actual value of the calibration signal. Detailed discussion of the nature and application of the correction is presented in Reference 7.

SECTION 2 - OVERALL ANALYSIS

2.0 INTRODUCTION

This section contains the overall analysis of the Saturn S-IC Model Base Heating Test Program (X - 8). It contains a composite of significant data obtained in the Cornell 8 by 8 Foot Transonic Wind Tunnel, Lewis 8 by 6 Foot Transonic Wind Tunnel, Lewis 10 by 10 Foot Supersonic Wind Tunnel, and the Cornell High Altitude Chamber. Data from these tests are reported in References 9 through 12. See Sections 3, 4, 5 and 6 for detailed analyses of the individual tests.

Considerable development of the short-duration technique occurred during the test program. Non-symmetrical exhaust was noted in the first tests in the Cornell Transonic Tunnel. CAL revised the mixer plate and testing was resumed in the CAL high-altitude facility. Flow symmetry from the nozzles continued unsatisfactory, and the means for measuring the oxygen-to-fuel (O/F) ratio was believed to be unreliable.

Prior to tests in the Lewis Research Laboratory 10-by 10-foot supersonic tunnel, the combustor was redesigned and a splash plate was introduced. Results from this series of tests indicate that the radiation and convection was considerably lower than estimated. Data repeatability was poor and motion pictures indicated continued combustion instability.

Before testing in the Lewis transonic tunnel extensive tests were run at CAL and some combustor redesign was accomplished. The instabilities of the previous test were traced to liquifaction of the ethylene. Preheating the ethylene eliminated the problem.

Configuration changes have also occurred during the two years in which tests have been conducted. Consequently, the configurations tested in one facility may be inconsistent with those of another facility. For example, during two tests (CAL Altitude Chamber and LRC 10 by 10), two gimbal patterns were run. These represented extreme cases; outboard engines gimballed as far as they physically could toward each other and toward the center engine. Before the LRC 8 by 6 test was conducted a nominal prototype gimbal pattern was established. Because of time limitations, this was the only gimbal pattern tested in the LRC 8 by 6 tunnel. Therefore, the plots in this section showing the effects of gimbaling do not have the same gimbal pattern for the entire altitude range.

2.0 (Continued)

Table I indicates that the altitude range covered in the CAL 8 by 8 foot tunnel and the Lewis 8 by 6 foot tunnel are the same even though the Mach range is different. This occurs because the Lewis tunnel cannot be operated on the trajectory altitude at a given Mach number. As a result a multiplicity of data points between altitudes of 10,000 and 35,000 feet are shown on some of the charts. A flag is placed on the symbols to designate that data which was obtained from the Lewis 8 by 6 foot tunnel:

Although the data are generally not compatible in magnitude the trends are generally similar and the data is useful in defining design criteria.

The following discussion relates geometry changes and the effect of hydrogen turbine exhaust injection over the range from 0 to 200,000 feet. Hydrogen is used to simulate turbine exhaust. Effect of using ethylene is discussed in Volume II Section 4.

2.1 BOUNDARY LAYER

The boundary layer thickness is dependent on the flow condition and can be estimated for a flat plate using well established theoretical equations. For laminar flow an equation after T. Von Karman may be used.

$$\frac{\delta}{x} = \frac{4.65}{(\text{Re}_x)^{\frac{1}{2}}}$$

Equation 1

where: δ = Boundary layer thickness
 x = Distance from the leading edge
 Re_x = Reynolds number (based on x)

For turbulent flow the equation is

$$\frac{\delta}{x} = \frac{3.77}{(\text{Re}_x)^{1/5}}$$

Equation 2

Although the equations are approximate and do not account for variations due to the model geometry they are adequate to determine the type of flow which occurs at the rear of the models for comparison with boundary layer data.

2.1 (Continued)

Boundary layer measurements are obtained in the three wind tunnels by the total pressure rakes illustrated in Figures 15 and 16. Actual total pressure in the boundary layer is determined by correcting the probe readings for the normal shock that stands in front of the rake. The boundary layer edge is defined as the point at which 0.998 of the free-stream velocity is reached. In all three tunnels, the measured boundary layer thickness coincides with the turbulent flow estimate. (See Figure 28.)

2.2 RADIATION

The source of radiation heating is the engine exhaust. On the prototype secondary radiation effects will occur from the heat shield and other heated components in the base region. Secondary radiation will not occur on the X-11 model tests since the extremely short burn times eliminate high structural temperatures.

Although the combustion characteristics and geometry of the prototype are essentially duplicated in the model tests, radiation heating rate simulation is unlikely for the following reasons:

- a) Model engine wall temperatures remain relatively cold and will tend to reduce the exhaust temperature.
- b) Free stream and engine exhaust mixing will not coincide between model and prototype due to size difference which may effect the onset of afterburning.
- c) Emissivity from carbon particles is related to the thickness of the gaseous medium. Since the model engines produce a relatively thin exhaust envelope, the emissivity may be considerably less than emissivity from the prototype.
- e) Turbine exhaust is simulated with hydrogen which will not produce the same emissivity as the very fuel rich prototype turbine exhaust.

The trends and relative configuration effects shown by the radiation test data are representative of the S-IC prototype. However, the data magnitude is believed low.

D5-15615

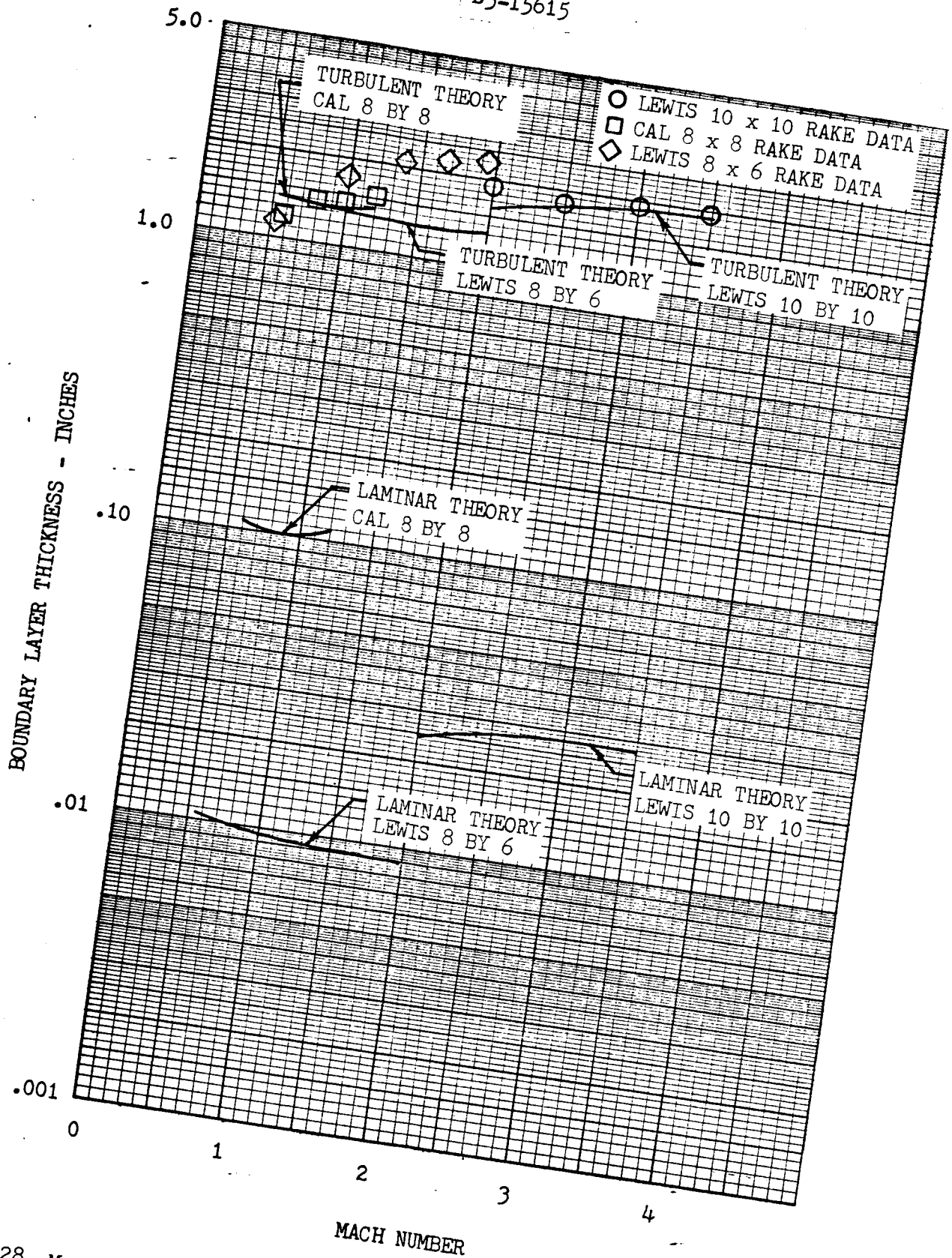


FIGURE 28 Model Boundary Layer Thickness Versus Theory

2.2.1 Radiation to Base

The effects of injecting turbine exhaust and varying the model configurations are shown in Figures 29 through 33. The data are average values for the five heating gages located on a ray between engines 3 and 4. (See Figure 19.) A dotted line is shown which is based on the radiation drop off from Saturn I Block II flight data. The curve was drawn by arbitrarily assuming a radiation heating rate of $1.0 \text{ BTU/FT}^2\text{SEC}$ at the 195,000 foot altitude, and is provided as a reference point.

All data from the Lewis 10-by 10-foot tunnel (50,000 to 100,000 feet) appear lower than data from other facilities. This is believed due to improper combustion.

There is no significant effect on radiation heating rates due to configuration changes or the addition of hydrogen turbine exhaust above 35,000 feet.

Below 35,000 feet data from the Lewis 8 by 6 tests are consistently 1.0 to $1.5 \text{ BTU/FT}^2\text{SEC}$ lower than equivalent data obtained from the CAL 8 by 8 tests. This is due to combustion variations and the off trajectory conditions in the Lewis 8 by 6 tunnel. This fact must be considered in making comparisons. However, the drop-off rate with altitude from both sets of data correlate well with the Saturn I Block II data. Addition of scoops and deflectors produce conflicting data, i.e., an increase in heating rate in the CAL 8 by 8 and a reduction in the Lewis 8 by 6. Operating with the center engine out or with the engines gimbaled appears to reduce the heating rate below 35,000 feet. Addition of hydrogen turbine exhaust has no consistent effect on the base radiation data.

2.2.2 Radiation to Fin

Instruments are located at four places on the aft face of the fin as shown in Figure 26. However, gage H64, located near the fin/fairing interface, is the only fin radiation gage which operated throughout the test series. Data shown in Figure 34 indicate that radiation to this gage is about 30 percent lower than average radiation to the base below 35,000 feet. The drop-off trend with increasing altitude is in line with Saturn I flight data.

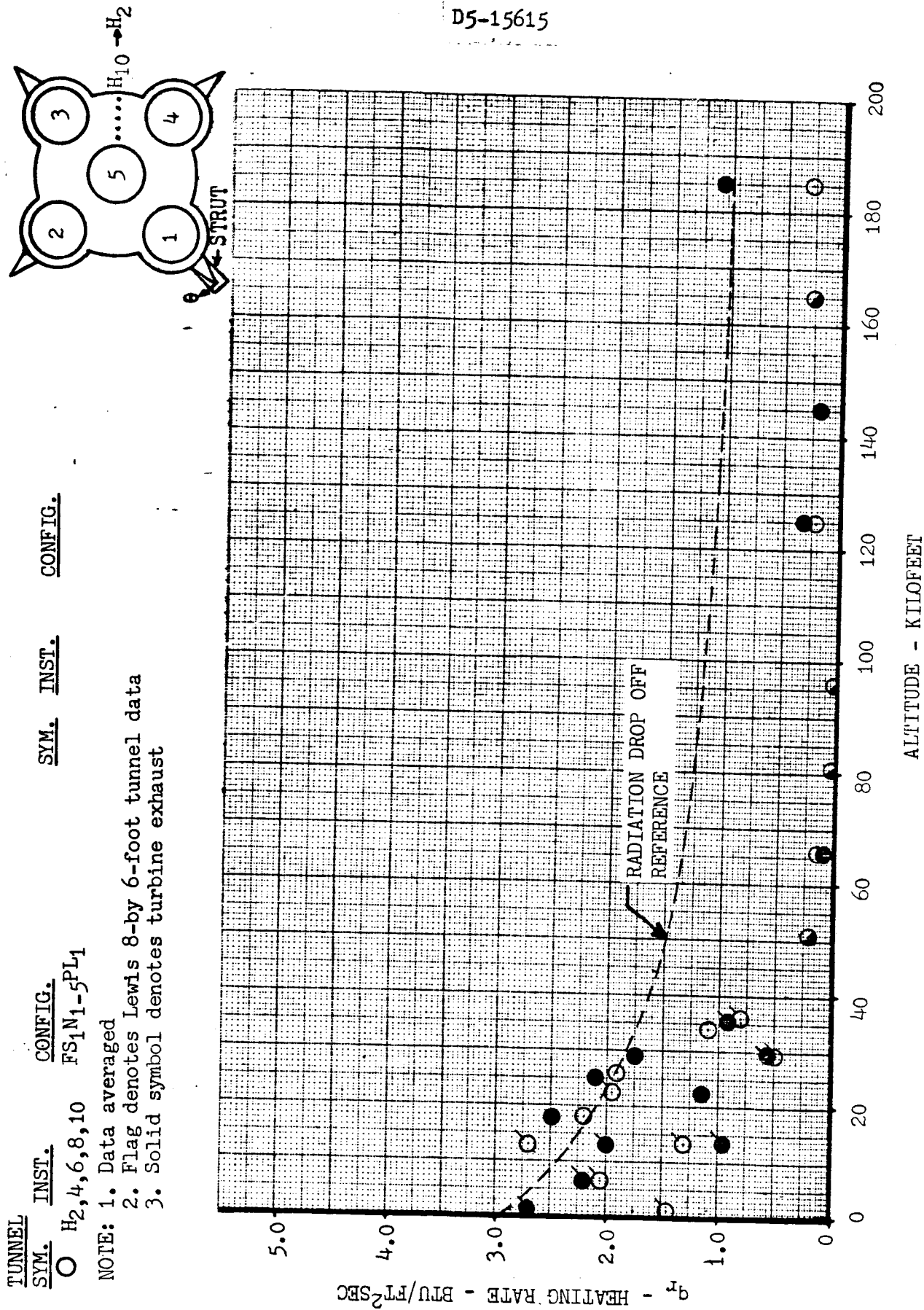
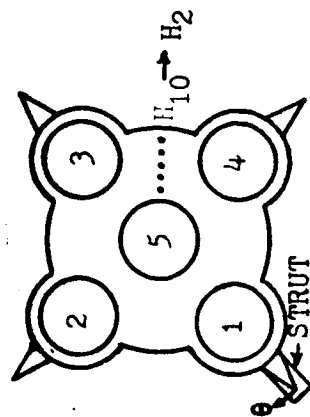


FIGURE 29 Base Heating - Radiation



TUNNEL SYM.	INST.	CONFIG.
○	H ₂ , 4, 6, 8, 10	FS ₁ N ₁₋₅ PL ₁
△	H ₂ , 4, 6, 8, 10	FS ₁ D ₁ SC ₁ N ₁₋₅ PL ₁
△	H ₂ , 4, 6, 8, 10	FS ₁ D ₁ SC ₂ N ₁₋₅ PL ₁

NOTE: 1. Data averaged
2. Flag denotes Lewis 8-by 6-foot tunnel data

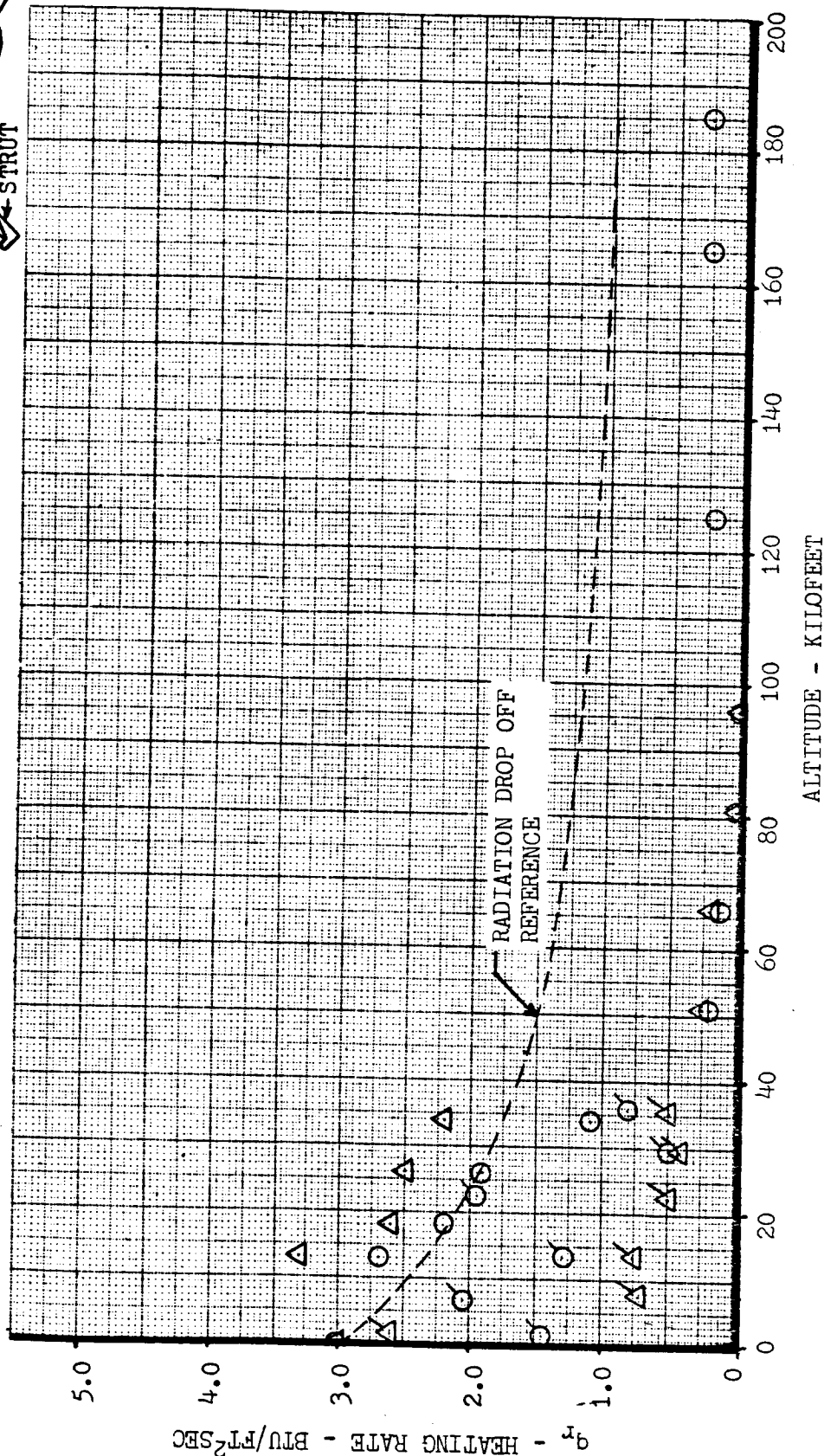
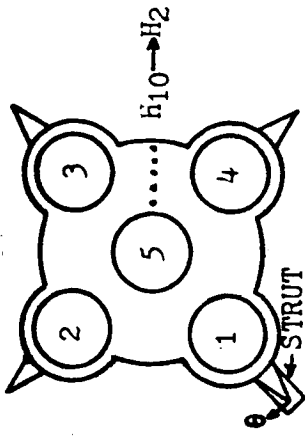


FIGURE 30 Base Heating - Radiation



TUNNEL	SYM.	INST.	CONFIG.	SYM.	INST.	CONFIG.
	○	H ₂ , 4, 6, 8, 10	FS ₁ N ₁ -5PL ₁			
	□	H ₂ , 4, 6, 8, 10	FS ₄ N ₁ -5PL ₁			

NOTE: 1. Data averaged
2. Flag denotes Lewis 8-by 6-foot tunnel data

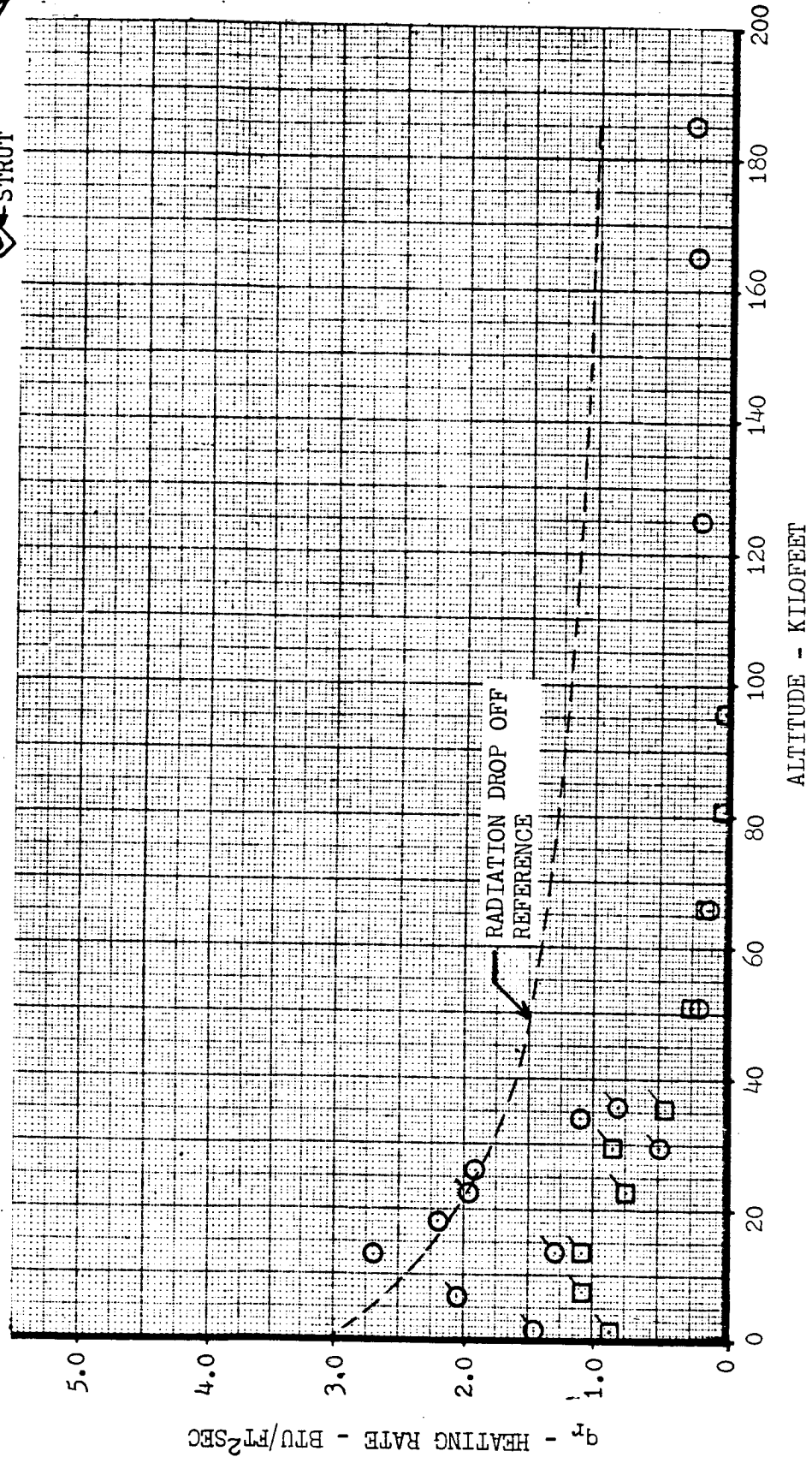
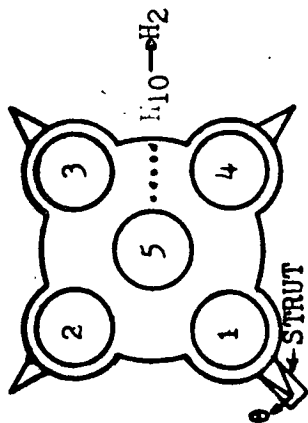


FIGURE 31 Base Heating - Radiation



TUNNEL SYM.	INST.	CONFIG.
○	H ₂ , 4, 6, 8, 10	FS ₁ N ₁ -5PL ₁
◇	H ₂ , 4, 6, 8, 10	FS ₁ N ₇ PL ₁

SYM. INST. CONFIG.

NOTE: 1. Data averaged
2. Flag denotes Lewis 8-by 6-foot tunnel data

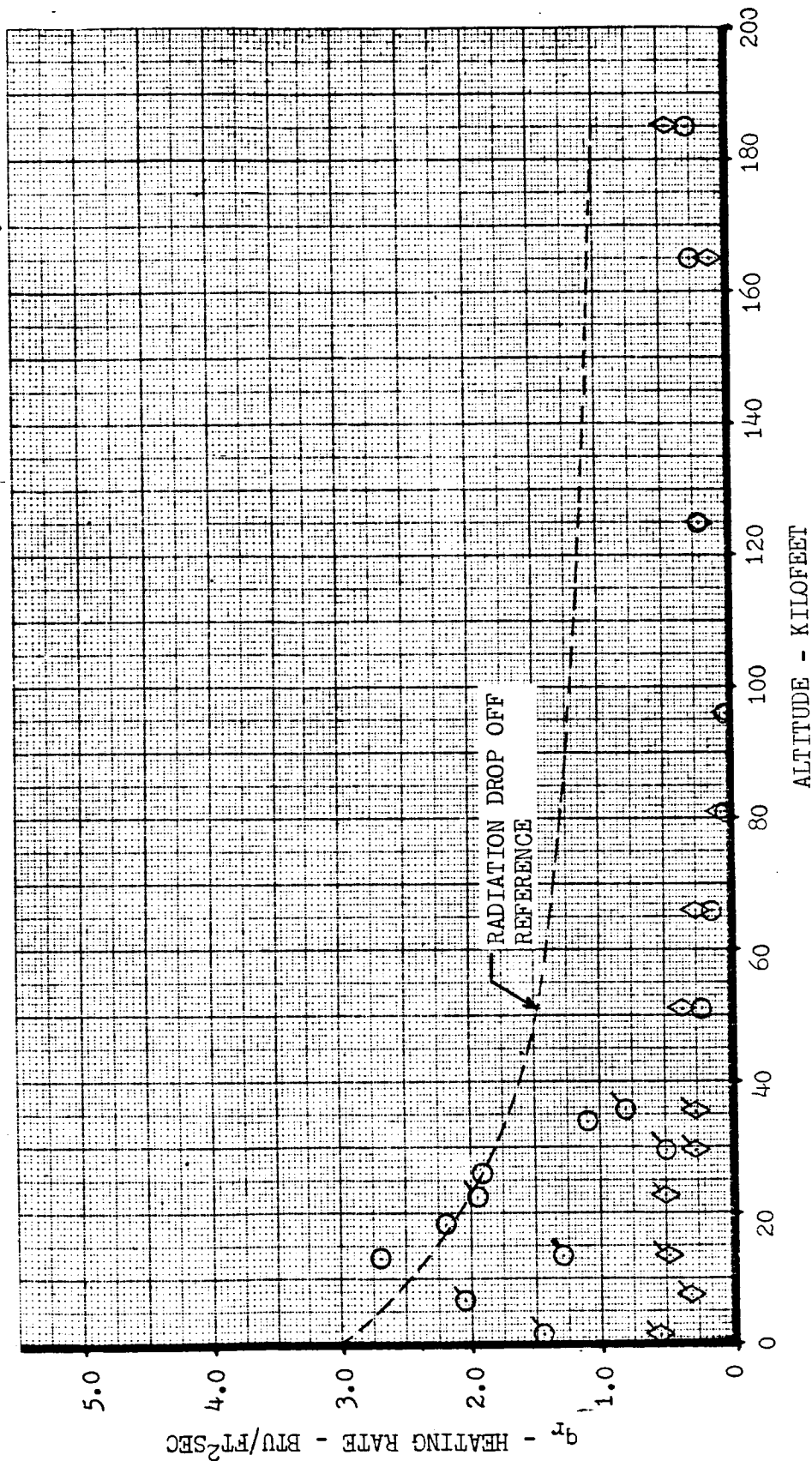
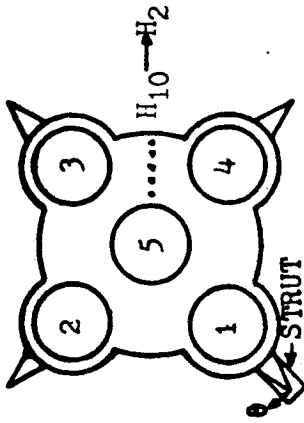


FIGURE 32 Base Heating - Radiation



TUNNEL SYM.	INST.	CONFIG.	SYM.	INST.	CONFIG.
○	H2, 4, 6, 8, 10	FS1N1-5PL1	◇	H2, 4, 6, 8, 10	FS1NG3NG6PL1
◊	H2, 4, 6, 8, 10	FS1D2NG7NG8PL1	◊	H2, 4, 6, 8, 10	FS1NG5NG6PL1

NOTE: 1. Data averaged
2. Flag denotes Lewis 8-by 6-foot tunnel data

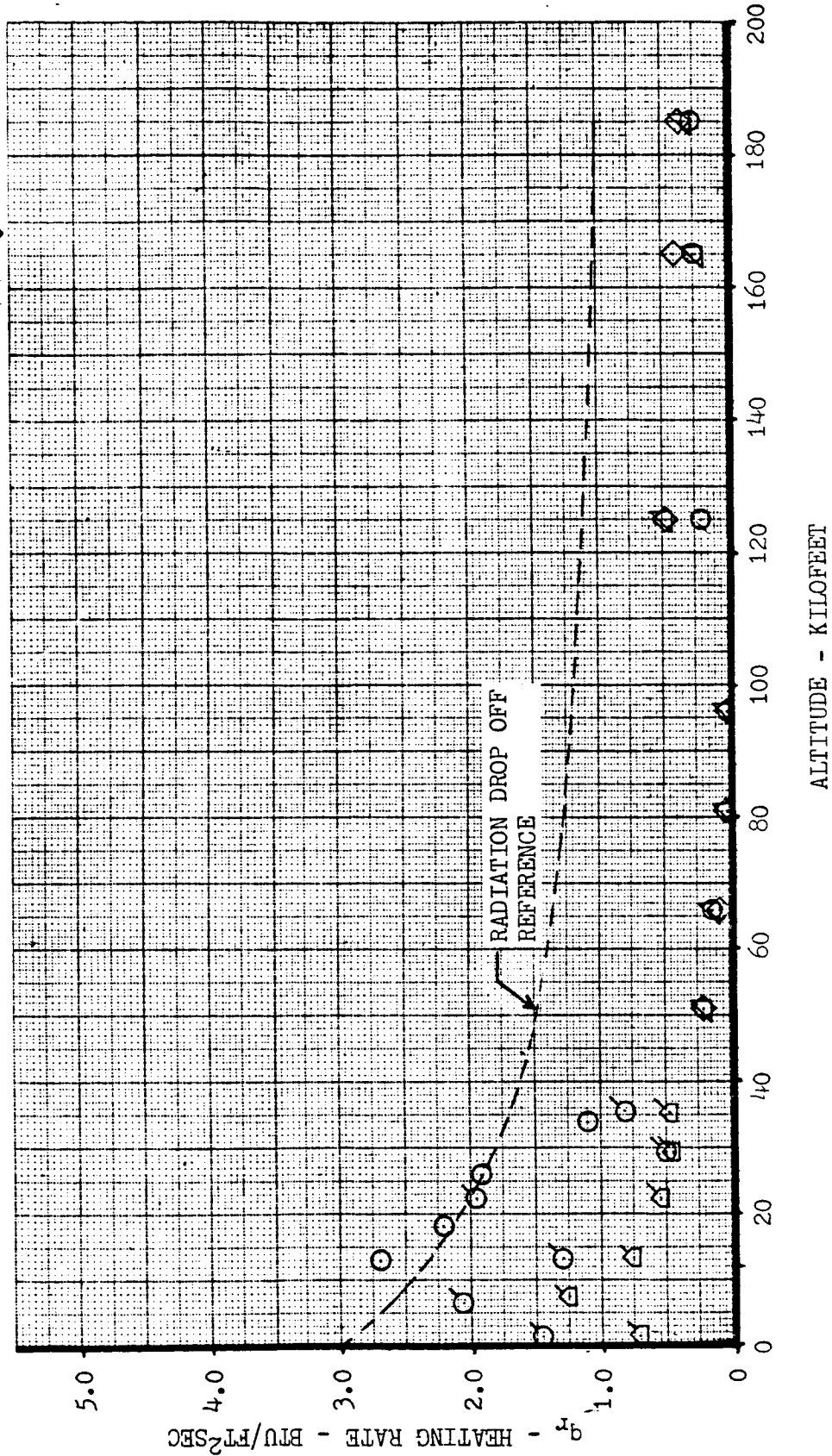
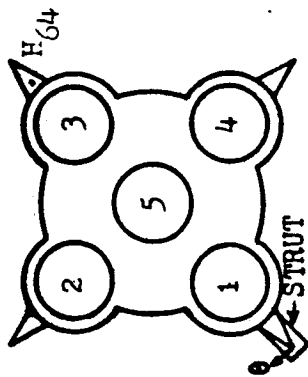


FIGURE 33 Base Heating - Radiation



TUNNEL SYM.	INST.	CONFIG.	SYM.	INST.	CONFIG.
○	H ₆₄	FS ₁ N ₁₋₅ PL ₁			
◻	H ₆₄	FS ₁ D ₂ N ₁₋₅ PL ₁			

NOTE: 1. Flag denotes Lewis 8-by 6-foot tunnel data
2. Solid symbol denotes turbine exhaust

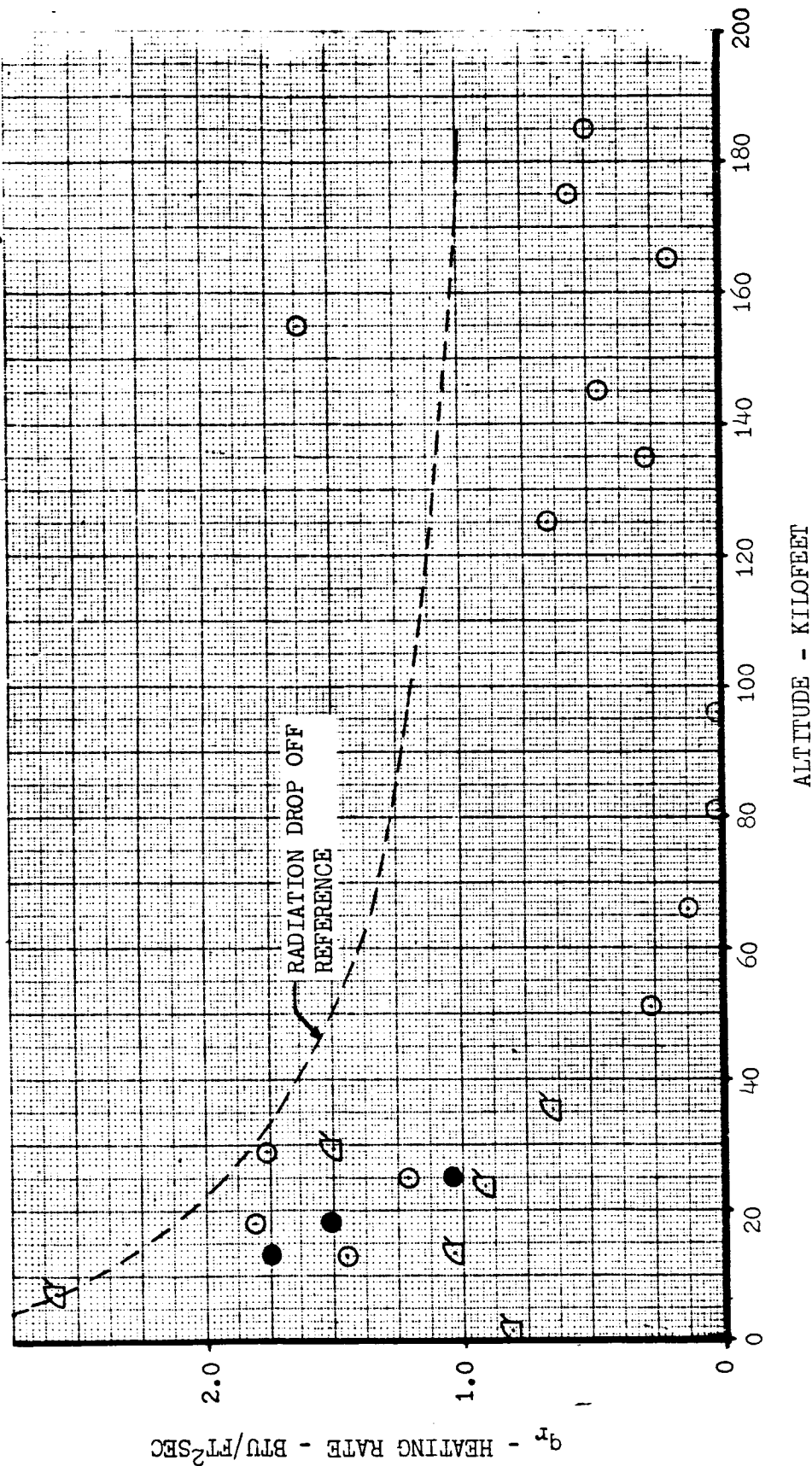


FIGURE 34 Fin Heating - Radiation

2.2.3 Radiation to Engine Fairing

Radiation gages are located on the inside surface of the fairing near the trailing edge facing the engine centerline. (See Figure 27.) Radiation to the inside fairing surface is approximately half that to the base which is in line with theory since the view factor to the near engine is negligible. (See Figure 35.)

2.2.4 Radiation to Engine (External)

Radiation gages are located on the external surfaces of the engines as shown in Figure 22 and 23. These gages suffered a high failure rate and consistent data are available only from gage H₂₂ which is located near the nozzle lip facing outboard normal to the engine centerline between engines 3 and 4. Data available, shown in Figure 36, indicate that radiation heating to the external surface of the engines is low and comparable to radiation to the fin. Radiation to other parts of the external engine nozzle surface will be even less severe.

2.2.5 Radiation to Engine (Engine Out - Internal)

An engine is plugged and instrumented to determine heating rates to an inoperative engine. (See Figures 24 and 25.) The same engine is used for center engine out and for outside engine out investigations. The configurations were tested only in the Lewis facilities and the CAL altitude chamber. Instruments are located on the nozzle lip (H_{54,56}) looking aft, and on the internal nozzle surfaces facing the nozzle centerline. Data shown in Figure 37 are for the lip only. Radiation to the inside of the nozzle does not exceed 0.70 BTU/FT²SEC for the center engine, and are under 1.0 BTU/FT²SEC for the outside engine except at 1600 feet altitude. Details of radiation to the inside of the engine are shown in Volume II of this document.

2.2.6 Comparison with Radiation Theory

Radiation from the engine exhausts is described by the equation

$$q = \sigma \epsilon F T^4$$

where: q = Heating rate
 σ = Steffan Boltzman constant
 ϵ = Emissivity
 F = Shape factor of the plume as seen from the point of calculation
 T = Temperature of the plume.

To obtain accurate results from this equation the exhaust plume shape, emissivity and temperature must be accurately known. Since these parameters are not known assumptions are made which allow the answers to be bounded.

TUNNEL SYM.	INST.	CONFIG.	SYM.	INST.	CONFIG.
○	H ₅₈	FS ₁ N ₁₋₅ PL ₁	Δ	H ₅₈	FS ₁ SC ₂ D ₃ N ₁₋₅ PL ₁
◻	H ₆₀	FS ₁ D ₂ N ₁₋₅ PL ₁			

NOTE: 1. Flag denotes Lewis 8-by 6-foot tunnel data
2. Solid symbol denotes turbine exhaust

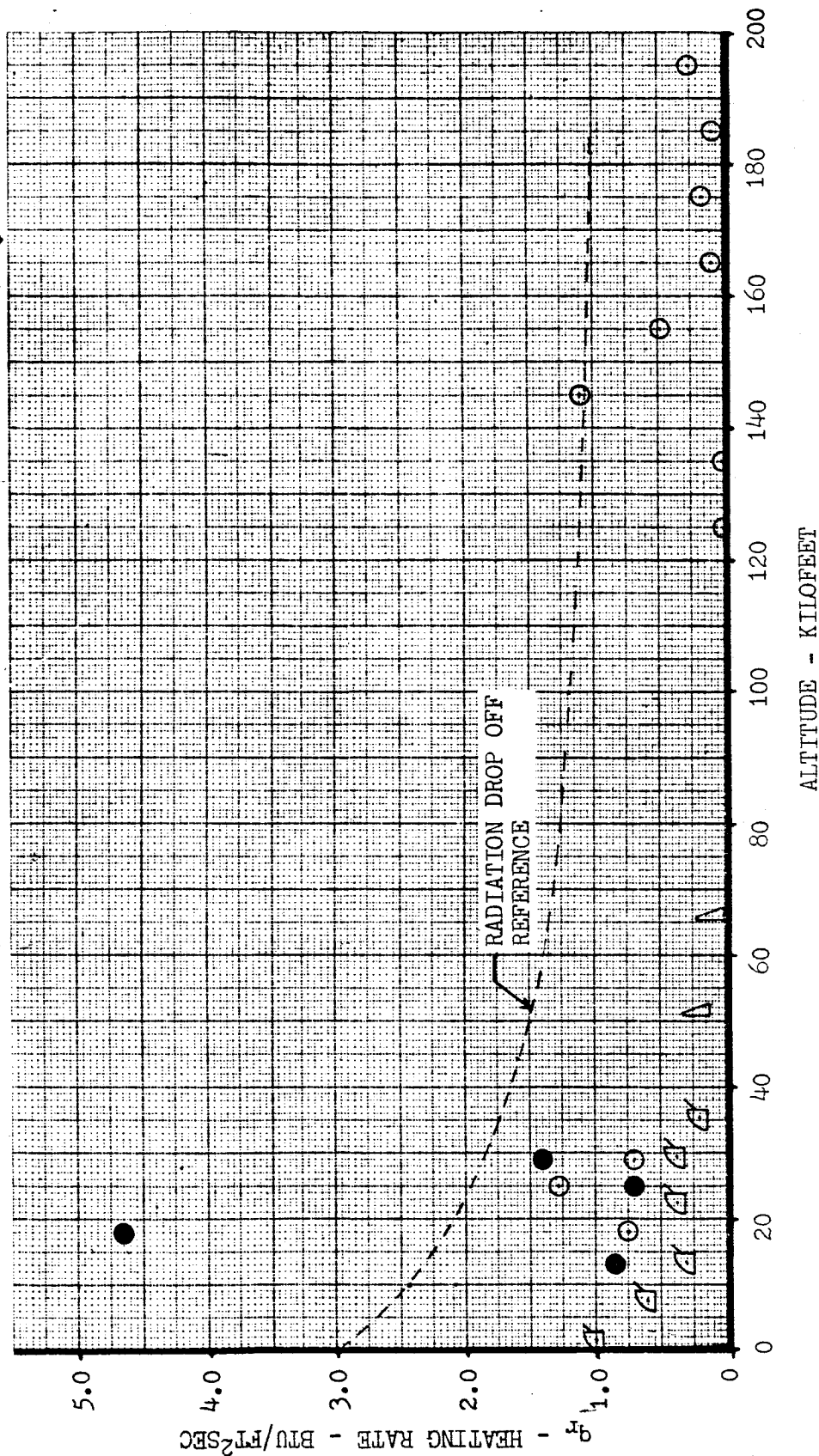
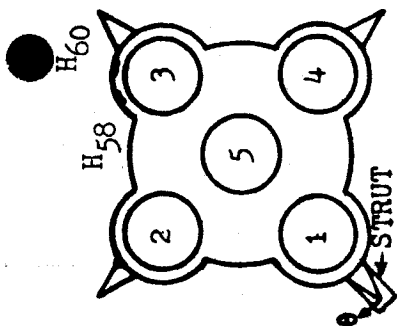


FIGURE 35 Engine Fairing Heating - Radiation

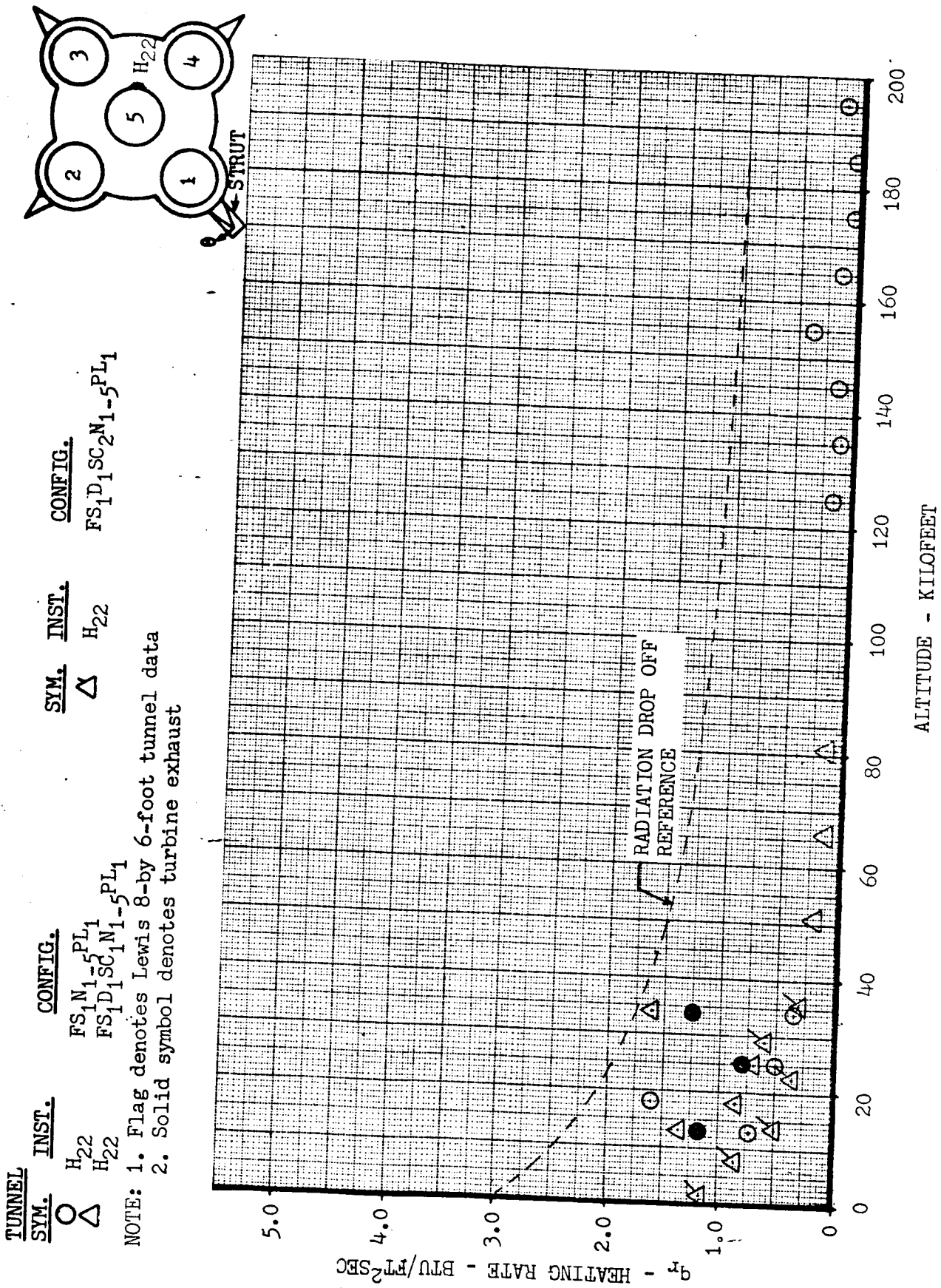
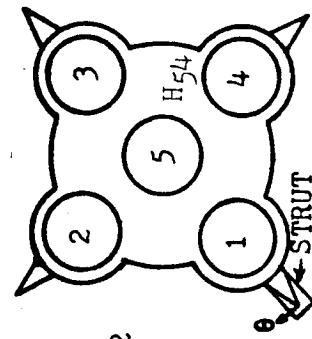


FIGURE 36 Engine Heating - Radiation (External)



TUNNEL SYM.	INST.	CONFIG.	SYM.	INST.	CONFIG.
○	H ₅₄	B ₁ FS ₁ N ₇ PL ₁	◇	H ₅₄	B ₄ FS ₁ D ₂ N ₁₀ G ₁₁ N ₆ N ₁₂ PL ₂
○	H ₅₄	B ₄ FS ₁ D ₂ N ₇ PL ₁			

NOTE: Flag denotes Lewis 8-by 6-foot tunnel data

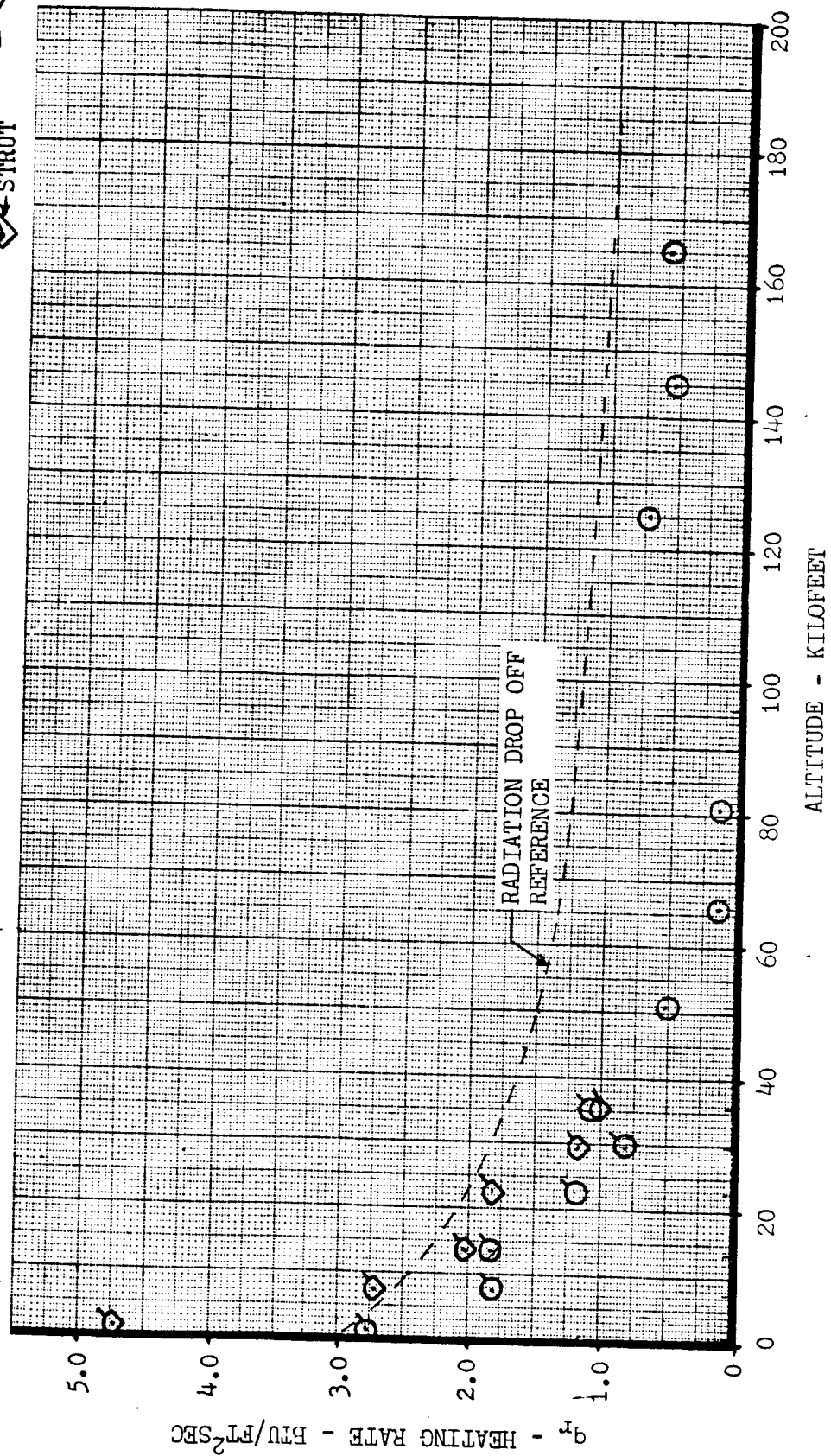


FIGURE 37 Engine Heating - Radiation (Engine Out)

2.2.6 (Continued)

A lower limit is determined by assuming radiation from hot non-luminous gases only. The theoretical predicted upper limit is determined by assuming an emissivity of 1.0 at sea level and reducing radiation at altitudes using the flight data from Saturn I Block II. Other assumptions and the calculation procedures are described in Appendix A.

Figure 38 compares the model data with the upper and lower limits described above, based on the model plume shown in Appendix A. The data shown are the highest average base heating values recorded for any of the configurations at any given altitude. Data in the CAL 8 by 8 tunnel approximates the upper theoretical prediction while the Lewis 10 by 10 data closely matches non-luminous hot gas theory.

2.3 CONVECTION

The flow field in the base region of the S-IC model is created by the interactions of the free stream flowing over the edge of the base, the free stream gases entering the base region through flow deflectors and engine fairing scoops, free stream impinging on the engine exhaust, and the impingement of engine plumes on each other.

The free stream flowing over the edge of the base, including the engine fairing, has the effect of creating a low pressure across the base without the nozzle flow. Magnitude of the pressure is generally expected to decrease with Mach number due to the momentum of the flow. Addition of deflectors and scoops will allow injection of mass into the base which will increase the base pressure. Addition of engine exhaust to the system has a variable effect dependent on altitude.

Impingement of the free stream air on the plumes at low altitude may create a condition similar to plume/plume impingement wherein exhaust gases may be mixed with free stream air and recirculated into the base region. Should this condition exist, combustion will occur and cause the condition occasionally noted on model and prototype tests known as "base burning." Base burning is largely alleviated by the use of flow deflectors on the base.

At low altitudes the engines are overexpanded and the exhaust plumes are expected to approximate the size of the nozzle diameter. Mixing between the free stream and the plume across the shear layer may cause some growth and lead to afterburning. In this condition the exhausts act as ejectors and may cause a reduction in base pressure greater than the reduction due to free stream flow over the base. However as the altitude increases and the plumes expand and begin to impinge, part of the impinging flow is turned toward the base and eventually the base pressure will exceed the ambient.

Since convective heating is primarily dependent on flow velocity and recovery temperature the flow deflectors and scoops are expected to have the predominant effect at low altitudes. With an increase in altitude recirculating hot gases will become predominant.

- NOTE: 1. Data shown are the highest average base heating values obtained for any of the configurations at a given altitude.
 2. Flag denotes Lewis 8-by 6-foot tunnel data

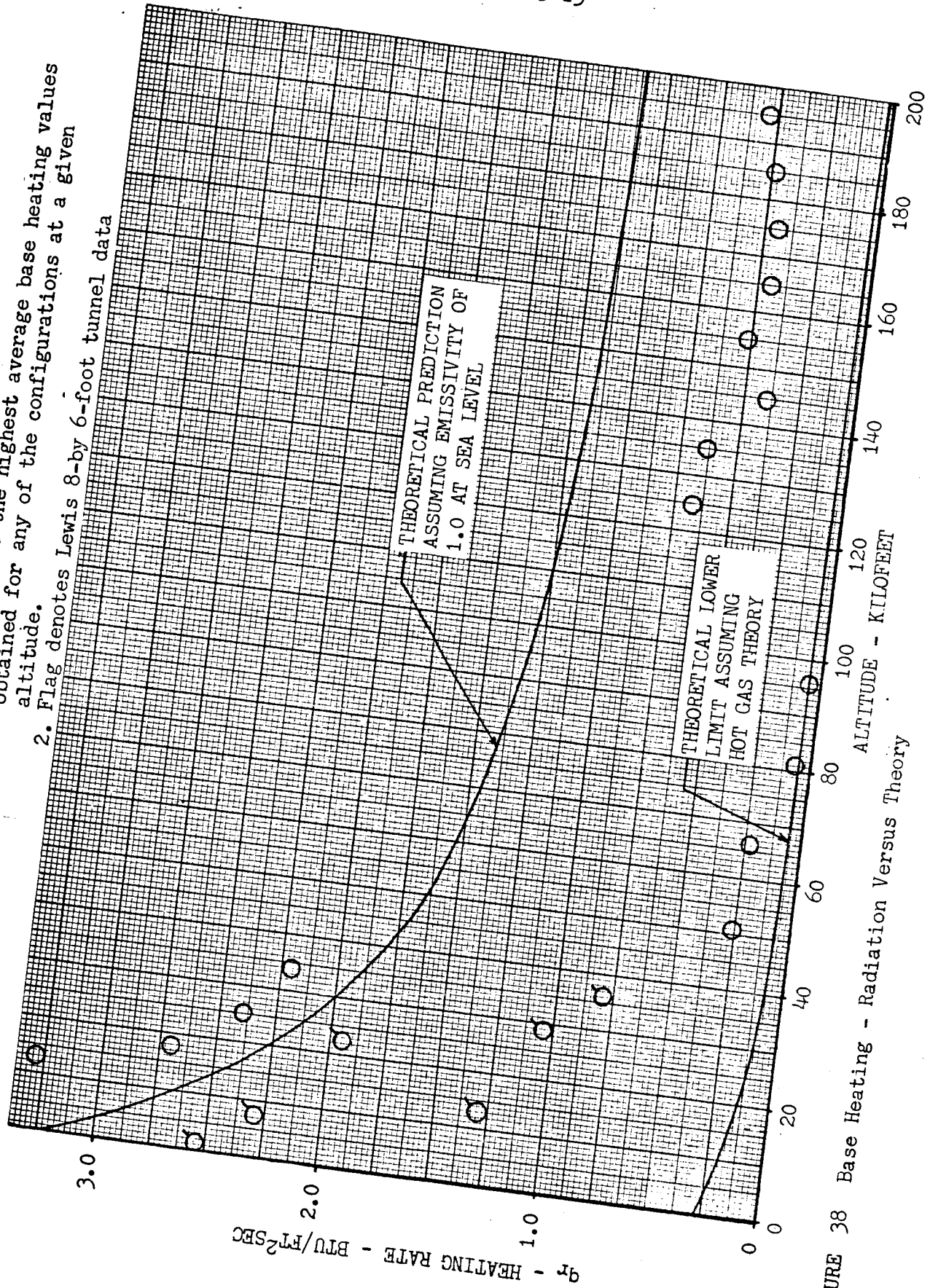


FIGURE 38 Base Heating - Radiation Versus Theory

2.3 (Continued)

With the above in mind many flow deflector and scoop combinations were tested in the CAL 8 by 8 facility. When testing began in the Lewis 10 by 10 facility heating rates were so low that the run schedule was adjusted to include primarily those configurations which would produce significant heating rates, i. e., configurations without scoops or deflectors and the gimbal patterns. Changes in prototype which eliminated the engine fairing scoops are reflected in the configurations tested in the Lewis 8 by 6 facility in that scoops were used in only one test series. The CAL high altitude tests were run in chambers without external flow and all convection is due to recirculation flow.

Model convective heating rate data are obtained by subtracting a measured radiative heating rate from a measured total heating rate. The Lewis 8 by 6 data are plotted according to trajectory altitude. Details of the instrumentation are available in paragraph 1.4.

2.3.1 Convection to Base

The effect of injecting hydrogen to simulate turbine exhaust is shown in Figures 39 and 40. Without scoops or deflectors there is a definite increase in the convective heating rate below 40,000 feet in both the CAL and Lewis facilities. With the addition of scoops and deflectors there is no difference between convection with or without turbine exhaust in the Lewis facility. However in the CAL facility it is noted that although the heating rate is diminished with addition of scoops and deflectors it is still significantly higher than the heating rate without turbine exhaust up to 40,000 feet.

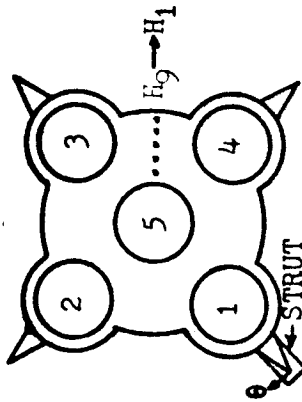
This difference at the low altitudes may be caused by one or both of the following reasons:

- a) A greater mass of scavenging air is forced into the base in the Lewis tunnel since the density of the free stream is higher at a given Mach number.
- b) The advent of turbine exhaust commences prior to engine ignition in the CAL tests.

Above 40,000 feet injection of hydrogen appears to reduce heating indicating that no burning is taking place.

Figure 41 shows a considerable reduction in convection heating with addition of scoops and deflectors, without turbine exhaust, again demonstrating the purging effect of flow over the base.

Data shown on Figures 40 and 41 obtained from the Lewis-10 by 10 (Mach 3.5 at 150,000 feet) indicate that base convection data obtained in an altitude chamber may be conservative.



TUNNEL
SYM. INST. CONFIG.

H₁, 3, 5, 7, 9 FS₁N₁-5PL₁

NOTE: 1. Data averaged
2. Flag denotes Lewis 8-by 6-foot tunnel data
3. Solid symbol denotes turbine exhaust

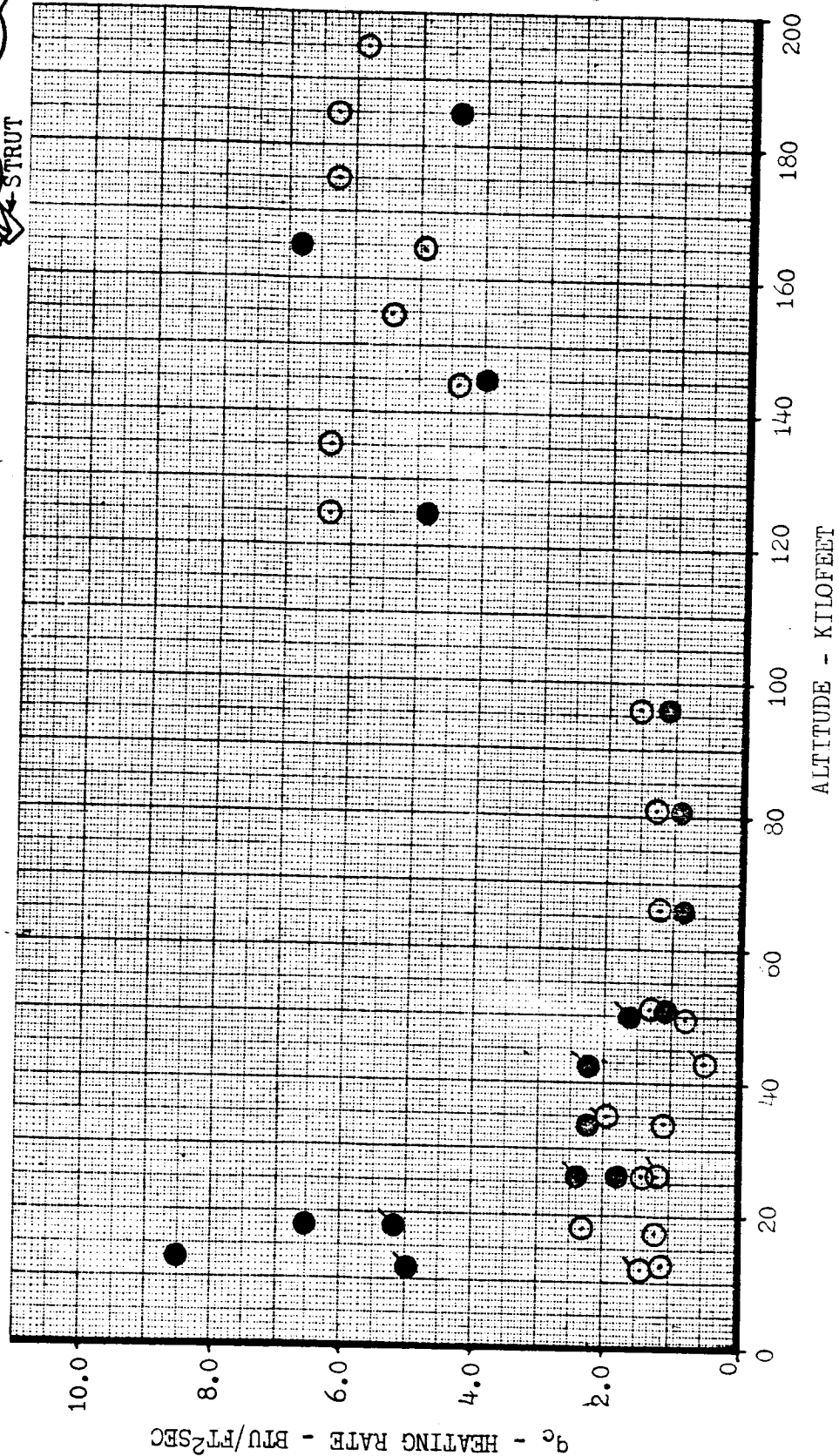
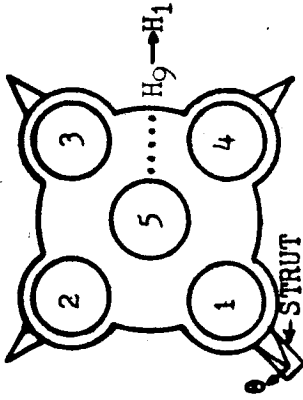


FIGURE 39 Base Heating - Convection



TUNNEL SYM.	INST.	CONFIG.
Δ	H ₁ , 3, 5, 7, 9	FS ₁ D ₁ SC ₁ N ₁ -5PL ₁
Δ	H ₁ , 3, 5, 7, 9	FS ₁ D ₁ SC ₂ N ₁ -5PL ₁
Δ	H ₁ , 3, 5, 7, 9	FS ₄ D ₁ SC ₁ N ₁ -5PL ₁

- NOTE: 1. Data averaged
 2. Closed symbol is with turbine exhaust
 3. Flag denotes Lewis 8-by 6-foot tunnel data

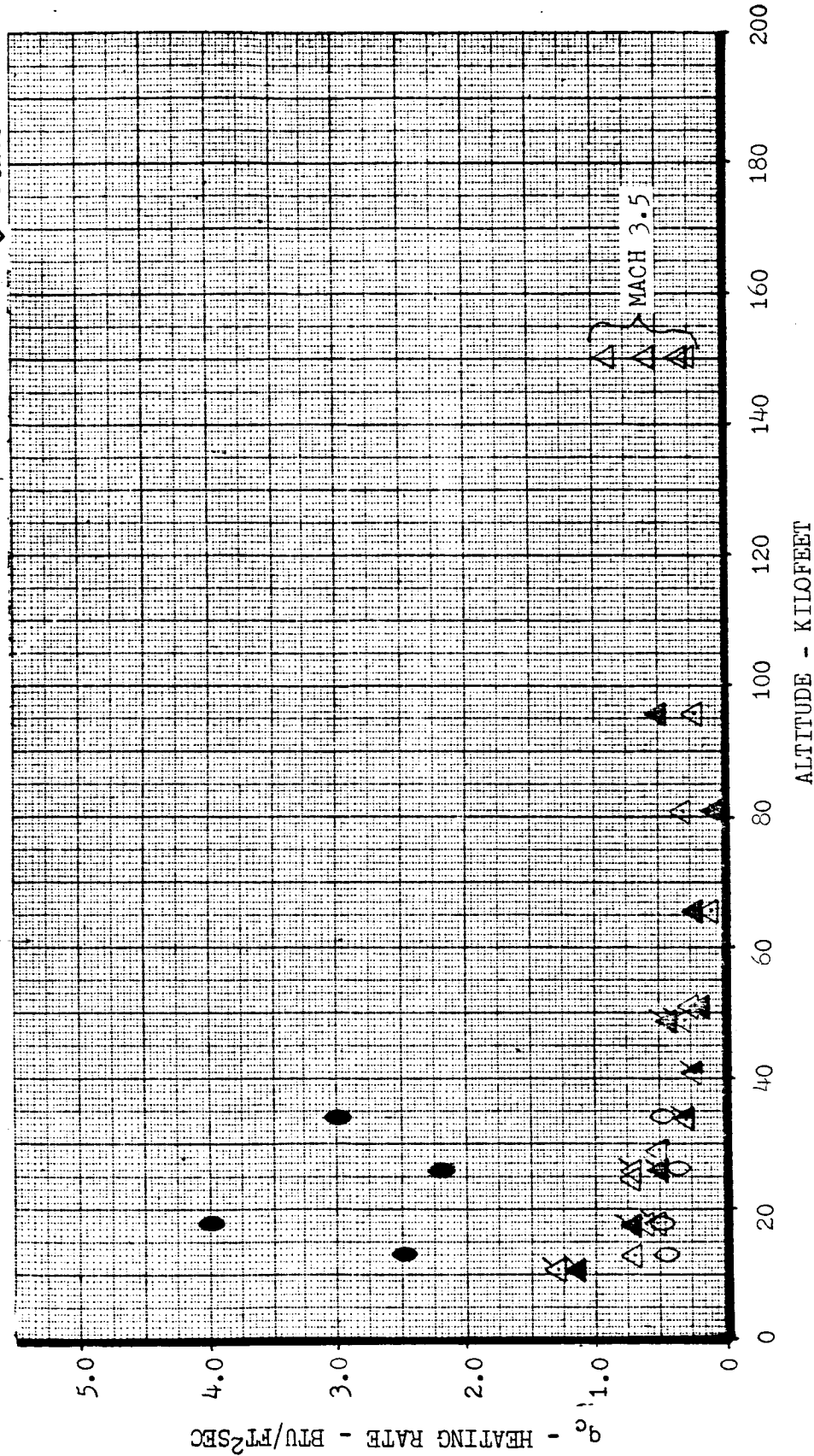
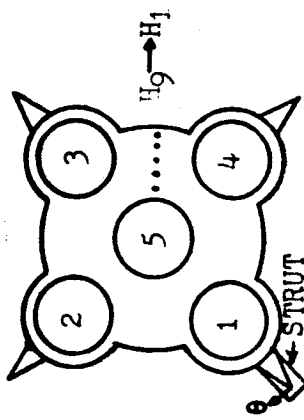


FIGURE 40 Base Heating - Convection



TUNNEL	SYM.	INST.	CONFIG.
	Δ	$H_1, 3, 5, 7, 9$	$FS D_1 SC N_1 - 5 PL_1$
	Δ	$H_1, 3, 5, 7, 9$	$FS D_1 SC N_1 - 5 PL_1$

NOTE: 1. Data averaged
2. Flag denotes Lewis 8-by 6-foot tunnel data

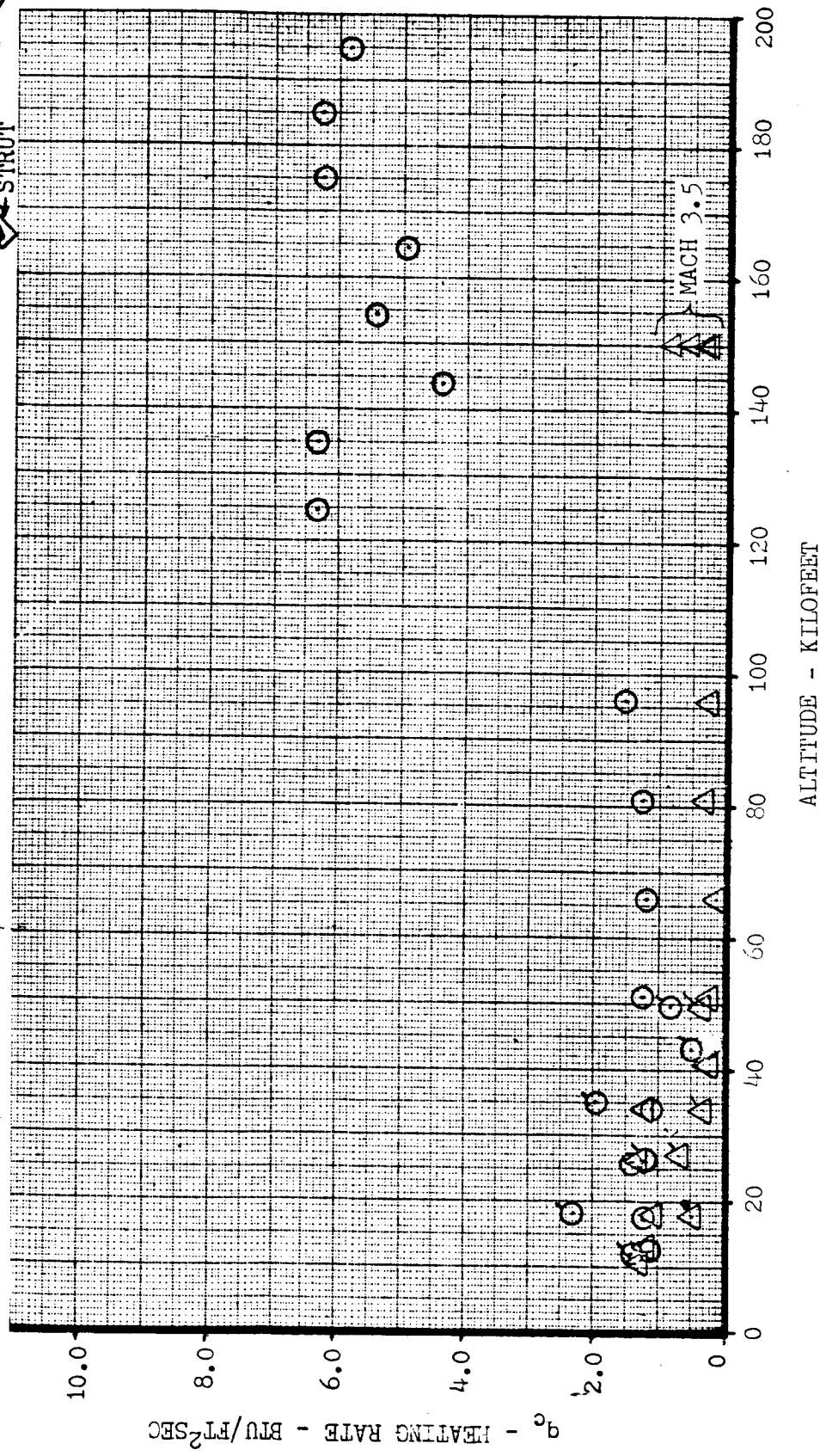


FIGURE 41 Base Heating - Convection

2.3.1 (Continued)

Shortening the engine fairings increases the base convective heating rate over the entire test range for a configuration without scoops or deflectors. (See Figure 42.) A similar trend for configurations with scoops below 34,000 feet is shown in Volume II, Section 3.0, paragraph 3.3.1.

Operating with the center engine out reduces the base convective heating throughout the test range. (See Figure 43.) Data for an outside engine out is available for the Lewis 8 by 6 foot test only and is shown in Volume II, Section 4.0.

Effect of gimbaling the engines is shown in Figure 44. Configuration NG₃NG₄ has engines 3 and 4 gimbaled toward each other 6 degrees. On configuration NG₅NG₆ engines 3 and 4 are gimbaled 8.5 degrees toward the center engine. Both of these patterns are extreme. Pattern NC₇NG₈ is based on realistic conditions which could occur if one engine went hard over. This pattern was only tested in the Lewis 8-by 6-foot tunnel.

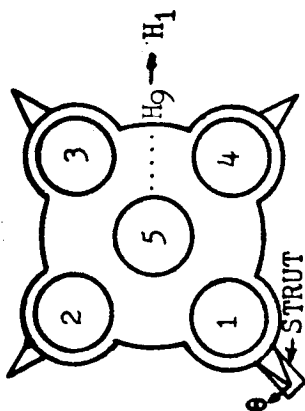
The data indicate that a hard over failure may have significant effect on base convective heating above approximately 80,000 feet. This may occur since the failure would cause two outboard engines to gimbal toward each other at near test angles which increases the plume impingement angle and creates greater recirculation in the closed quadrant. When the engines are gimbaled toward the center engine there is no significant change in the base heating data.

2.3.2 Convection to Fin Base

Data on the base of the fin are obtained from gage H₆₃ which is located near the fin/fairing interface. (See Figure 26.) All the data available above 50,000 feet are shown on Figure 45. The data obtained indicates that the fin heating rate with the short engine fairing (S₄) is approximately constant at 1.0 BTU/FT²SEC and relatively unaffected by turbine exhaust. Other data shown in the range of zero to 50,000 feet are representative of a normal fairing length with or without deflectors and indicate a slight reduction in the heating rate.

2.3.3 Convection to Engine Fairing

The locations of the engine fairing heating gages are shown in Figure 27. The only consistent gage is H₅₇ which is located on the inside surface of the engine fairing near the aft edge, 65 degrees from the fin centerline. Heating rate increases almost linearly with altitude reaching a value of approximately 3.0 BTU/FT²SEC (see Figure 46) or about half of the heating rate to the base. Addition of scoops and deflectors causes a reduction in the convective heating level. Without scoops injection of turbine exhaust caused a large increase in heating rate at low altitudes indicating base burning. No turbine exhaust data are available with scoops and deflectors in the CAL 8 by 8 facility.



TUNNEL SYM.	INST.	CONFIG.	SYM.	INST.	CONFIG.
○	H ₁ , 3, 5, 7, 9	FS ₁ N ₁ -5 _{PL1}			
□	H ₁ , 3, 5, 7, 9	FS ₄ N ₁ -5 _{PL1}			

NOTE: 1. Data averaged
2. Flag denotes Lewis 8-by 6-foot tunnel data

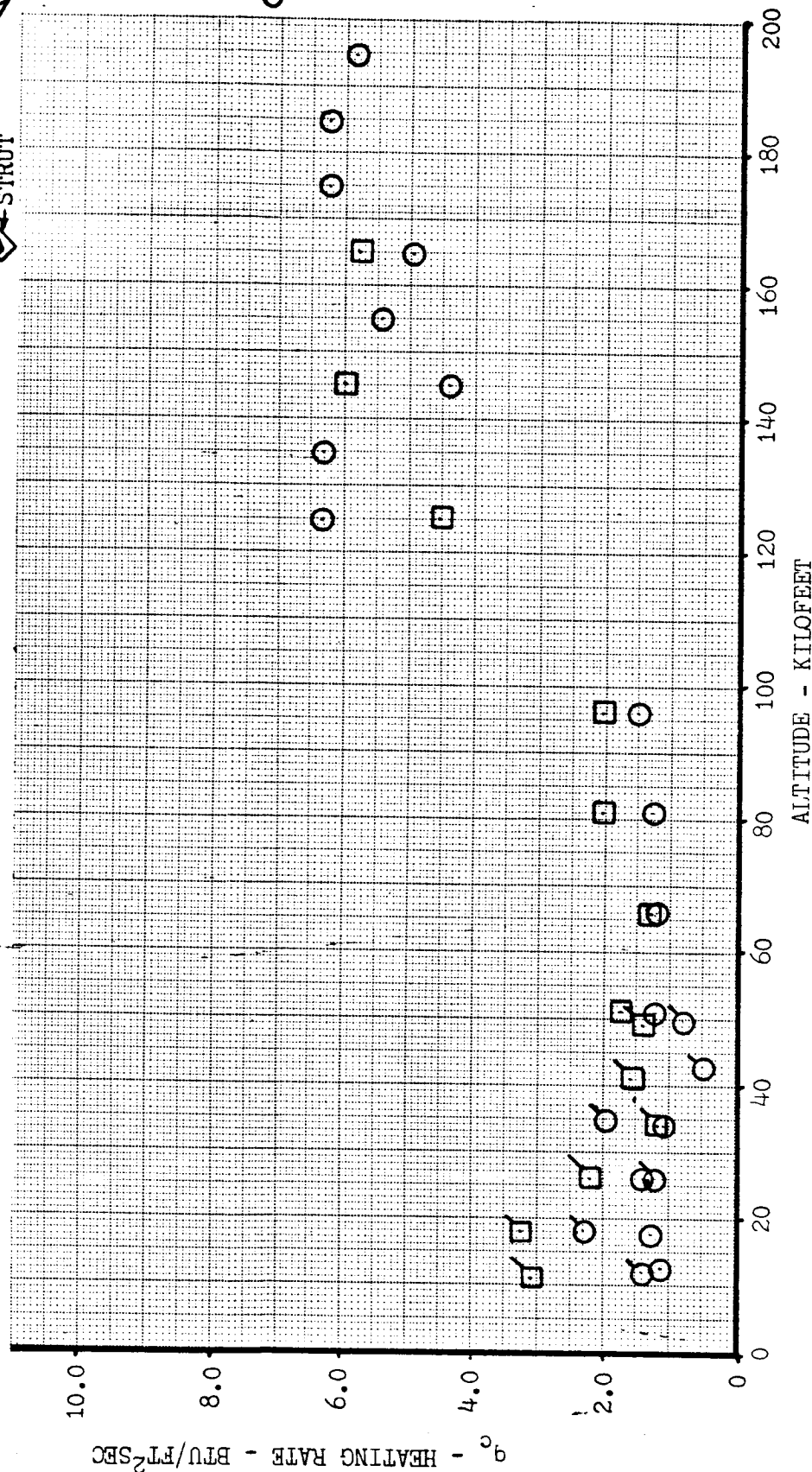


FIGURE 42 Base Heating - Convection

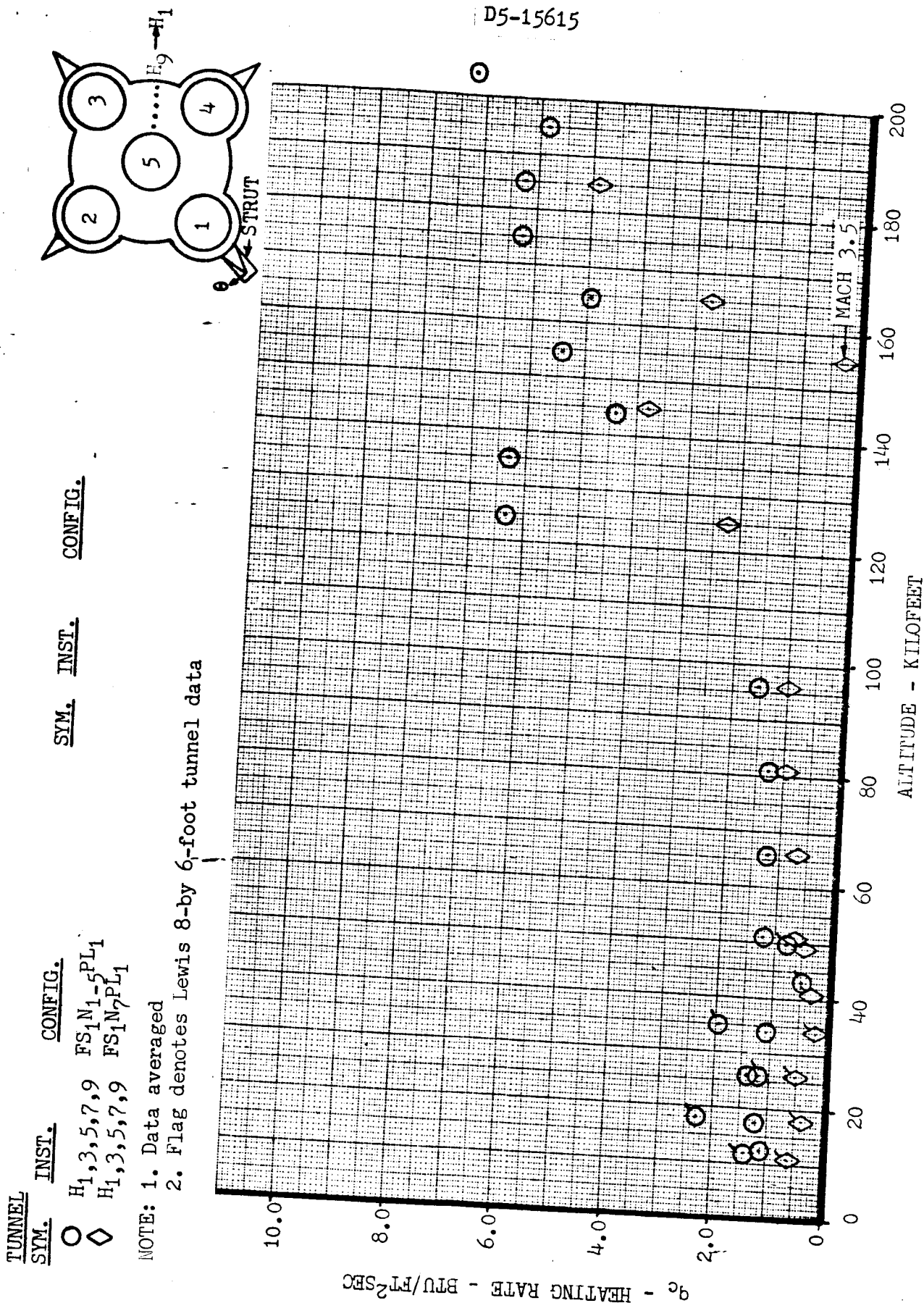


FIGURE 43 Base Heating - Convection

2.3.4 Convection to Engine

Total heating gages are located on the external surfaces of the engines as shown in Figures 22 and 23. Most of this instrumentation failed during transonic wind tunnel tests so that data in this range are available only from gages H₂₁ which is located near the nozzle lip of the center engine and H₂₉ which is located on the center engine nozzle near the throat. In the supersonic and high altitude tests considerable data are available especially for the gimbal patterns. For all configurations over the entire range heating near the lip is higher than that recorded at any other point on the engine. Axial temperature distributions are shown in Volume II under paragraphs 5.3.3 and 6.2.3.

Data from gage H₂₁ and H₂₉ are shown in Figure 47 for the configuration without flow deflectors or scoops, (FS₁N₁₋₅PL₁). Engine heating near the lip is seen to be highly dependent on altitude and clearly reflects the degree of plume impingement. Convection to the nozzle near the throat (H₂₉) is unaffected by altitude and without turbine exhaust remains under 2.0 BTU/FT²SEC throughout the test range.

Data from the CAL 8-by 8-foot transonic tunnel indicate base burning at low altitude (under 25,000 feet) when hydrogen is injected to simulate turbine exhaust. Although all the data is not shown this also occurs with deflectors and/or scoops. (See Volume II, Paragraph 3.3.3.) In the Lewis 8-by 6-foot tunnel no data are available for gage H₂₉ with turbine exhaust due to instrumentation failure.

Center engine heating effects with gimbled engines are shown in Figures 48 and 49 for altitudes above 50,000 feet. Data on Figure 48 are for a configuration with engines 3 and 4 gimbled at 8.5 degrees toward the center engine in Figure 49. Instrument locations not previously described include H₂₃ which is near the lip facing engine 3 and H₂₇ which is in line with H₂₃ located just aft of the turbine exhaust manifold.

With both configurations convection to gage H₂₃ is significantly less than to gage H₂₁. This indicates that flow is stagnated between engines 3 and 5. It is also evident that convection heating will not be a problem at points below the lip on the center engine.

No data are available on the outside engines. This is unfortunate since the heating rates are likely to be considerably higher there since the flow is moving outboard away from the center engine and will flow around the outside engines. The higher heating rates are expected to work toward the base with increasing altitude eventually reaching and affecting the heating on the base.

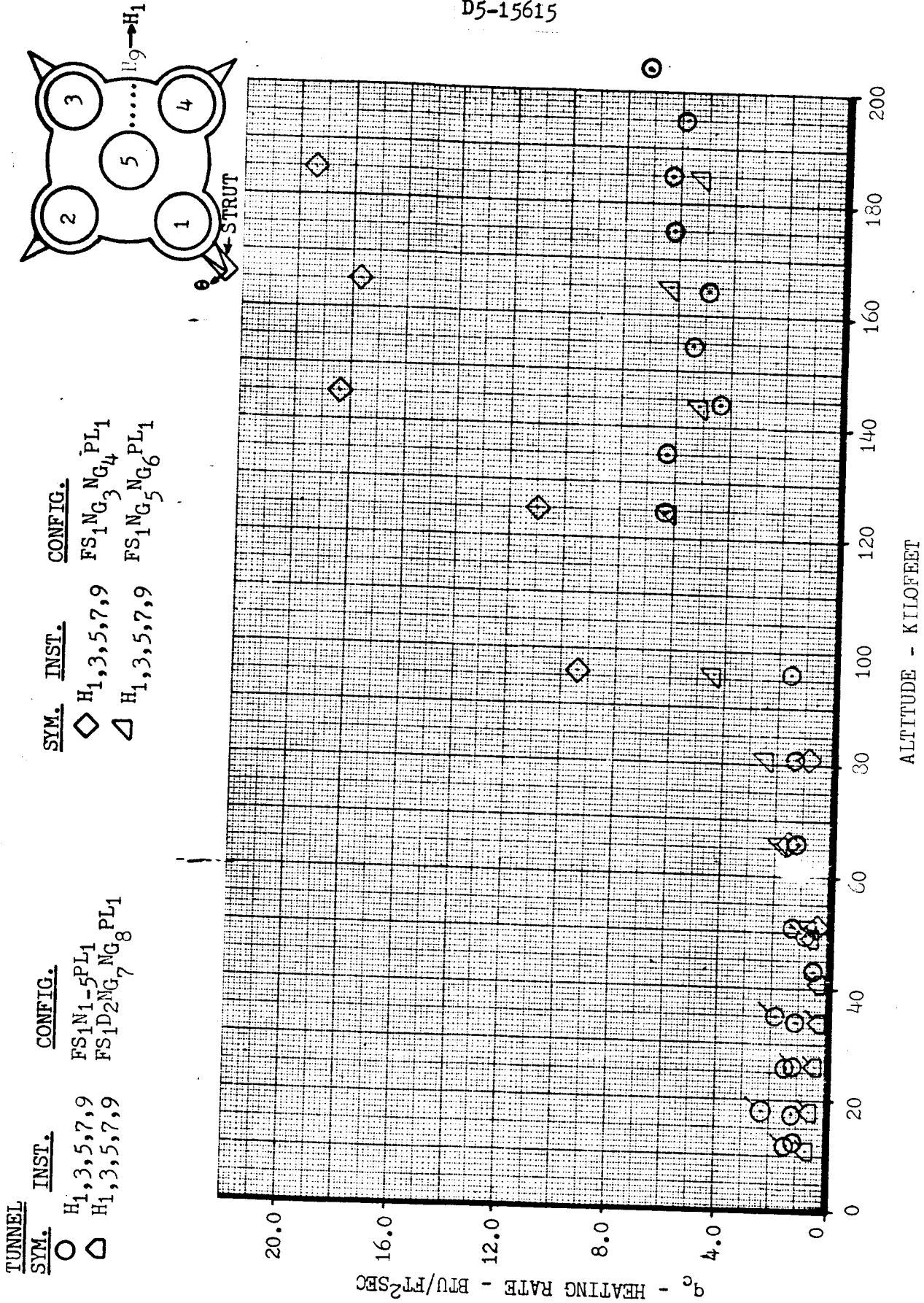
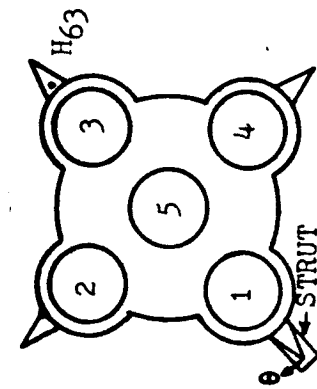


FIGURE 44 Base Heating - Convection



TUNNEL SYM.	INST.	CONFIG.	SYM.	INST.	CONFIG.
○	H63	FS ₁ N ₁₋₅ PL ₁	◇	H63	FS ₄ SC ₁ N ₁₋₅ PL ₁
□	H63	FS ₄ N ₁₋₅ PL ₁			

NOTE: 1. Flag denotes Lewis 8-by 6-foot tunnel data
2. Solid symbol denotes turbine exhaust

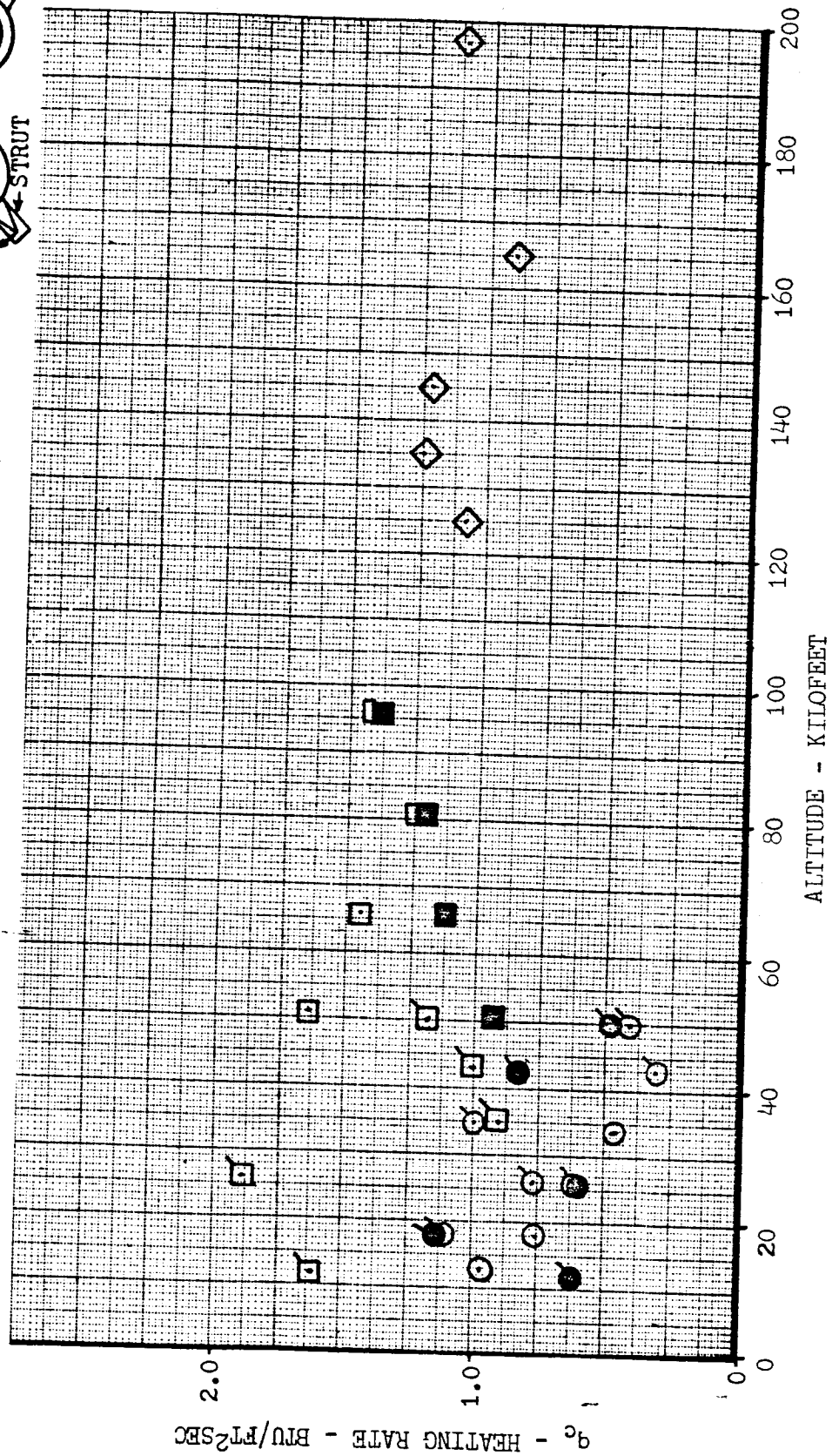
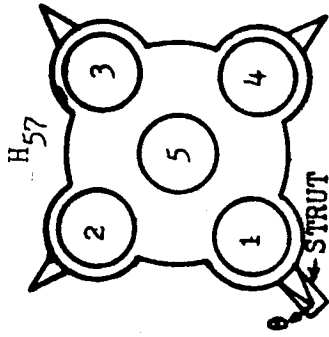


FIGURE 45 Fin Heating - Convection



TUNNEL SYM.	INST.	CONFIG.
○	H ₅₇	B ₁ FS ₁ N ₁₋₅
△	H ₅₇	B ₁ FS ₁ SC ₁ D ₁ N ₁₋₅

NOTE: Solid symbol denotes turbine exhaust

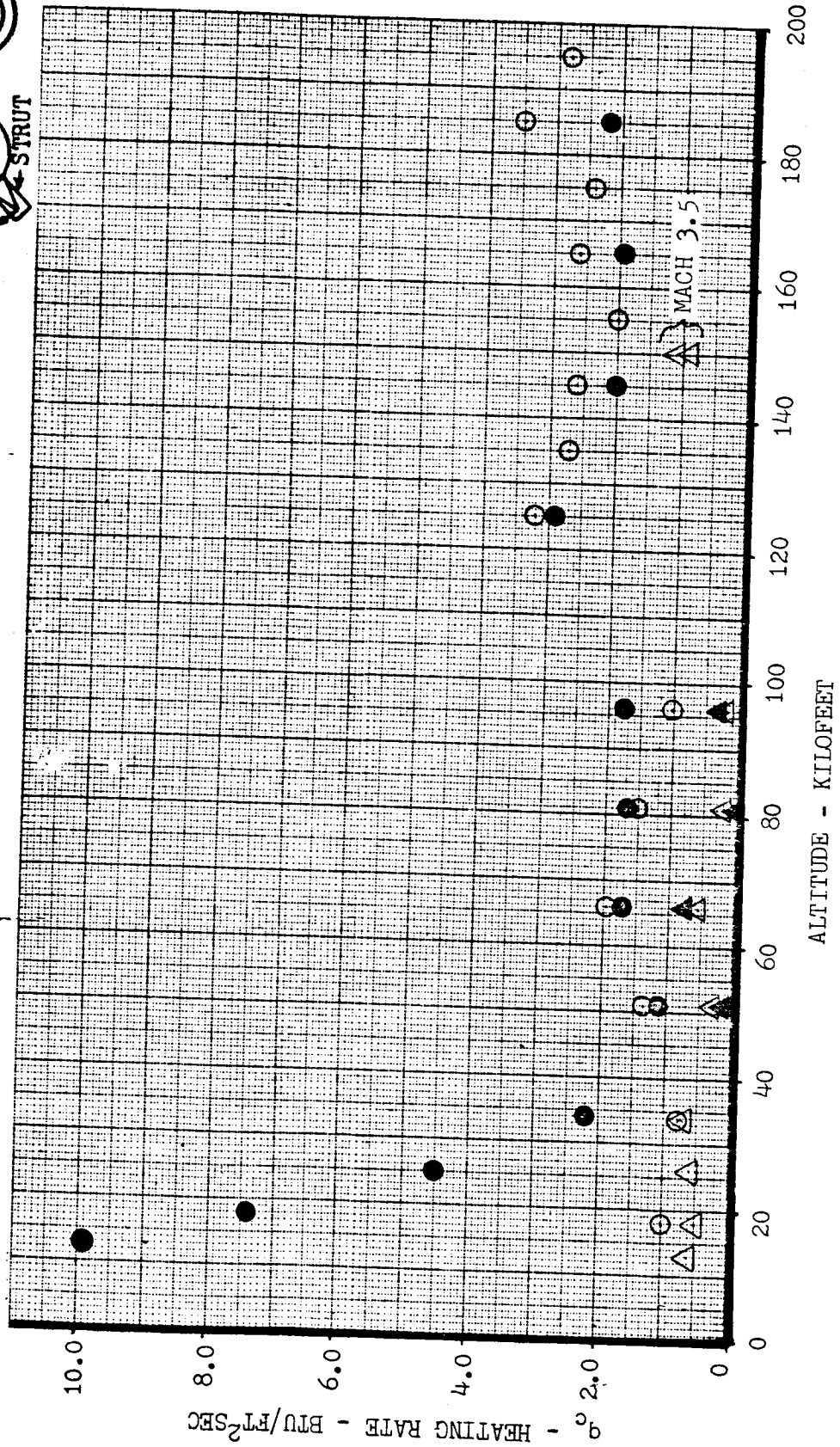
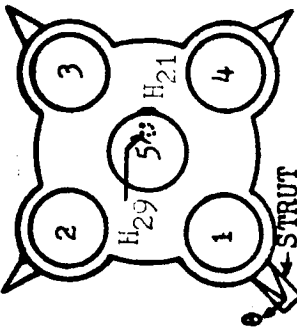


FIGURE 46 Engine Fairing Heating - Convection



<u>TUNNEL</u>		<u>INST.</u>	<u>CONFIG.</u>
<u>SYM.</u>			
○		H ₂₁	FS ₁ N ₁ -5PL ₁
△		H ₂₉	FS ₁ N ₁ -5PL ₁

SYM. INST. CONFIG.

NOTE: 1. Flag denotes Lewis 8-by 6-foot tunnel data
2. Solid symbol denotes turbine exhaust

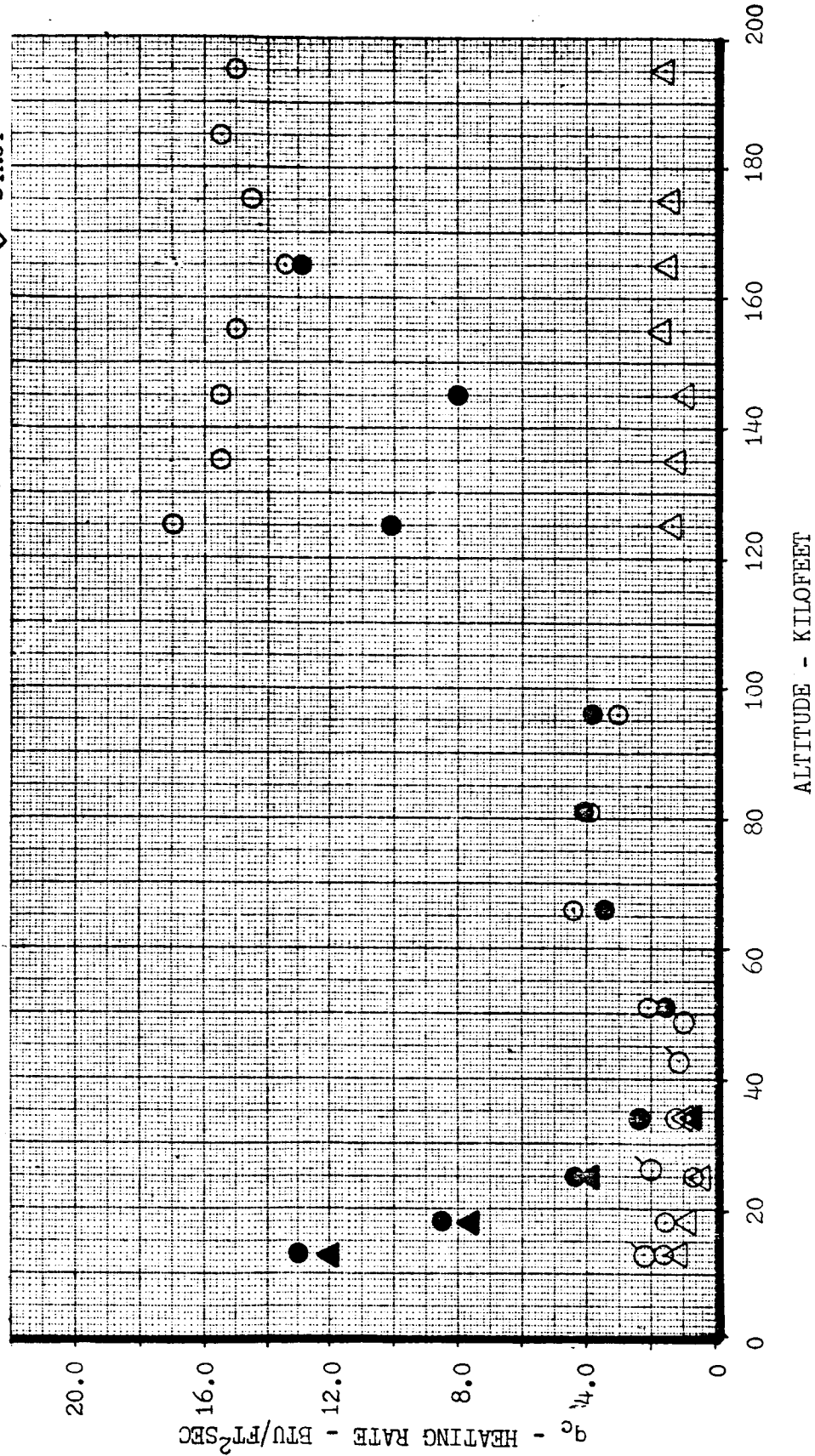


FIGURE 47 Engine Heating Convection - (External)

TUNNEL

SYM. INST.

CONF.

B₁FS₁NG₃NG₄PL₁

B₁FS₁NG₃NG₄PL₁

SYM.

INST.

CONF.

B₁FS₁NG₃NG₄PL₁

B₁FS₁NG₃NG₄PL₁

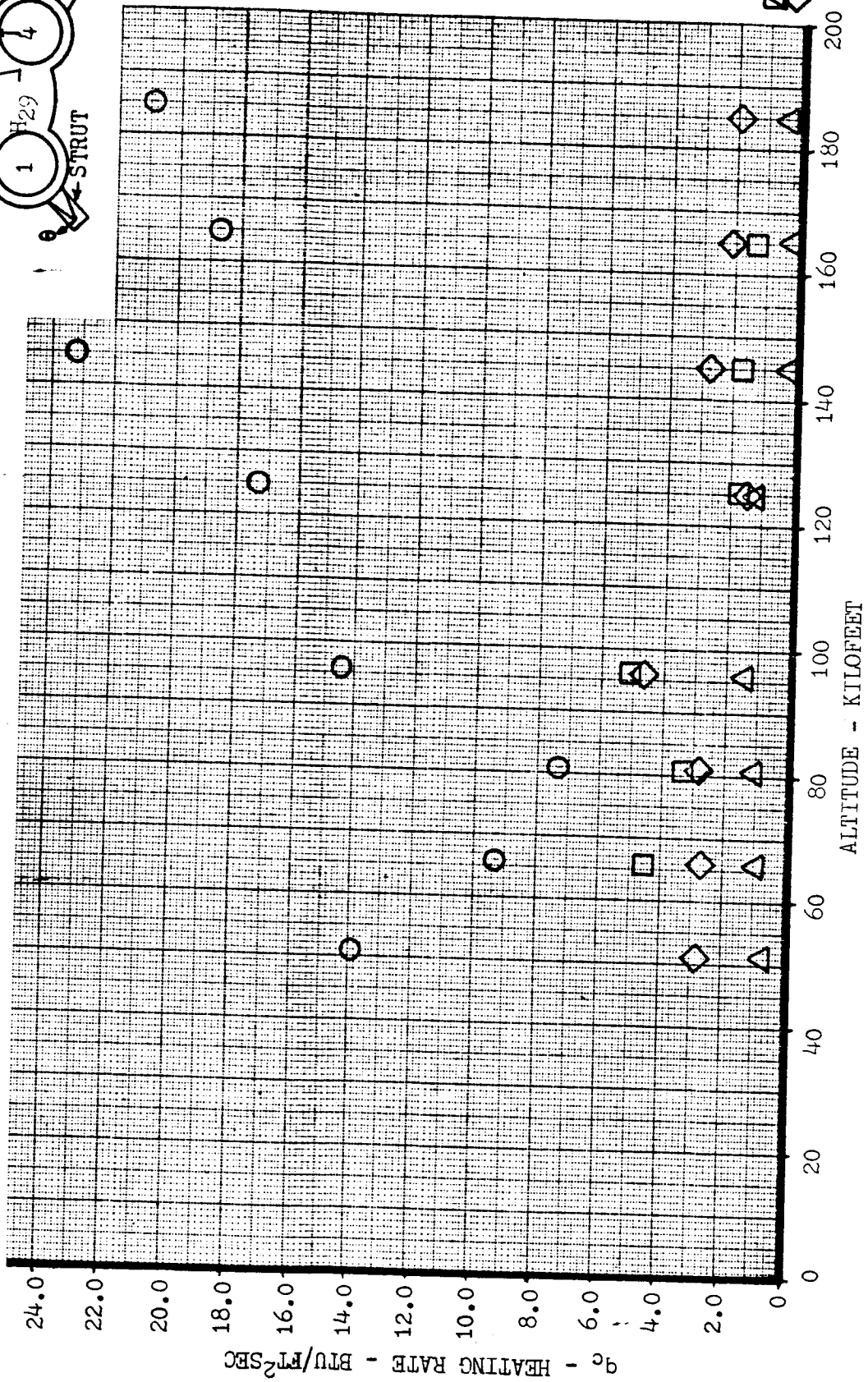
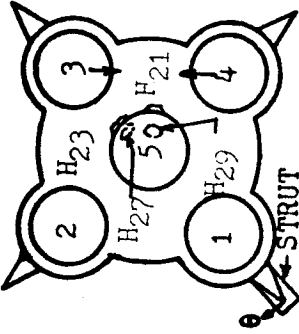


FIGURE 48 Engine Heating - Convection (External)

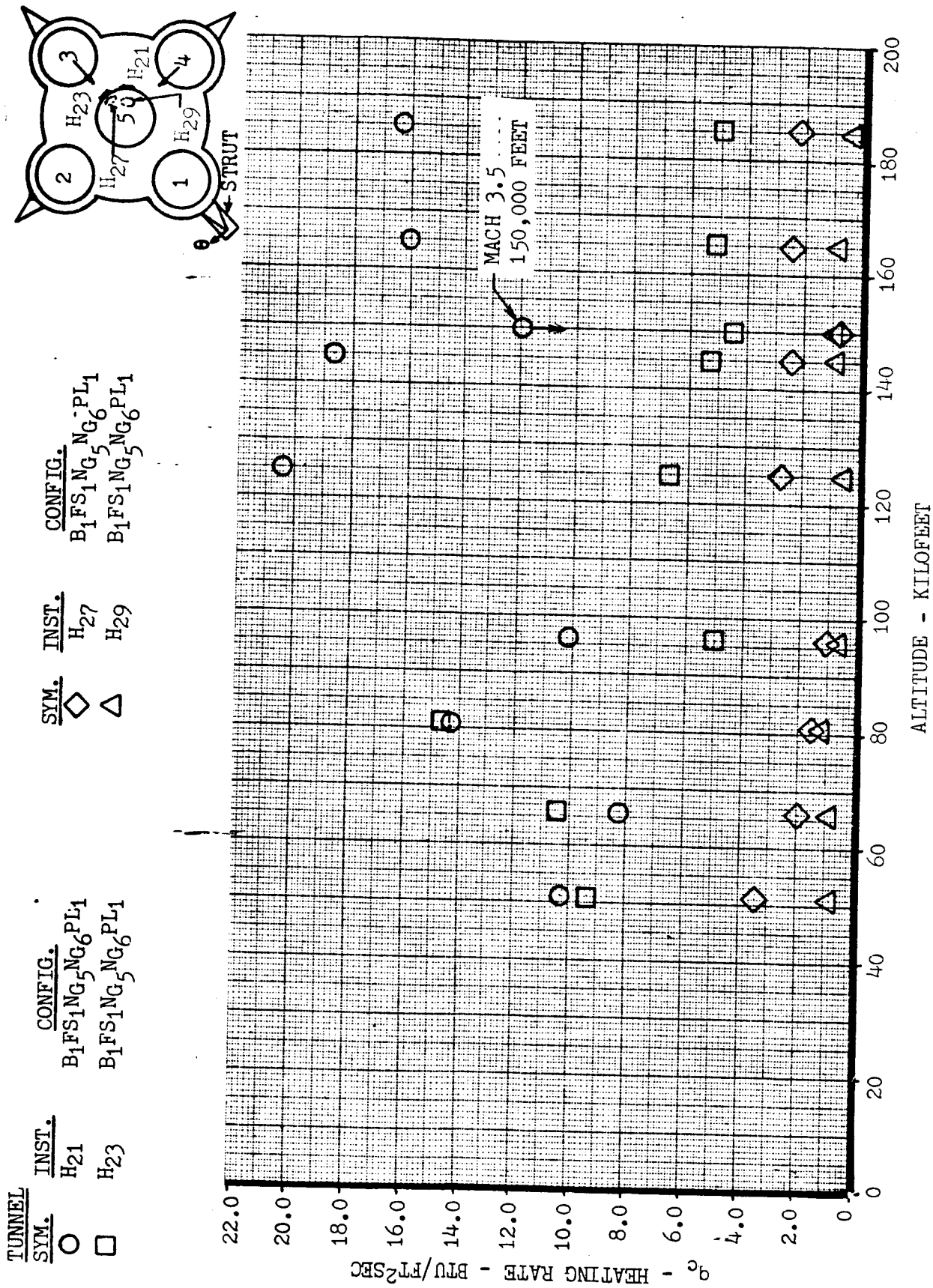


FIGURE 49 Engine Heating - Convection (External)

2.3.5 Comparison with Convective Theory

The convective heating rate is calculated using the equation

$$q_c = h_c (T_G - T_W) \quad \text{Equation 4}$$

where h_c is the heat transfer coefficient and T_G is the base gas temperature. T_W is the wall temperature which, for comparison with model test data, can be assumed to be 70°F. The theoretical determination of both the base gas temperature and the heat transfer coefficient are discussed in detail in Appendix B.

Determination of the recovery temperature (t_r) is essential to a good convection heating rate estimate since the fluid properties used in estimating h_c are dependent upon t_r as well as the velocity of the gas. The heated base plate described in paragraph 1.1.5 was used in the CAL altitude chamber and the LRC 8-by 6-foot tunnel in an attempt to determine the recovery temperature. (See paragraphs 4.6 and 6.5.)

Figure 50 shows the data obtained from the hot base plate compared with the theoretically calculated base gas temperature from Appendix B. It is evident that the measured temperatures at low altitude are higher than the theoretical calculation but at high altitude the theory is about double the measured data. The theoretical base gas temperature at high altitude could be lowered if it were assumed that the recirculating gas is mixing with air in the base.

The convective base heating data with and without scoops is shown in Figure 51 and compared with the theoretical calculations developed in Appendix B. Theoretically there should be no convective heating below 40,000 feet for the no-scoop configuration and the scoop configuration should have no convective heating below 55,000 feet. The theory does not consider free stream flow impinging on the exhaust plume, however, which would cause some recirculation earlier than 40,000 or 55,000 feet. The data (Figure 51) indicates some convective heating at the low altitudes which is not predicted by the current theory. At the higher altitudes the theoretical curves rise much more rapidly than the experimental data although the heating rates are about the same magnitude. High altitude experimental data is slightly higher than the theoretical calculations.

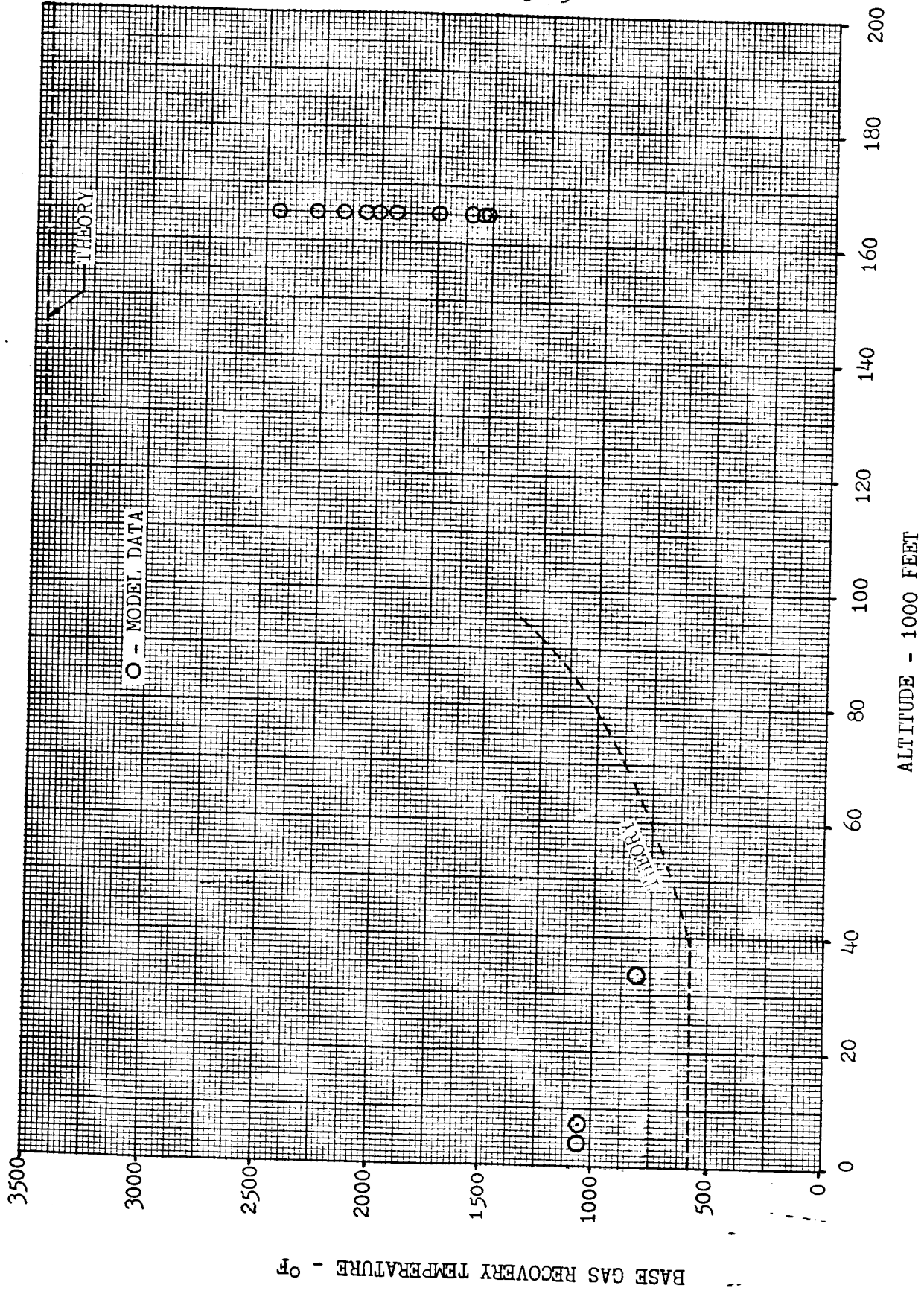


FIGURE 50 Base Gas Temperature - Comparison with Theory

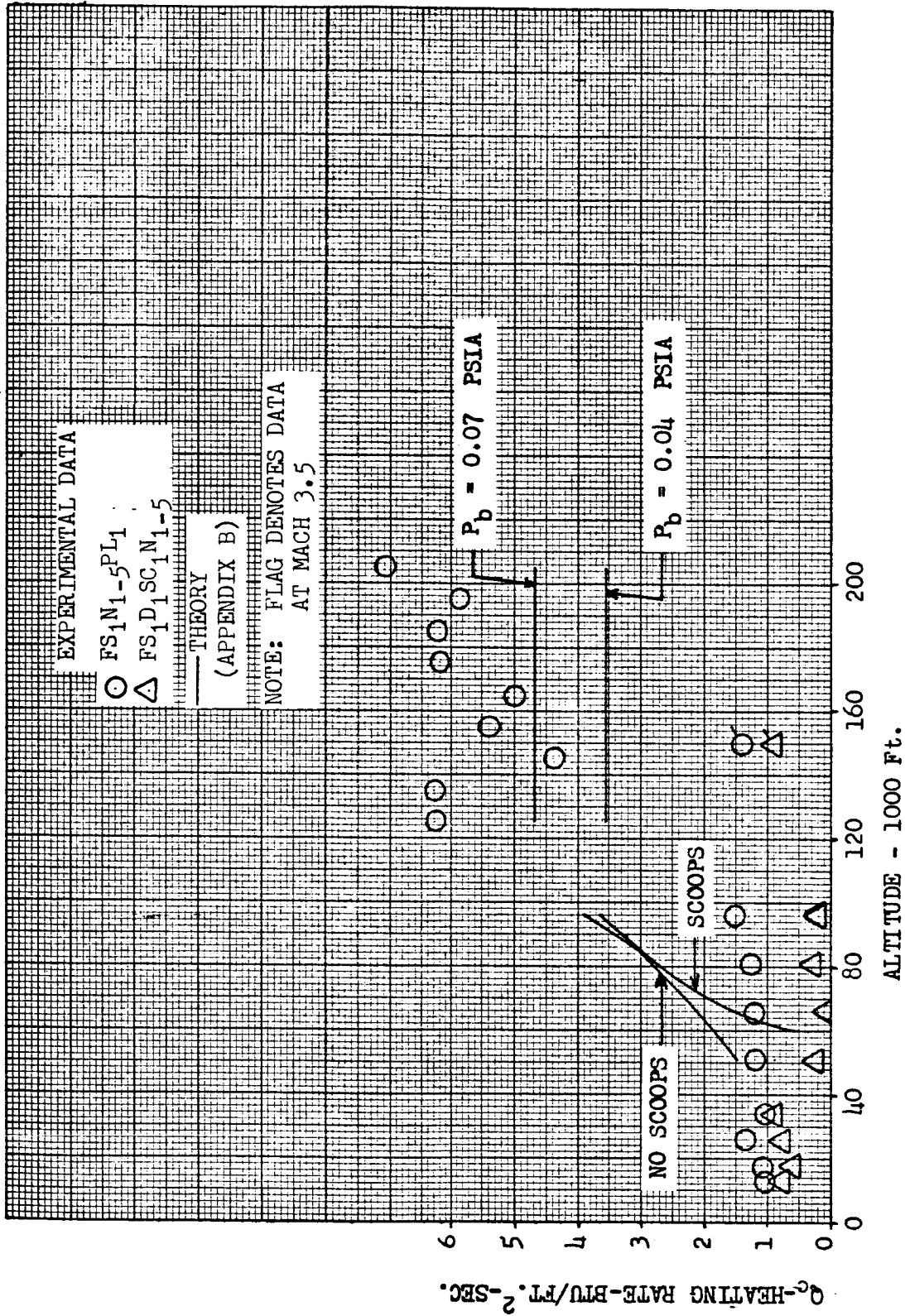


FIGURE 51 Convective Heating-Comparison With Theory

2.4 BASE PRESSURE

Static pressure data are available on the base only. Seven pressure instruments are located on the PL₁ base plate (see Figure 19); three located along rays between engines 1 and 2 and between engines 2 and 3 with a single gage located between engines 2 and 5. Pressure measurements are obtained by measuring an engine off base pressure and adding the measured gage in pressure during the engine firing.

Pressure data using base plate PL₂ are also available for the Lewis 8 by 6 foot tunnel tests. PL₂ is instrumented with 16 gages located in all quadrants as shown in Figure 20. These data were specifically obtained for comparison with cold flow tests and are shown in Volume II paragraph 4.6.

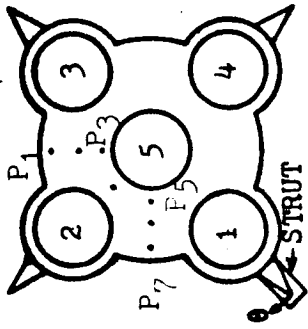
Pressure data were taken in the CAL 8-by 8 tunnel and Lewis 10 by 10 tunnel before the engines fired. This data is shown in Figures 52 and 53 and is compared with the engines-on data. Figure 52 shows the no-scoop configuration and Figure 53, the scoop configuration. In both figures it is noted that when the engines are operating, there is a distinct base pressure increase. It is also evident that the no-engine-flow base pressure is higher with scoops on as would be expected.

Data from PL₁ are used in Figures 54 through 58 to indicate configuration effects. Since various of the instruments were inoperative during the tests the data are averaged. Data in the altitude range of 51,000 to 96,000 feet do not include readings from gage P₃ which appear abnormally high in all runs.

No attempt has been made to correct the Lewis 8 by 6 tunnel data for the trajectory mismatch. No comparisons are shown which include data from the CAL 8 by 8 foot tunnel and the Lewis 8 by 6 foot tunnel on the same chart. Although the data from the two tunnels are different, comparison of effects of configuration variations is still possible.

Turbine exhaust is seen to have negligible effect on base pressure at low altitudes. From 60,000 feet up there is a slight increase in base pressure. (See Figure 54.)

Figure 55 indicates an increase in base pressure with the advent of flow deflectors and fairing scoops through 100,000 feet. Since there is no external flow in the CAL high altitude pressure chamber the effects of scoops were not obtained.



TUNNEL
SYM.

INST.

SYM.

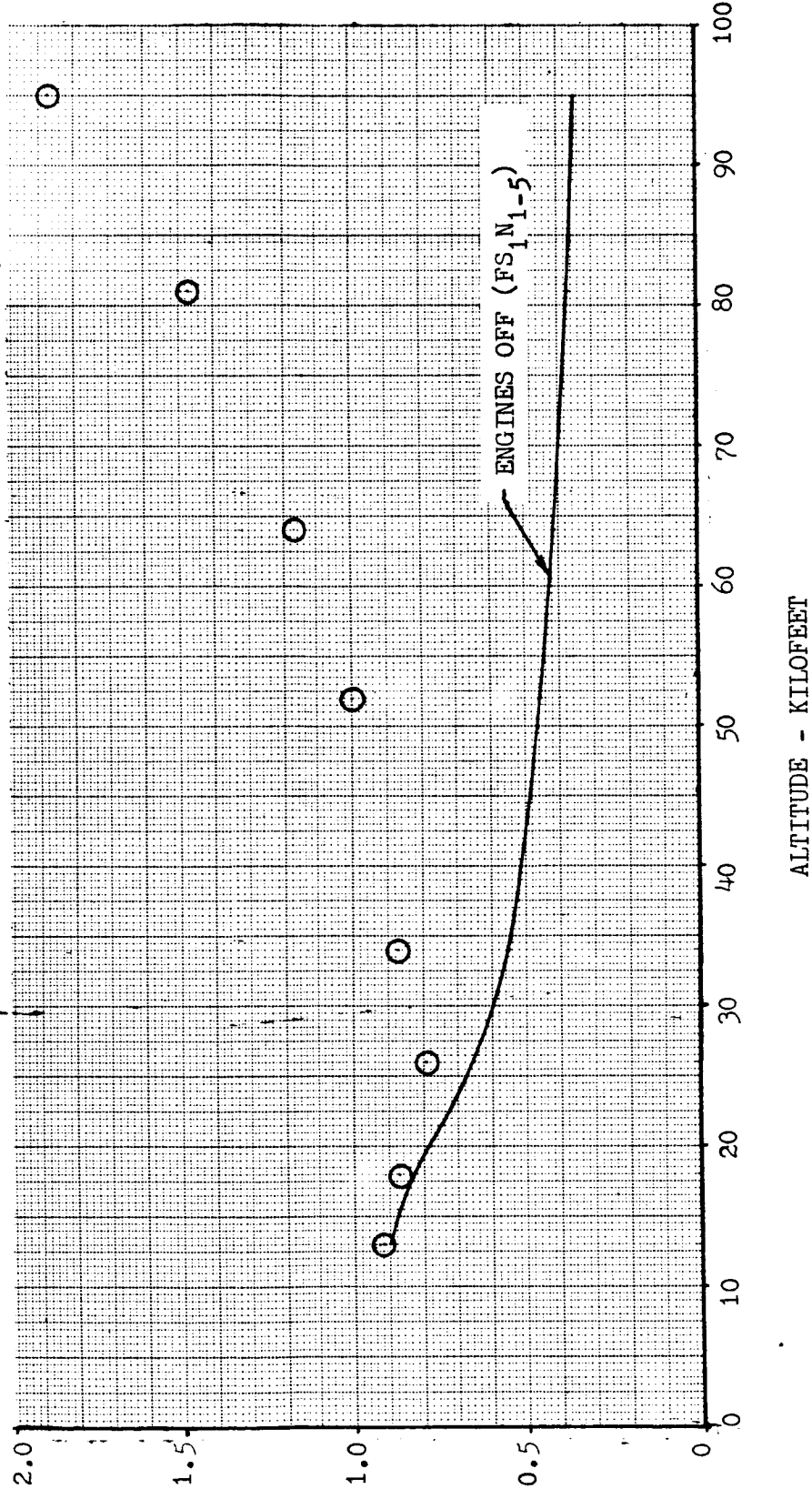
INST.

CONFIG.

CONFIG.

○ P_{1,2,3,4,5,6,7} FS₁N₁₋₅PL₁

RATIO - BASE TO FREE STREAM STATIC PRESSURE - P_b/P_∞



ALTITUDE - KILOFEET

FIGURE 52 Base Pressure

TUNNEL
SYM. INST. CONFIG.
 Δ P_{1,2,3,4,5,6,7} FS₁D₁SC₁N₁₋₅PL₁

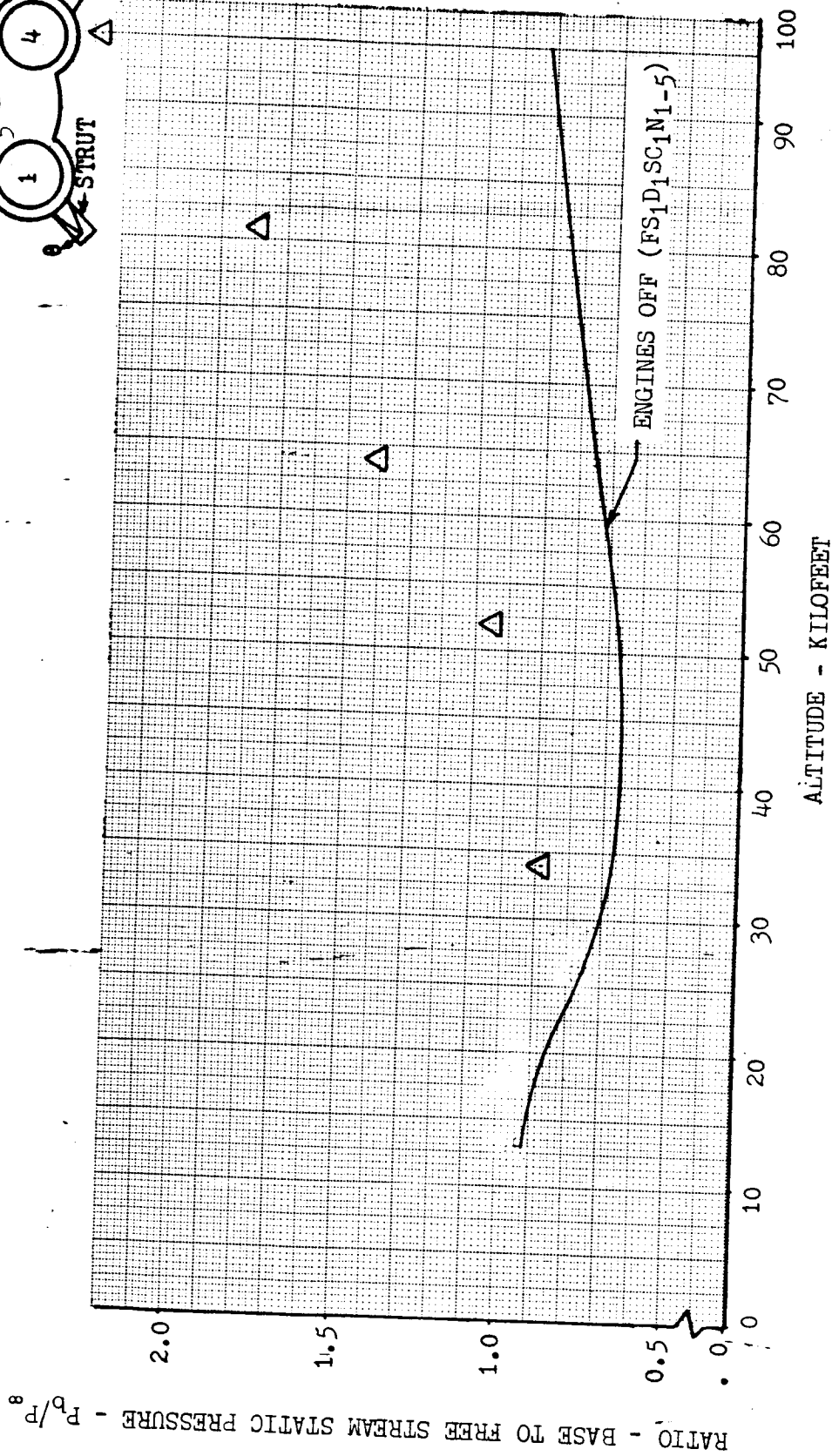
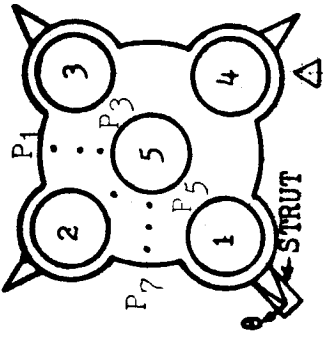


FIGURE 53 Base Pressure

TUNNELSYM. INST.CONFIG.○ $P_{1,2,3,4,5,6,7}$ $FS_1 N_{1-5} PL_1$

NOTE: 1. Data are averaged

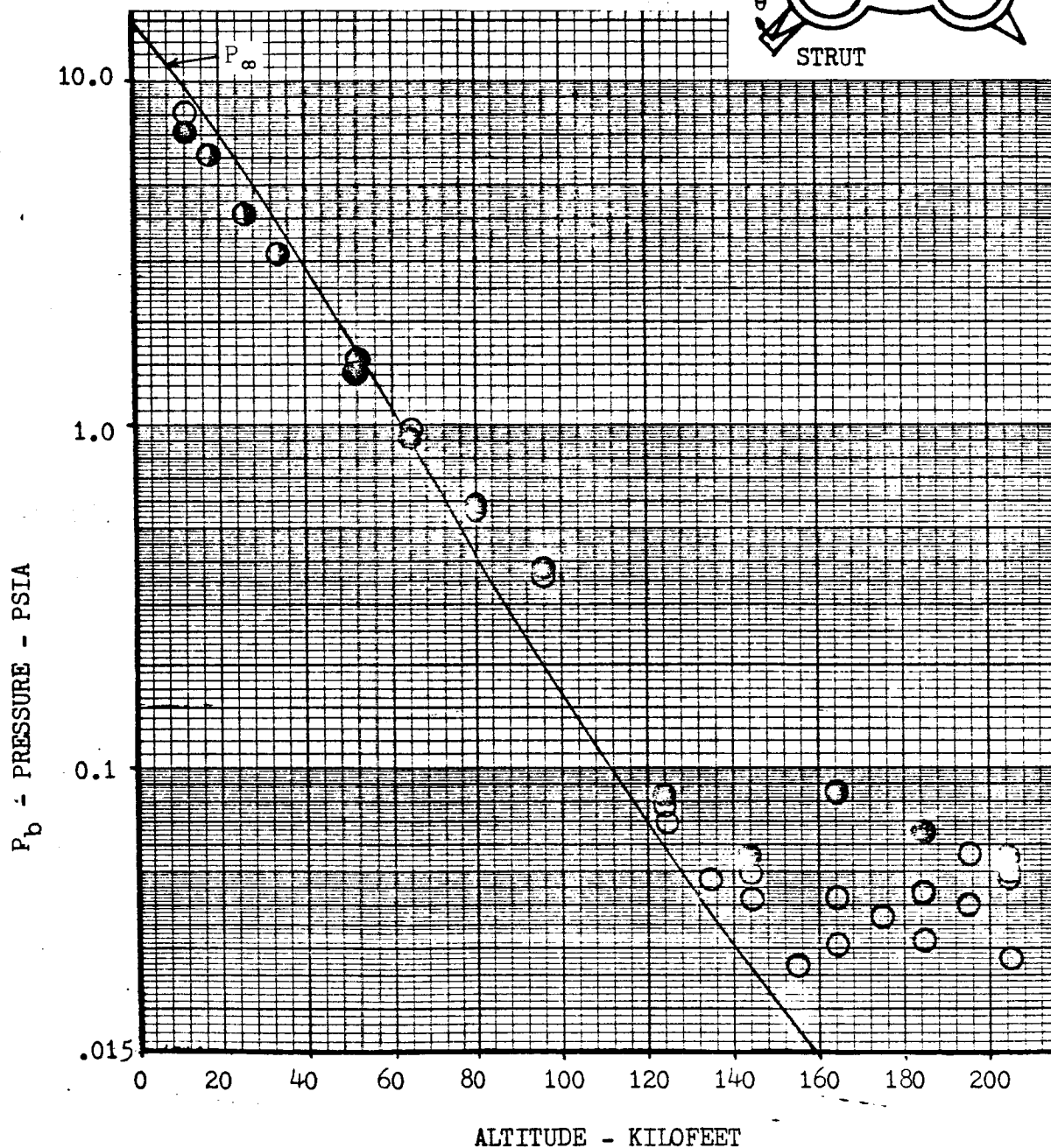
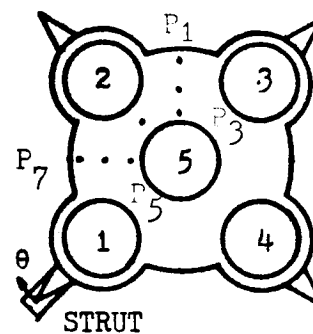
2. Solid symbol denotes turbine exhaust (H_2)

FIGURE 54 Base Pressure - Turbine Exhaust Effect

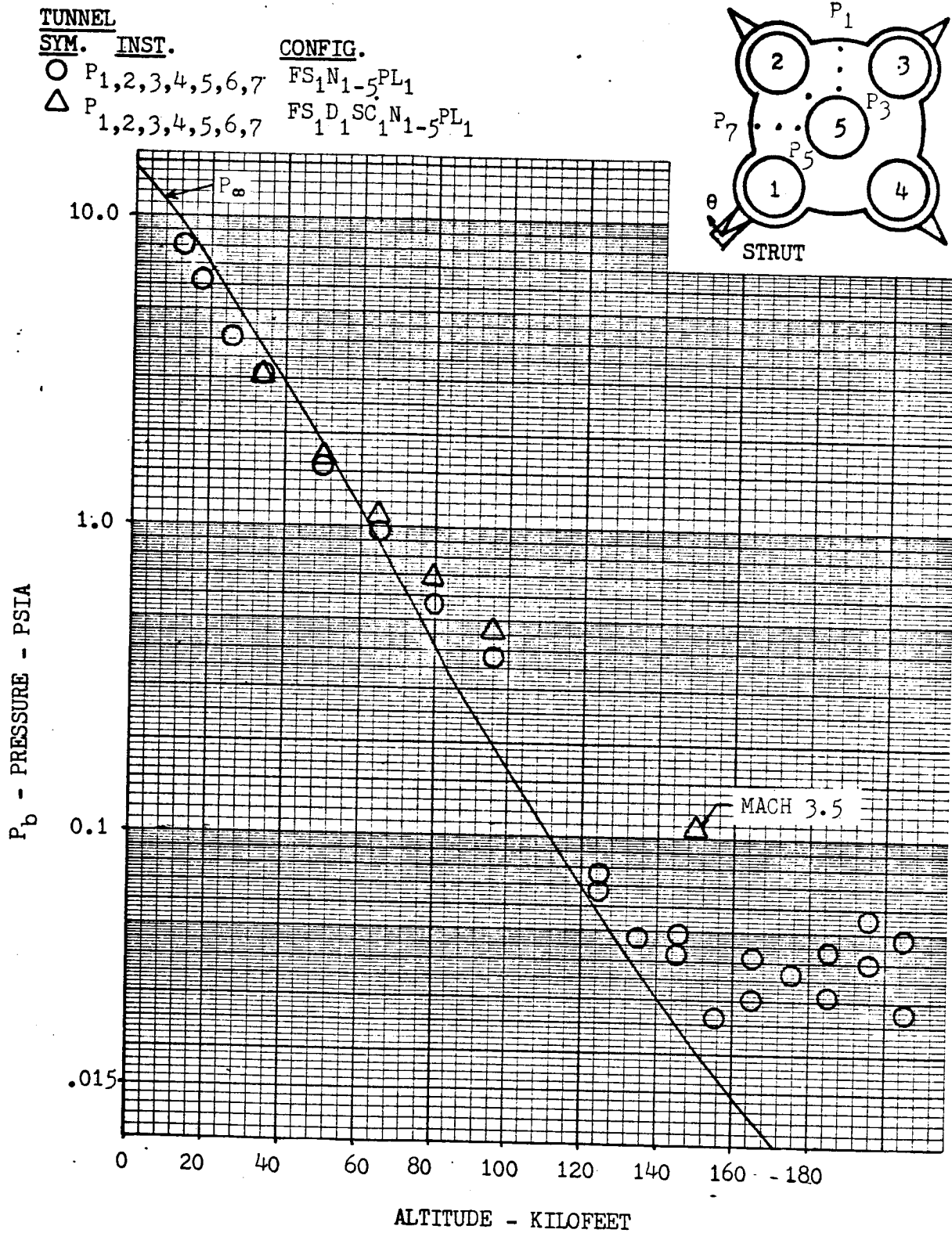


FIGURE 55 Base Pressure - Scoop and Deflector Effect

2.4 (Continued)

The effects of engine fairing length are shown in Figures 56 and 57. Reduction of fairing length where scoops and deflectors are present (see Figure 56) causes a slight reduction in base pressure at low altitudes. No data are available with this configuration from 40,000 to 125,000 feet. Without scoops and deflectors shortening the fairing causes a reduction in base pressure through 100,000 feet. (See Figure 57.) The data under 50,000 feet for this configuration are obtained from the Lewis 8-by 6-foot tunnel test.

For a condition where the center engine fails the average base pressure will be reduced throughout the flight range tested. (See Figure 58.) The low altitude data are from the Lewis 8 by 6 tunnel. All the data provide some gross similarities. All data are lower than the Patrick reference pressure below 50,000 feet. Above 50,000 feet the base pressure for all configurations is higher than the Patrick reference pressure. In general the data closely follow the reference pressure up to 145,000 feet after which the base pressure remains constant and may begin to increase. This condition will occur only when the flow between the outboard engines has become sonic.

Data taken in the Lewis 10 by 10 foot tunnel at Mach 3.5 and 150,000 feet shown on Figures 55 and 58, indicate that the pressure data from the high altitude tests may be low. However, the high altitude data are useful in that they establish the low pressure which will occur in flight and thus establish a lower limit for base pressure instrumentation requirements and an extrapolation limit.

2.4.1 Comparison with Pressure Theory

Engines-off base pressure is analytically calculated in Appendix C using an empirical base pressure coefficient curve from Mach 0.8 to 1.2 and above Mach number 2.5 the standard Newtonian base pressure-coefficient equation for a circular cylinder is used. Figure 59 shows the theoretically and empirically calculated base pressure compared with engines-off base pressure data with and without scoops. The theory is above the experimental data in the low altitude range but then closely approximates the no scoops base pressure at the higher altitudes. Differences between theory and data are caused by the engines and engine fairings.

The base pressure during engine firing is compared with the theoretically calculated scoop exit static pressure and Korst's theory in Figure 60. The experimental base pressures are below the scoop exit static pressures in all cases.

Korst's theory at the higher altitudes predicts a much higher base pressure than that measured on the base.

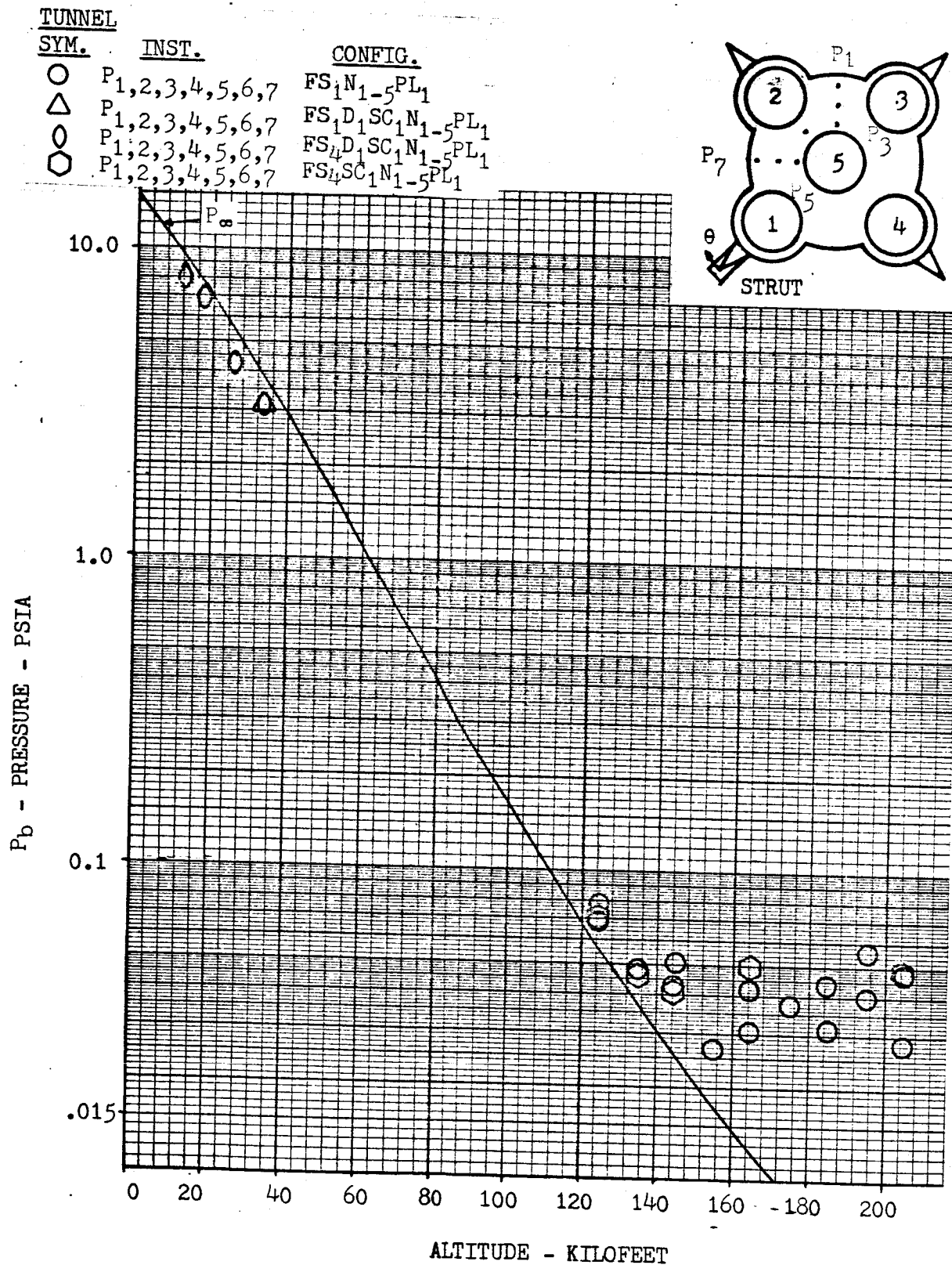


FIGURE 56 Base Pressure - Engine Fairing Length Effect

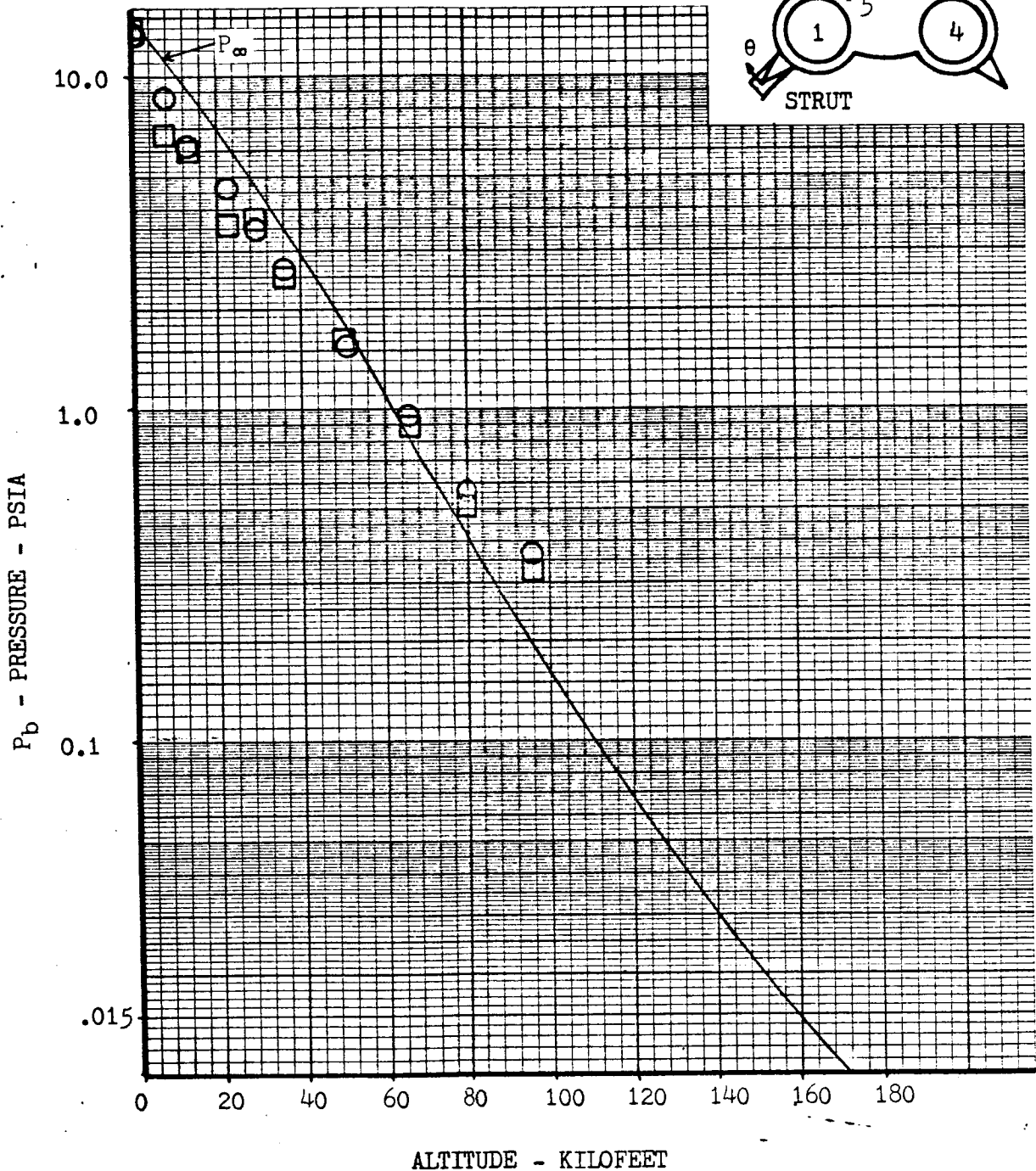
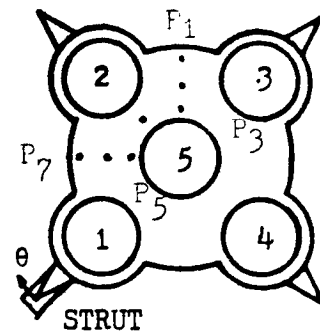
TUNNELSYM. INST.CONFIG.○ P_{1,2,3,4,5,6,7}FS₁N₁₋₅PL₁NOTE: Data are
averaged□ P_{1,2,3,4,5,6,7}FS₄N₁₋₅PL₁

FIGURE 57 Base Pressure - Engine Fairing Length Effect

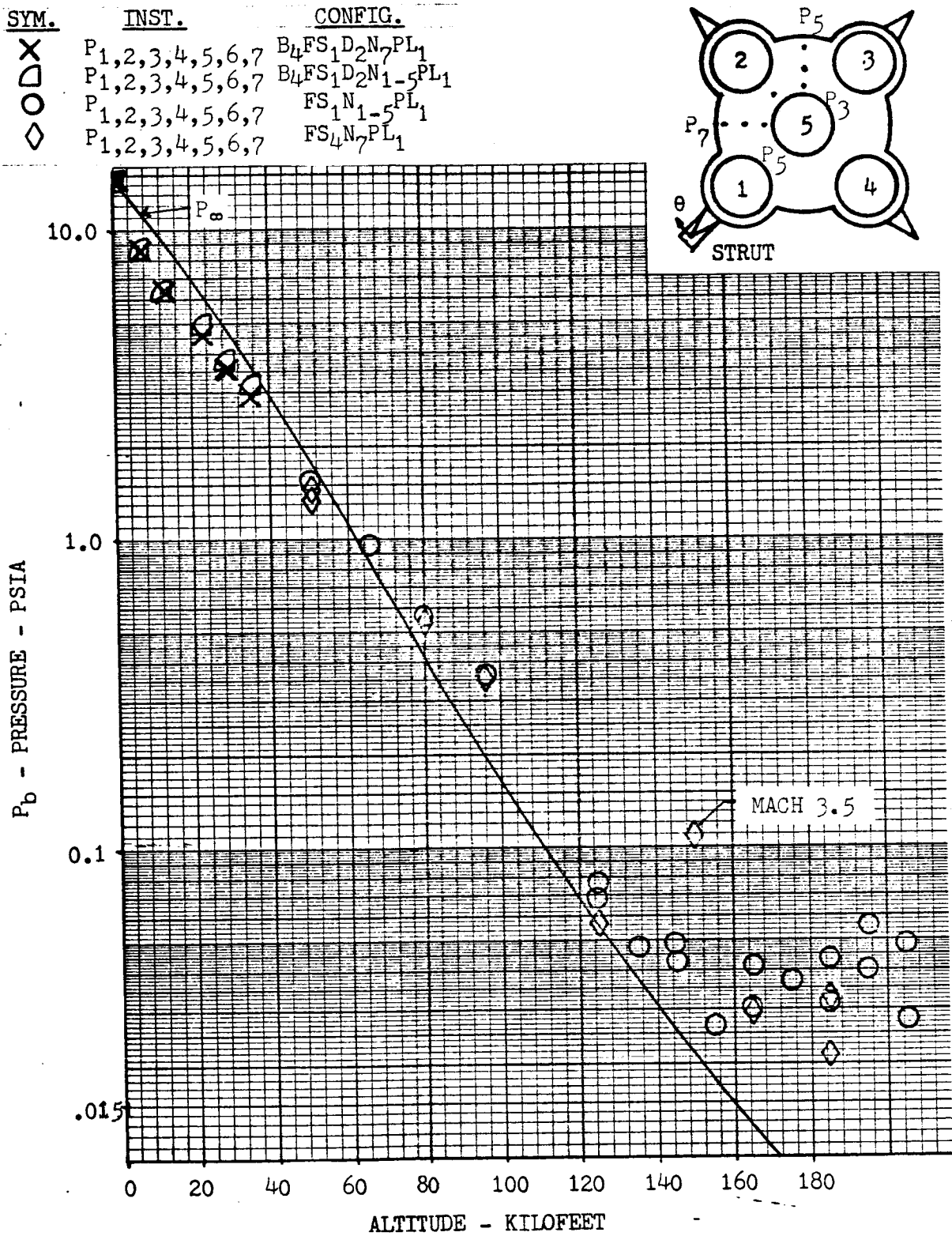


FIGURE 58 Base Pressure - Engine Out Effect

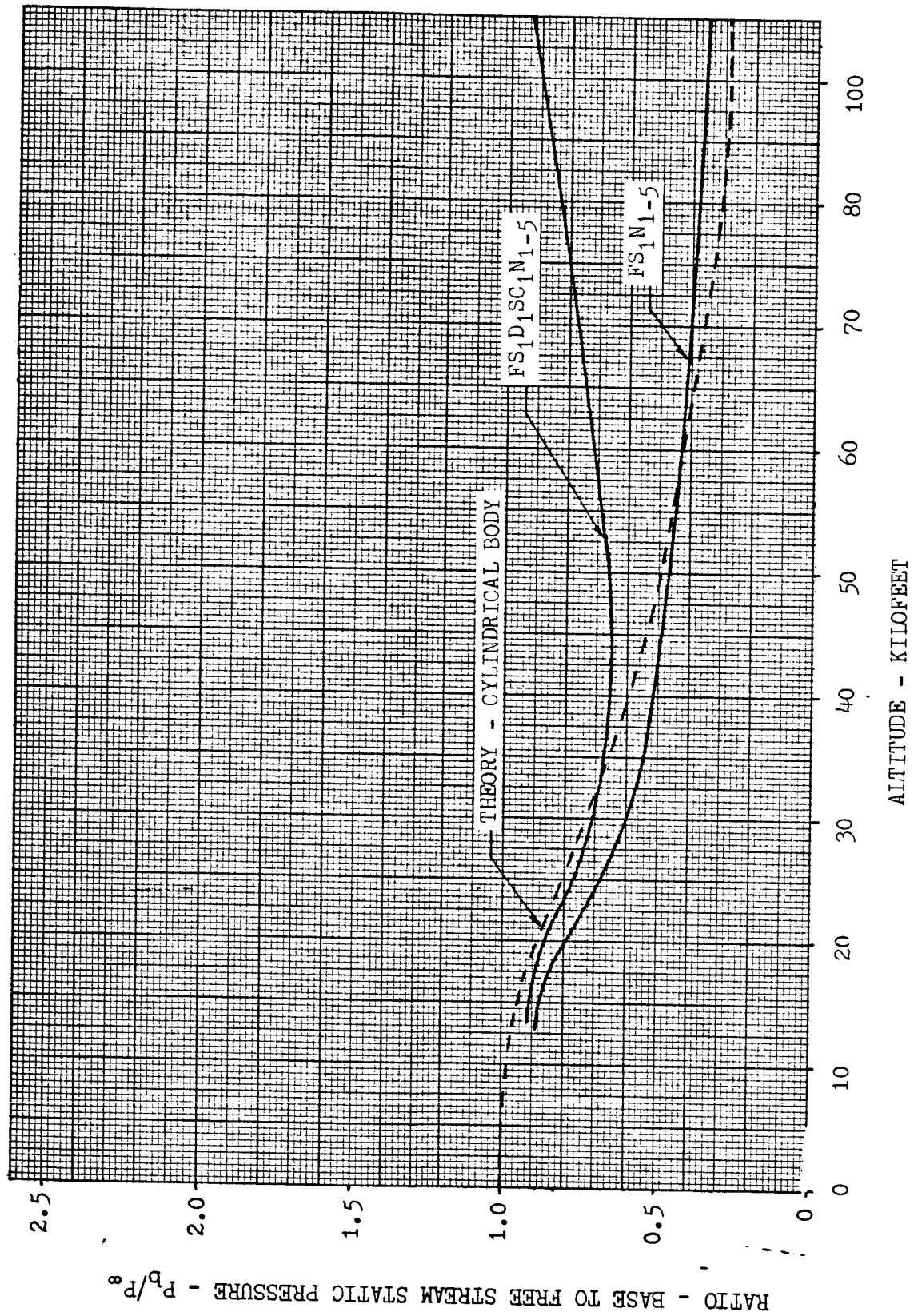


FIGURE 59 Engines Off Base Pressure Comparison

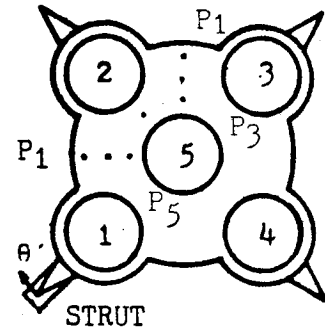
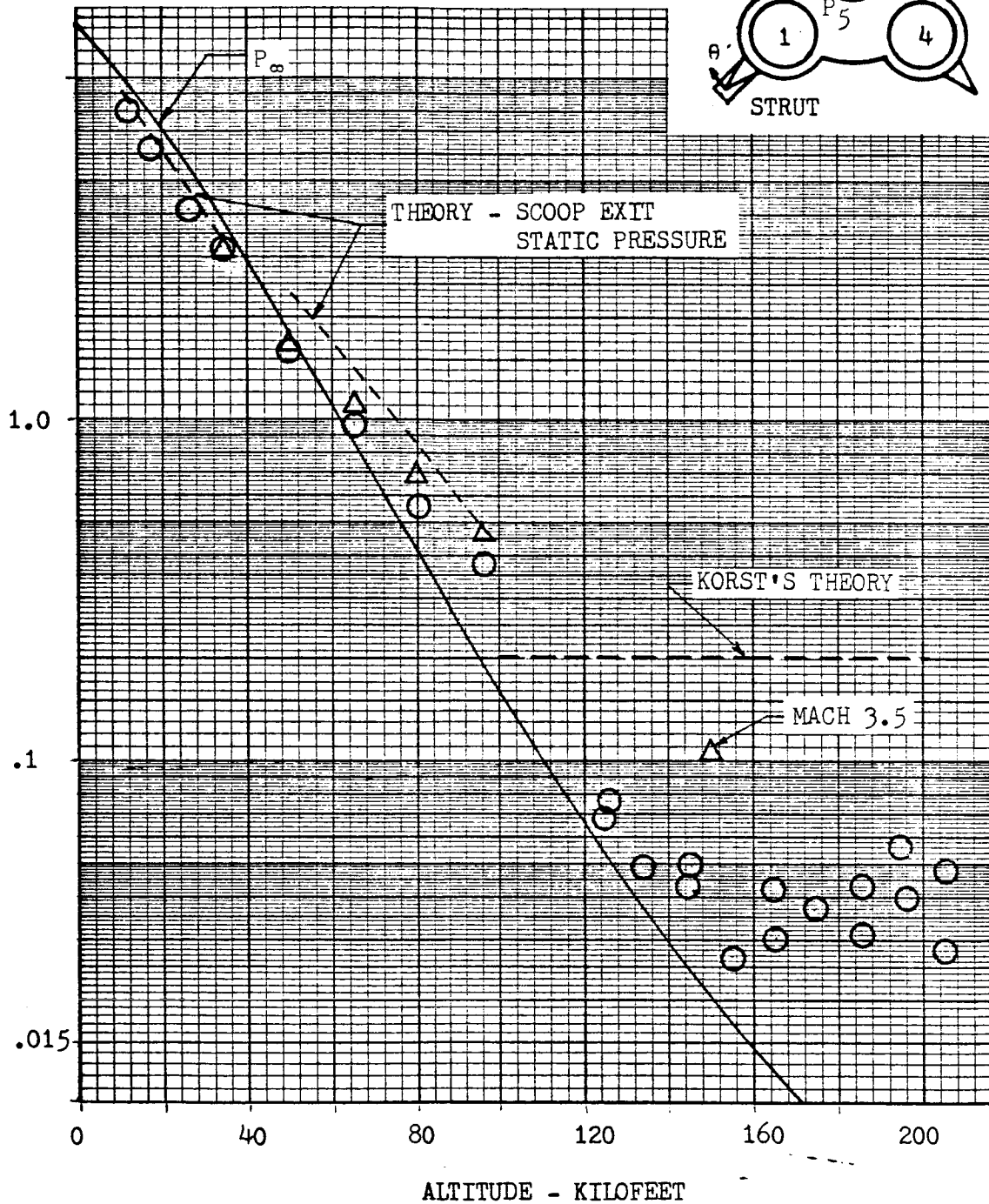
TUNNELSYM. INST.CONFIG. $P_{1,2,3,4,5,6,7}$ $FS_1 N_{1-5} PL_1$ $P_{1,2,3,4,5,6,7}$ $FS_1 D_1 SC_1 N_{1-5} PL_1$  P_b - PRESSURE - PSIA

FIGURE 60 Base Pressure Comparison with Theory

2.5 CONCLUSIONS

- a) In all three wind tunnels the measured boundary layer thickness on the body near the base of the vehicle coincides with turbulent flow theory.
- b) The trends and relative configuration effects shown by the radiation test data are representative of the S-IC prototype; the actual data magnitude is low.
- c) Hydrogen turbine exhaust does not affect radiation.
- d) Configuration changes have little if any effect on radiation.
- e) Hydrogen turbine exhaust significantly increases convective heating below 40,000 feet, has no effect for 40,000 - 100,000 feet, then slightly reduces the heating level above 125,000 feet when no scoops are present.
- f) Addition of deflectors significantly reduces convection heating. However, some evidence indicates that some base burning may exist with deflectors on.
- g) Convective heating is a minor contributor to base heating below 100,000 feet altitude unless base burning occurs. Data at Mach 3.5 at an altitude of 150,000 feet indicates that convective heating rates may be less than 4.0 BTU/FT²SEC. throughout the flight.
- h) High convection heating rates will occur on the nozzle lips above 120,000 feet. Center engine convection heating will be low except well aft on the nozzle throughout the flight. Outboard engines probably have much higher heating loads than the center engine.
- i) The base pressure essentially follows the free-stream ambient pressure to 145,000 feet. Above 145,000 feet base pressure is constant indicating that flow is outboard between the nozzles and has reached sonic velocity.
- j) Turbine exhaust has no effect on base pressure. Adding scoops and deflectors increases base pressure in the lower altitudes. A short fairing or operating with the center engine out will reduce base pressures.
- k) Hot base plate data indicates that a minimum of exhaust gases are present in the base region at low altitudes. Considerable exhaust gases reach the base at high altitudes. Results correlate with pressure and convection data.

APPENDIX A - THEORETICAL RADIATION

1.0 INTRODUCTION

The calculation procedures and references which were used to determine the theoretical radiation heating level on the model base are discussed below. Two theoretical radiation heating estimates were made. One estimate assumed all radiation experienced on the model base resulted from hot non-luminous gases in the model exhaust, and was, therefore, a lower limit for theoretical model radiation. The upper limit estimate utilized the view factors and plume characteristics made in the hot gas estimate but, assumed a heavy concentration of carbon particles and consequently an emissivity of 1.0. The hot gas estimate is described in the following paragraphs.

2.0 HOT NON-LUMINOUS GAS RADIATION

Non-luminous gases which are found in the gaseous oxygen-gaseous ethylene combustion process are water vapor, carbon monoxide, and carbon dioxide. These gases have emitting wave-lengths in the temperature range of the model exhaust. The emissivity of the gases at any location in the plume (which will directly determine the radiative heating rate at the same location) can be best determined by methods suggested by Hottel and described in detail in Reference 8.

2.1 Plume Characteristics

The plume characteristics including shape, constituents, and temperature and pressure profiles must be accurately defined.

Plume characteristics were predicted in the supersonic flight region by the method of characteristics computer program described in Reference 13. Computer calculated temperature and pressure profiles for the model plume at 51,000 feet are shown in Figures 1A and 2A respectively to illustrate typical computer results.

The computer program considers only one plume expanding to free stream pressure, and therefore cannot predict the effect of impingement or interaction with other plumes. Under sea level conditions the plume expansion is associated with mixing and afterburning. Plume interaction occurs well downstream from the nozzle exit. At higher altitudes the plumes impinge near the nozzle exit plane and the hot gas analysis based on a single plume which is not confined will be conservative (in terms of view factors). The analysis would not, however, include the effect of the increase in plume temperature or change in emissivity which will occur when the plumes interact.

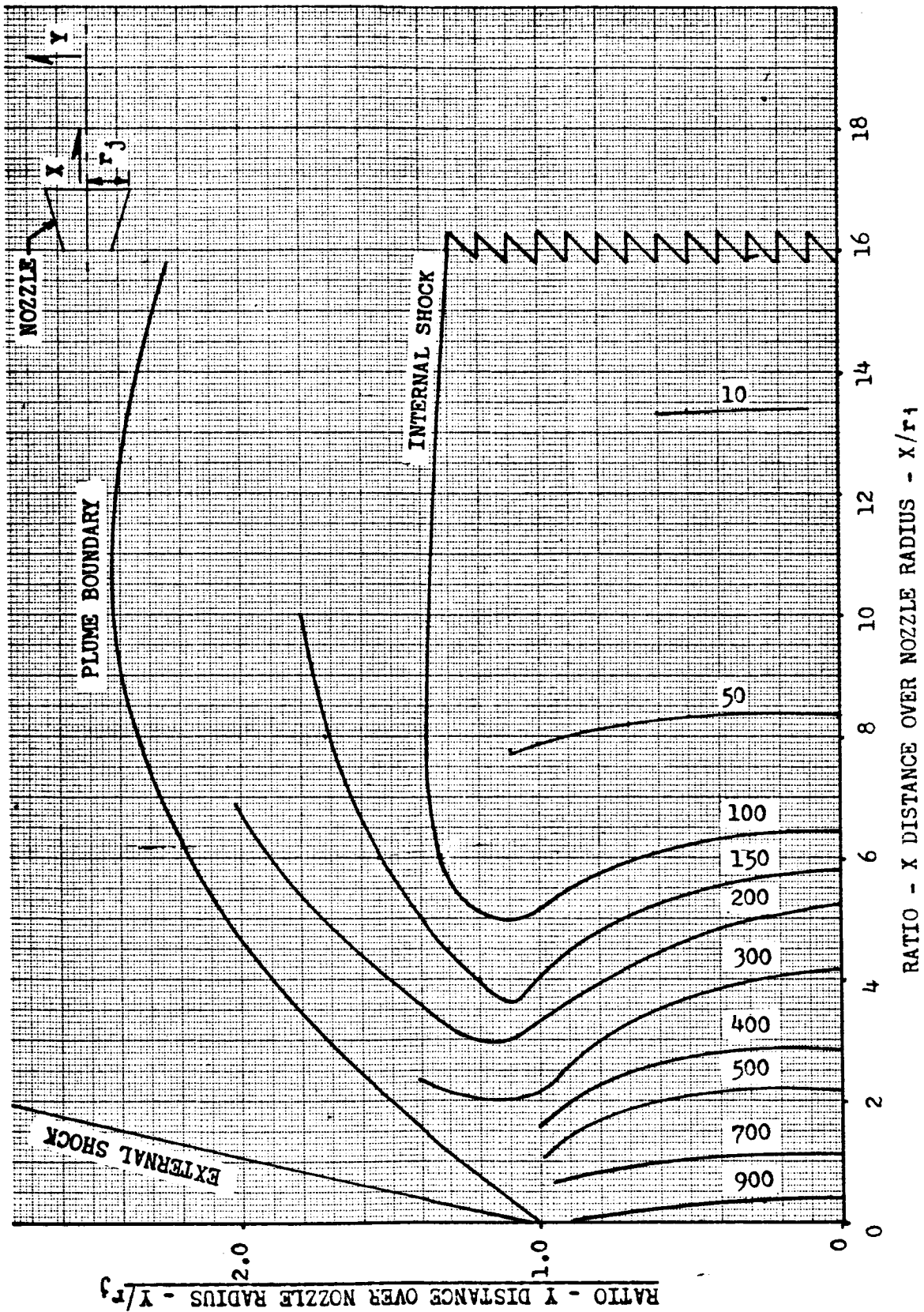


FIGURE 1A Theoretical Plume Pressure Distribution - 51,000 Feet

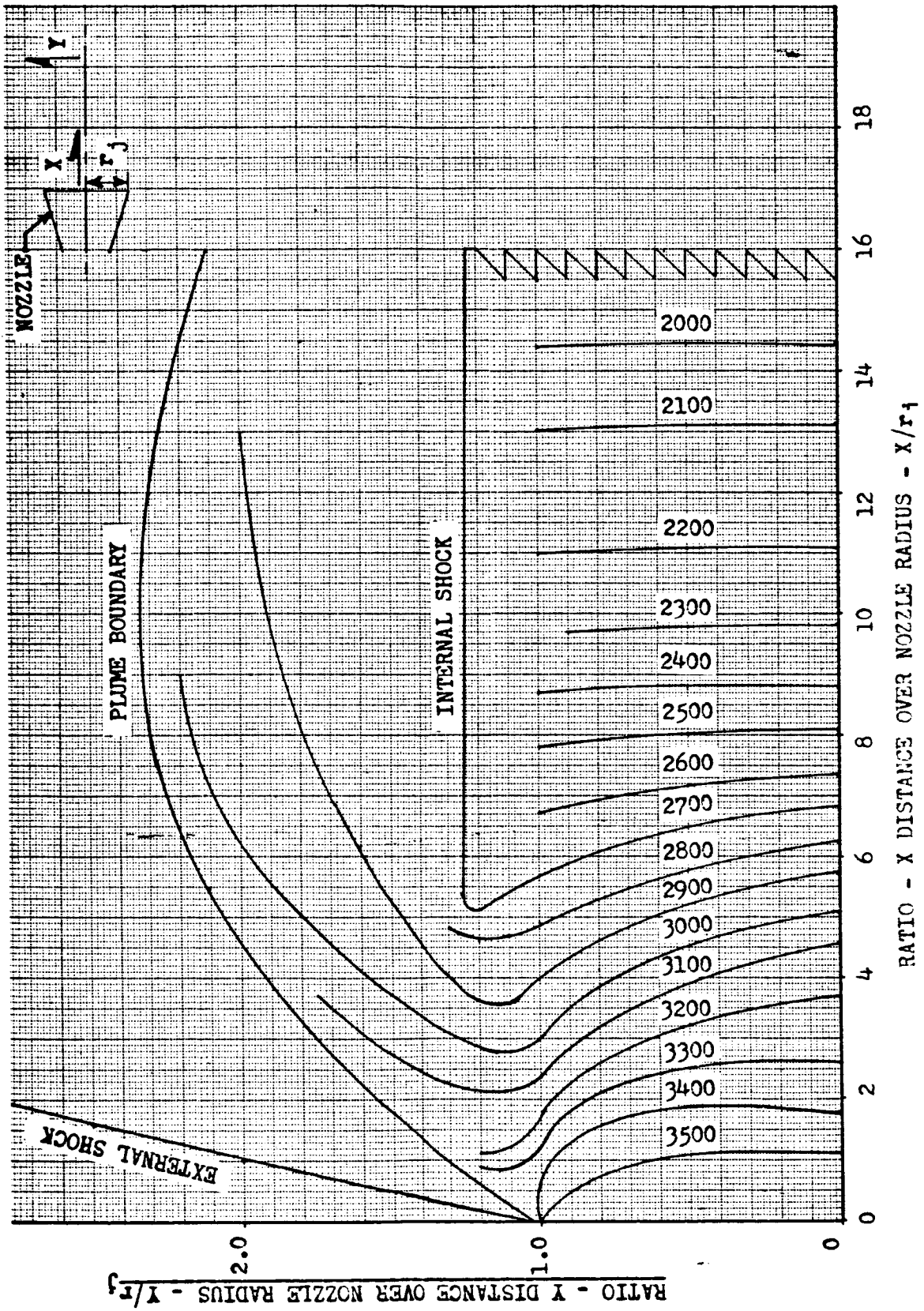


FIGURE 2A Theoretical Plume Temperature Distribution - 51,000 Feet

2.1 (Continued)

The analysis was simplified by representing the plumes with analytical models made up of several cylindrical sections. The sea level plume was represented by a cylinder with a diameter equal to the model nozzle exit diameter. The total plume cylinder was further divided into four smaller cylinders as shown in Figure 3A. An average temperature for each subcylinder was determined theoretically assuming an inviscid flow field without afterburning. All cylinders of the sea level plume were assumed to have a pressure of one atmosphere.

Analytical models for plumes at higher altitudes were made up of stacked cylinders of varying diameters. By simulating the analytical plume (Figures 1A and 2A) in terms of cylinders and annulus areas, the view factors could be determined by a simplified method.

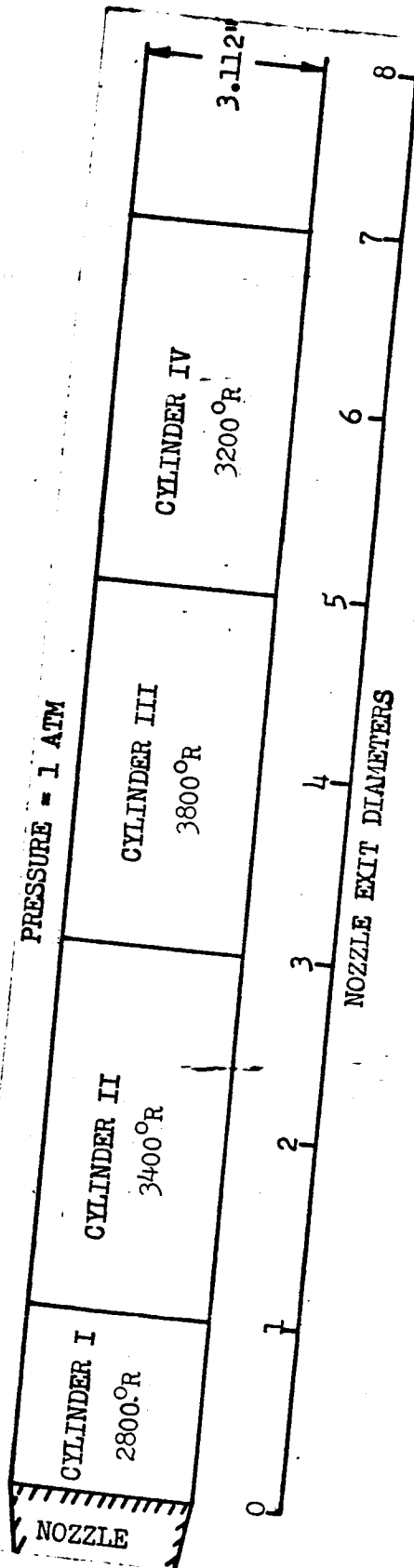
2.2 View Factors

View factors, from a point on the base to each cylinder of all five model plumes, were determined by the "Unit Sphere Method" suggested by Herman and Nusselt and outlined in Reference 14. This method was applied to both the single diameter cylinder of the sea level plume and the varying diameter cylinders of the higher altitude plumes.

2.3 Emissivity

The emissivity of the non-luminous gases for each cylinder was determined by knowing the mean beam length, the partial pressure of each of the non-luminous gases, and the cylinder average temperature. The mean beam length (L), or emission length for an infinite cylinder is equal to the cylinder (plume) diameter. The partial pressure of each constituent gas in the plume is proportional to the mole fraction of each gas to the total exhaust mass. The product of the partial pressure (P_c) and mean beam length (L) are used with the average temperature of the plume cylinder to determine the gas emissivity using the curves of Reference 15.

Drop-off in the hot gas radiation curve (lower limit) reflects the decrease in emissivity and change in view factors that result as the altitude is increased.



VIEW FACTORS

	CYLINDER I	CYLINDER II	CYLINDER III	CYLINDER IV
0	.838	.02987	.00683	.00276
210	.05734	.03246	.00956	.00399
225	.05863	.02062	.00556	.00244
225	.04915	.02020	.00491	.00196
270	.04298	.01292	.00255	.00099
225	.04364			

PRODUCTS OF COMBUSTION

	%
H ₂ O	33.4
CO	34.9
CO ₂	35.1

CYLINDER	EMISSIVITY
I	.053
II	.0733
III	.1092
IV	.0323

FIGURE 3A Radiation Plume Analytical Model - Sea Level

2.4 Radiative Heating

Each cylinder's contribution to the total hot gas radiation heating rate at a point on the base was calculated using Equation 1 below,

$$q_r = F \sigma \epsilon T^4 \quad \text{Equation 1}$$

The total radiation from the model plumes may be represented by Equation 2.

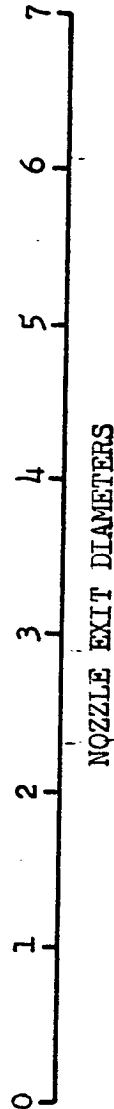
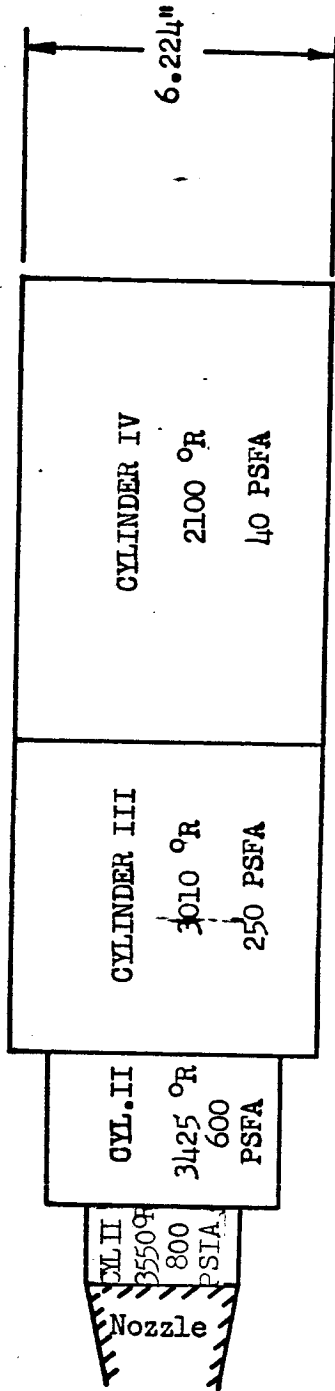
$$q_{rt} = \sum_{n=1}^n F_n \sigma \epsilon_n T_n^4 \quad \text{Equation 2}$$

Where n refers to each cylinder division of plume. View factors, emissivities and temperatures for the sea level plume and the plume at 51,000 feet are shown in Figures 3A and 4A.

3.0 HOT LUMINOUS GAS RADIATION

The luminous gas radiation calculations (upper limit) were made using the temperatures used in the non-luminous gas calculations and assuming at sea level that the emissivity is one.

A sea level radiation calculation was then made assuming the plume shape shown in Figure 3A. S-I Block II flight data was then used to predict the drop-off in radiation with altitude as shown in Figure 5A since the decrease in emissivity could not be determined.



VIEW FACTORS

	r/R	CYLINDER I	CYLINDER II	CYLINDER III	CYLINDER IV
210	.838	.03676	.08219	.02021	.00124
225	.900	.03795	.10524	.00587	.00071
225	.650	.03300	.10446	.00449	.00000
270	.450	.02739	.06410	.02634	.00263
225	.400	.03041	.09166	.01060	.00008

PRODUCTS OF COMBUSTION

PRODUCTS OF COMBUSTION	%	CYLINDER	EMISSIVITY
H ₂ O	33.4	I	.00516
CO	34.9	II	.00547
CO ₂	15.1	III	.00341
		IV	.00863

FIGURE 4A Radiation Plume Analytical Model - 51,000 Feet

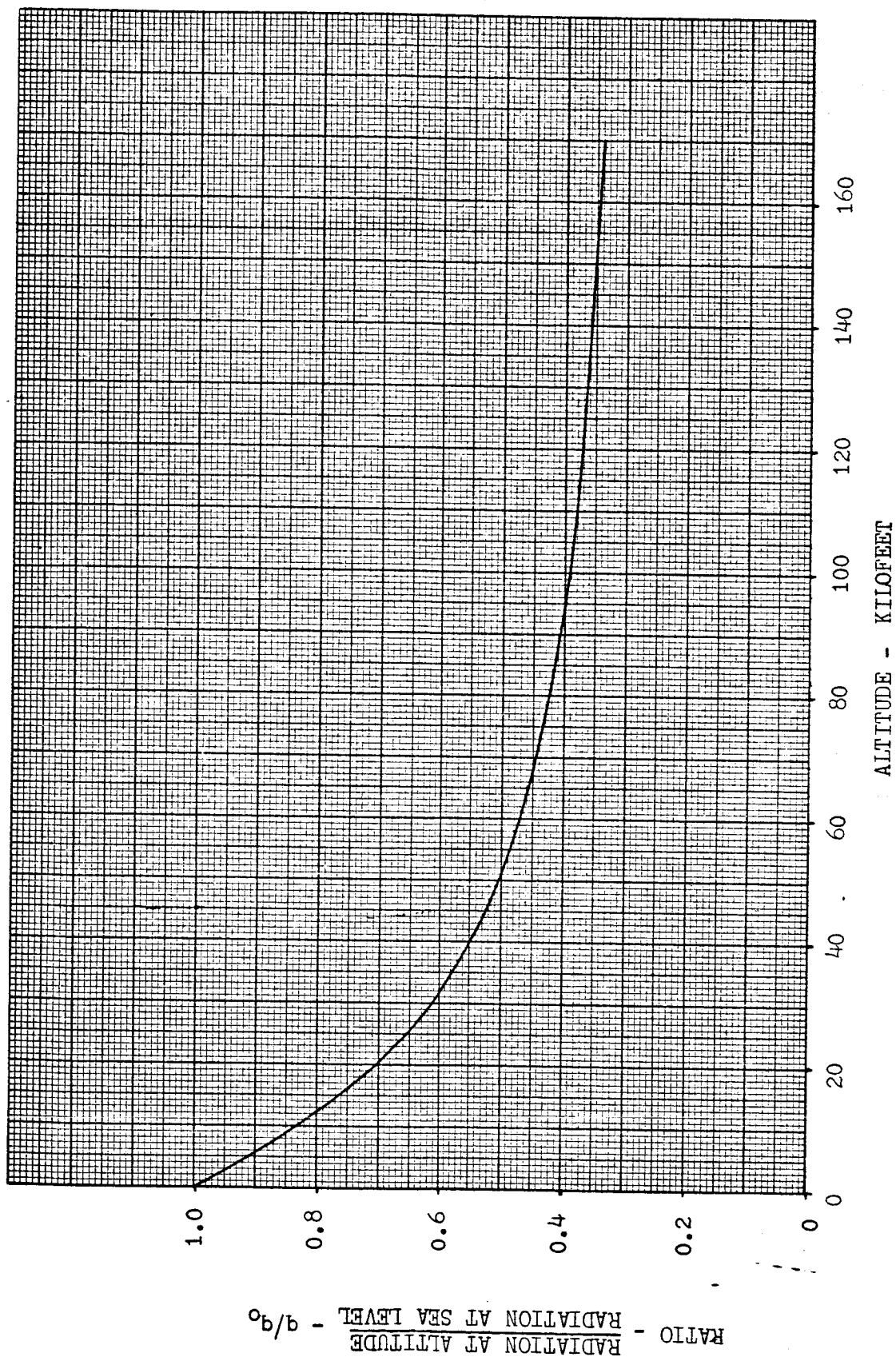


FIGURE 5A S-IC Base Region Altitude Radiation Variation

APPENDIX B - THEORETICAL CONVECTIVE HEATING

1.0 INTRODUCTION

The convective heating rate is a function of the base gas temperature, heat transfer coefficient and wall temperature. The base gas temperature is difficult to predict theoretically but is near the free stream air temperature at the low altitudes and some fraction of the engine stagnation temperature at the high altitudes. The heat transfer coefficient is also very difficult to define; however, a stagnation point calculation is made for comparison purposes. The wall temperature of the base and components was approximately 70°F during the model tests and is used for the theoretical calculations. Convective heating calculations are made for a no-scoop configuration and a scoop configuration.

2.0 SCOOPED AIR

The mass of air scooped into the base region by the 10 percent scoops was obtained from Figure 10 Reference 16 and shown in Figure 1B. Calculations are made for the CAL 8 by 8, Lewis 8 by 6, and Lewis 10 by 10 tunnel. Reductions in the mass flow due to the scoops being immersed in a turbulent boundary layer and friction in the scoops are considered.

The free stream temperature and Mach number of the three test facilities are used in Equation 1 to determine the necessary temperature of the scooped air in the base, assuming $\gamma = 1.4$ for air and a recovery factor of 1.90 for turbulent flow.

$$T_{\text{air}} = T_{\infty} \left(1 + \frac{\gamma - 1}{2} M^2 \right) \quad \text{Equation 1}$$

Figure 2B shows the air temperature calculated for the CAL 8 by 8 tunnel and the Lewis 10 by 10 tunnel.

3.0 RECIRCULATED GAS

The amount of recirculated exhaust gas from the engines is estimated using compressible two-dimensional jet mixing theory developed by Korst (Reference 17). Model parameters are used in the base heating computer program which is modified to simulate a five engine configuration. The program computes only the recirculated gas in the center area. These calculations do not consider recirculation due to the external air impinging on the jet exhaust. Figure 3B shows the recirculated gas flow for the configurations with and without scoops in the Lewis 10 by 10 foot Supersonic Wind Tunnel and with no external flow in the high altitude chamber. Theory predicts no recirculated mass into the base region in the test range of the Lewis 8 by 6 or CAL 8 by 8 wind tunnels.

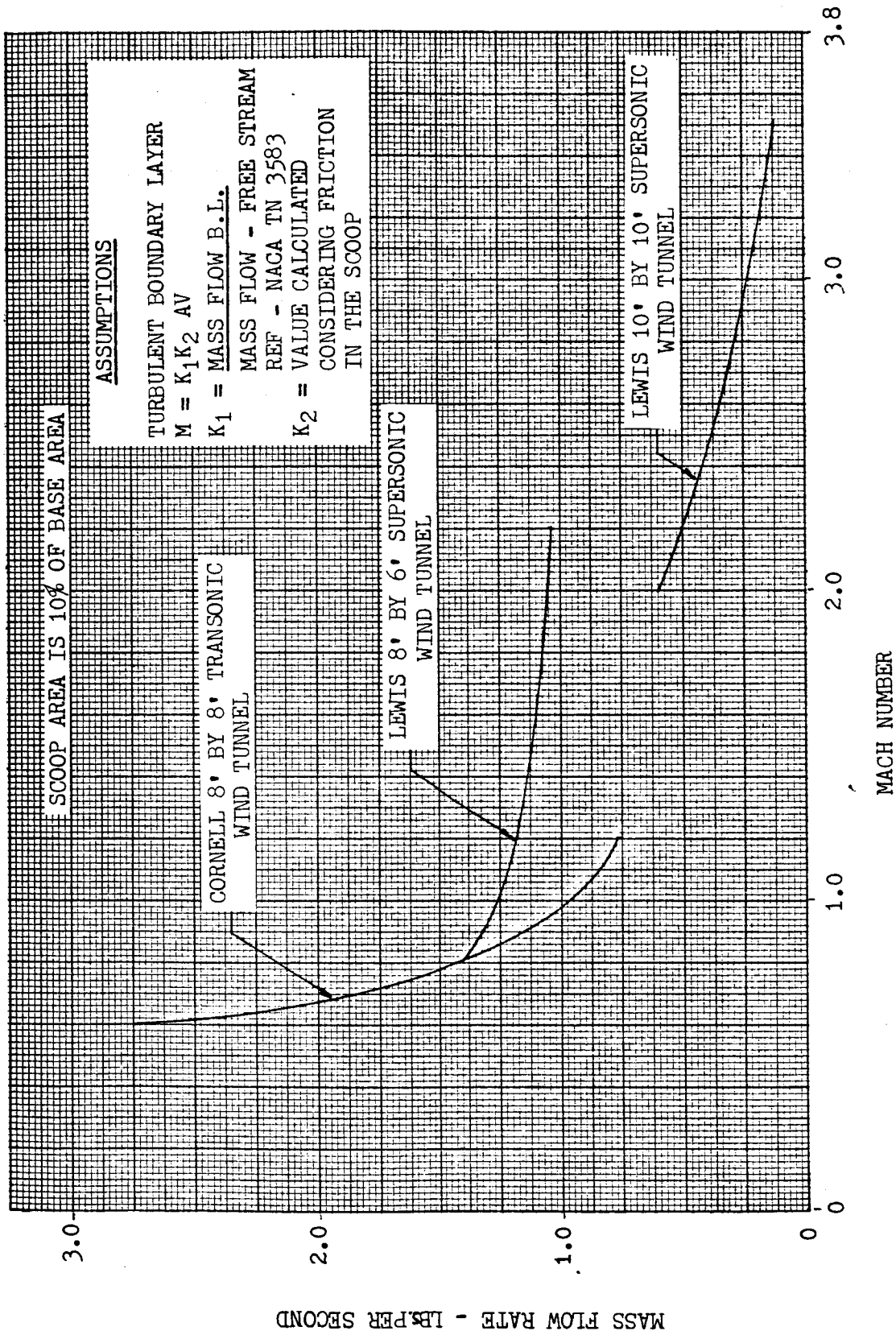


FIGURE 1B Mass Flow of Air Into Base

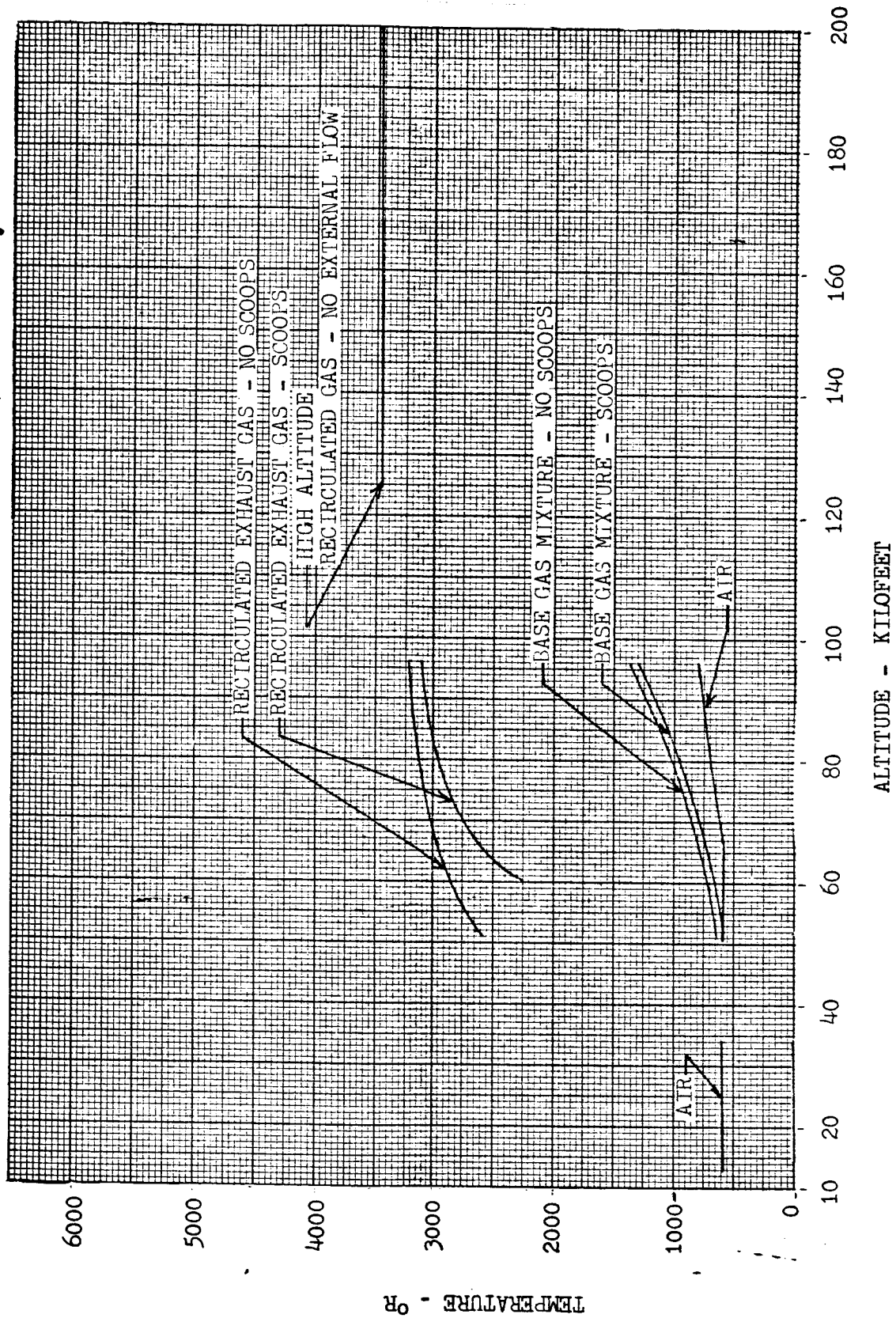


FIGURE 2B Theoretical Base Gas Temperature

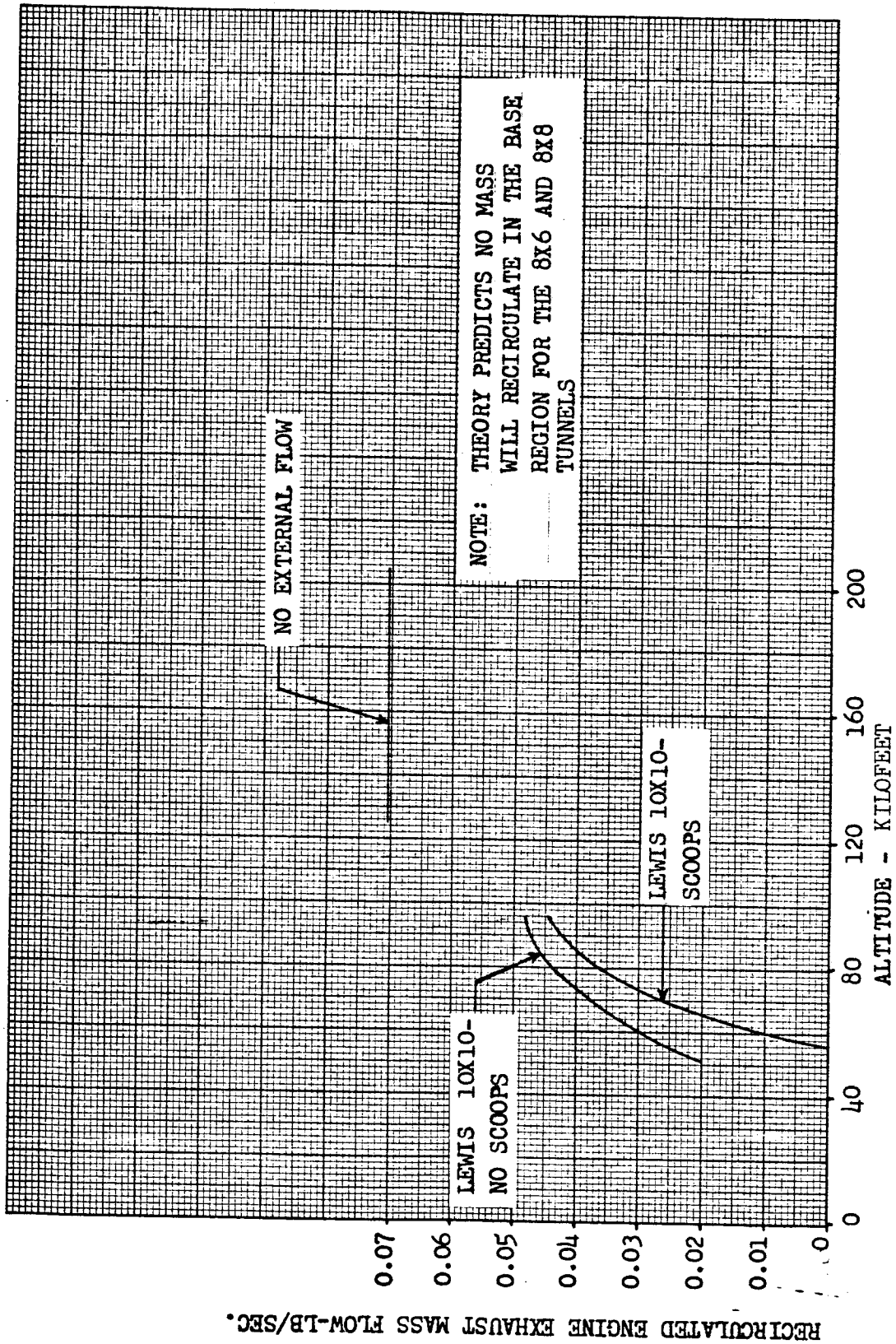


Figure 3B Theoretical Recirculated Gas Flow

3.0 (Continued)

The recirculated gas temperature is estimated using the recirculated mass flow and assuming that this mass originates from the nozzle boundary layer. Nozzle boundary layer calculations using turbulent boundary layer equations and assuming heat transfer are made. The total temperature in the boundary layer is then evaluated using Equation 2.

$$\frac{T_o - T_w}{T_{o\infty} - T_w} = \left(\frac{Y}{\Delta}\right)^{1/p} \quad \text{Equation 2}$$

The boundary layer calculations evaluated Δ to be .0219 feet at the model nozzle exit and p is 5.68. (Δ is the momentum thickness.)

It is assumed that 1/8 of the mass being recirculated is originating from each of the four outboard engines and 1/2 originates from the center engine. Boundary layer mass flow is integrated from the nozzle surface to a point in the boundary layer which produces the predicted mass flow from jet mixing theory. (See Figure 38.) The temperature of the gas over this integrated mass is averaged to produce the recirculated gas temperature. This gas temperature is shown in Figure 2B.

4.0 BASE GAS TEMPERATURE

The gas in the base region of the model consists of a mixture of the recirculated exhaust products and scooped air, each at different temperatures. The percent of air and recirculated gas in the total mixture is shown in Figure 4B as a function of altitude and configuration. Complete mixing of the air and the recirculated mass resulted in the mixture recovery temperature shown in Figure 2B.

5.0 HEAT TRANSFER RATE

Van Driest's equation for the stagnation point heating rate (Reference 18, equation 3) for subsonic as well as supersonic flow is used to make convective base heating rate calculations.

$$q_{con} = \frac{0.570}{Pr^{0.6}} \sqrt{\frac{4 V_{\infty}}{D}} \rho_{\infty} \mu_{\infty} C_p (T_r - T_w) \quad \text{Equation 3}$$

and

Pr = Prandtl No. (.833)
 V_{∞} = Base Gas Velocity
 D = Base Diameter
 ρ_{∞} = Base Gas Density
 μ_{∞} = Base Gas Viscosity
 C_p = Base Gas Specific Heat
 T_r = Base Gas Temperature
 T_w = Wall Temperature

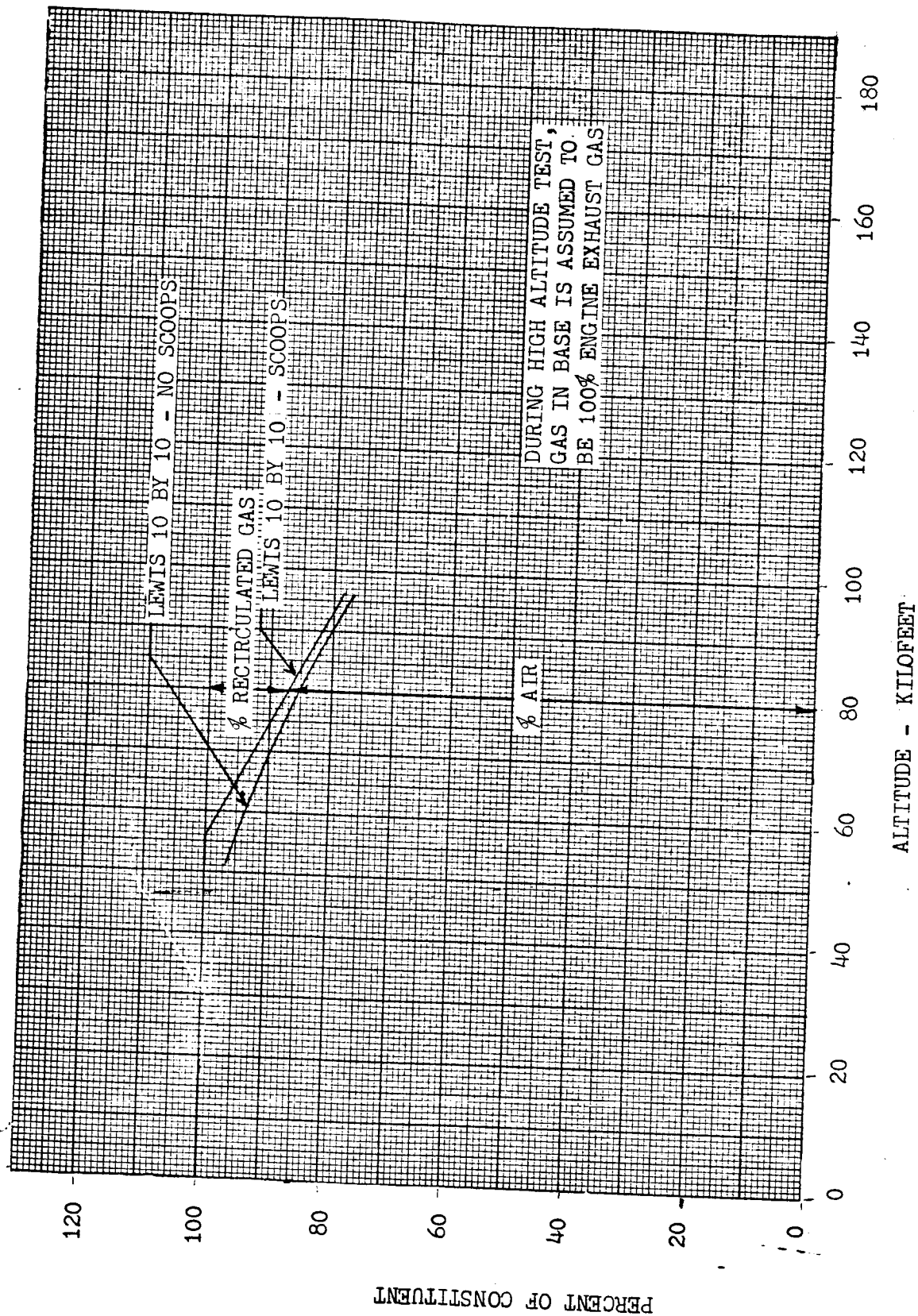


FIGURE 4B Percent of Air and Recirculated Gas in Base Region - Theoretical

5.0 (Continued)

It is assumed that the flow Mach number toward the base is one. The gas velocity is then evaluated using the recirculated gas temperature and calculating the speed of sound. The density is calculated using the measured base pressure for the appropriate altitude and configuration (Figure 56) and the base gas temperature. D is assumed to be 8.8 inches, the model base diameter. C_p and Pr are assumed constant.

Equation 3 is evaluated using base properties with and without scoop configurations and this evaluation is shown in Figure 5B.

The assumption of Mach 1 flow toward the base is expected to agree reasonably well with high altitude data but is used only for comparison in the low altitude range.

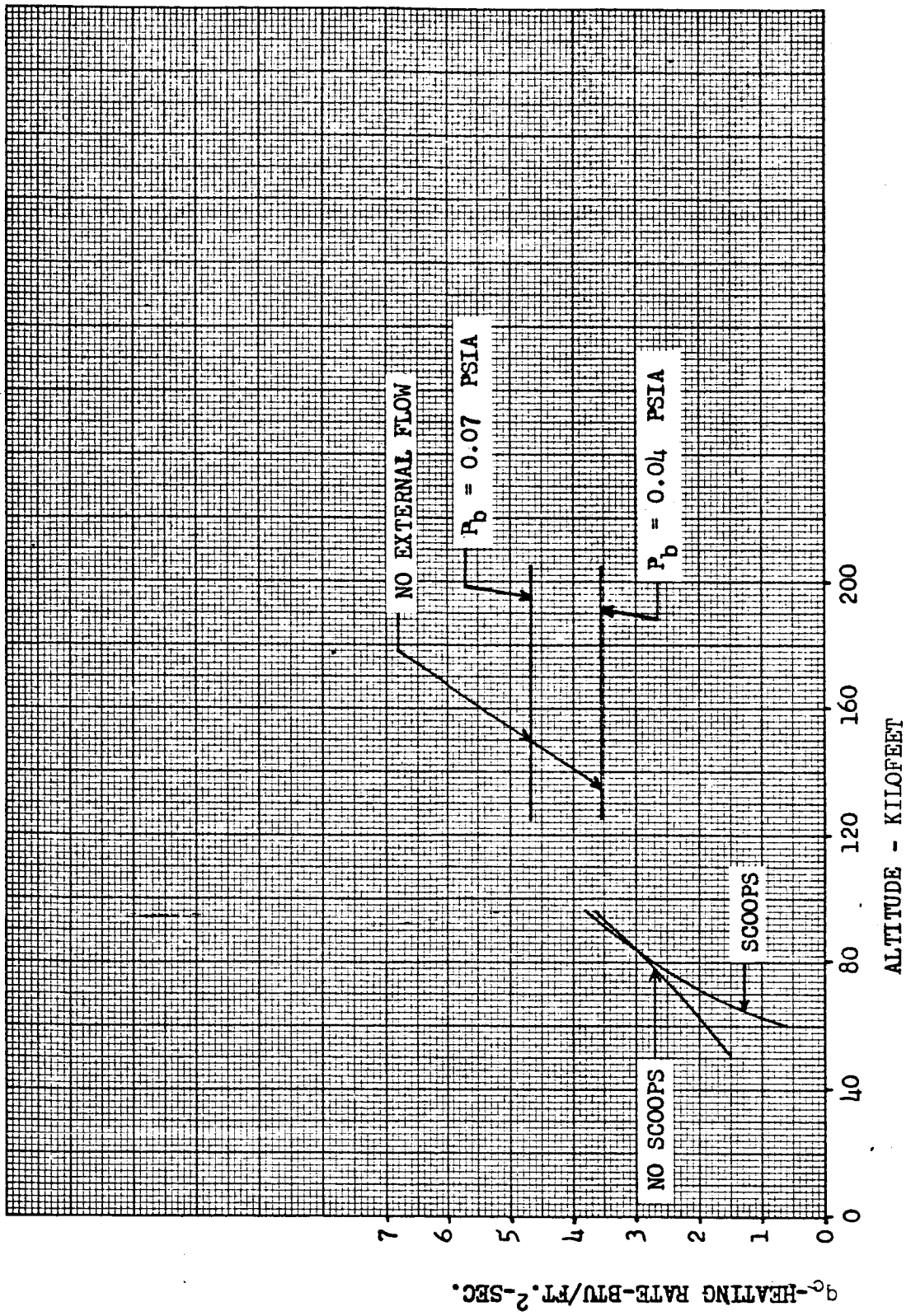


Figure 5B Theoretical Convective Heating Rate

APPENDIX C - THEORETICAL BASE PRESSURE

1.0 INTRODUCTION

Theoretical base pressure calculations are made for the "engines-off" condition as well as engines on. The "engines-off" calculation is made using empirical base pressure coefficient data from unpublished data and a procedure reported in Reference 19. The "engines-on" base pressure calculations are made using the scoop exit static pressure at low altitudes and Korst's reduced Mach number concept (Reference 17) at high altitude.

2.0 ENGINES OFF

The "engines-off" base pressure is shown in Figure 1C and is calculated using the base pressure coefficient shown in Figure 2C. The base pressure coefficient is for a short circular cylinder and is based on an accumulation of experimental data from Mach 0 to 3.0. The coefficient above Mach 3.0 is based on the equation,

$$C_{pb} = - \frac{1}{M_{\infty}^2}$$

3.0 ENGINES ON

3.1 Flow Deflector Exit Static Pressure

The flow deflector exit pressure is calculated for comparison with model test data at low altitudes. The procedure used is the same as outlined in References 20 and 21. Figure 3C, 4C and 5C are used to determine the average scoop inlet total pressure, average scoop inlet Mach number and scoop exit ~~total~~ pressure. Assuming the exit Mach number is equal to the inlet Mach number, the exit static pressure can then be evaluated. The boundary layer thickness on the cylindrical boundary near the base is obtained from Paragraph 2.1 (experimental data) and divided into 0.375 inches to produce the r/δ ratio. The scoop height (r) for the 10 percent scoops is 0.375 inches.

Figure 6C shows the flow deflector exit static pressure plotted as a function of altitude assuming a friction factor, $4 fL/D$, equal to 0.15.

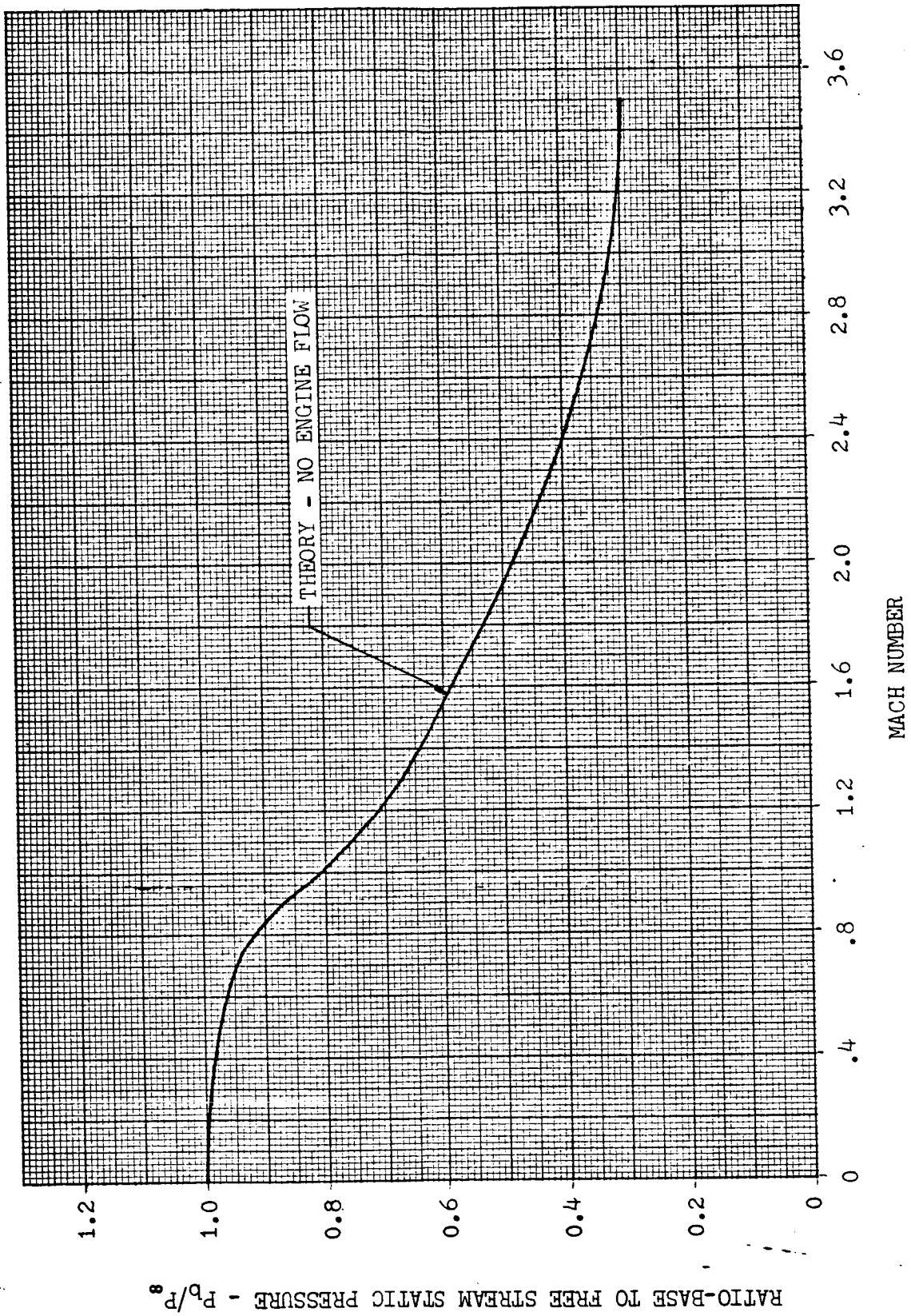


FIGURE 1C No Engine Flow Base Pressure

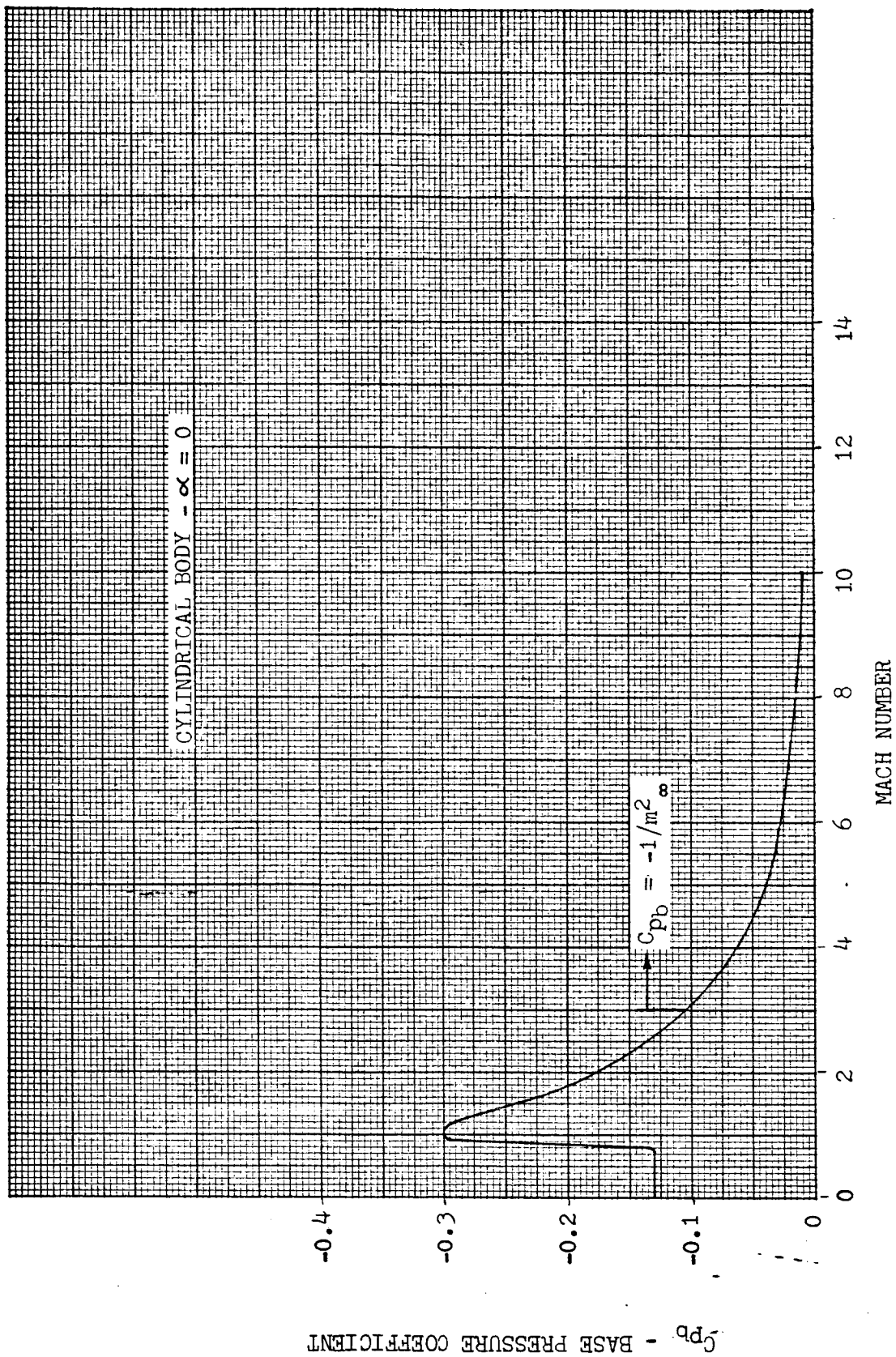


FIGURE 2C Theoretical Base Pressure Coefficient

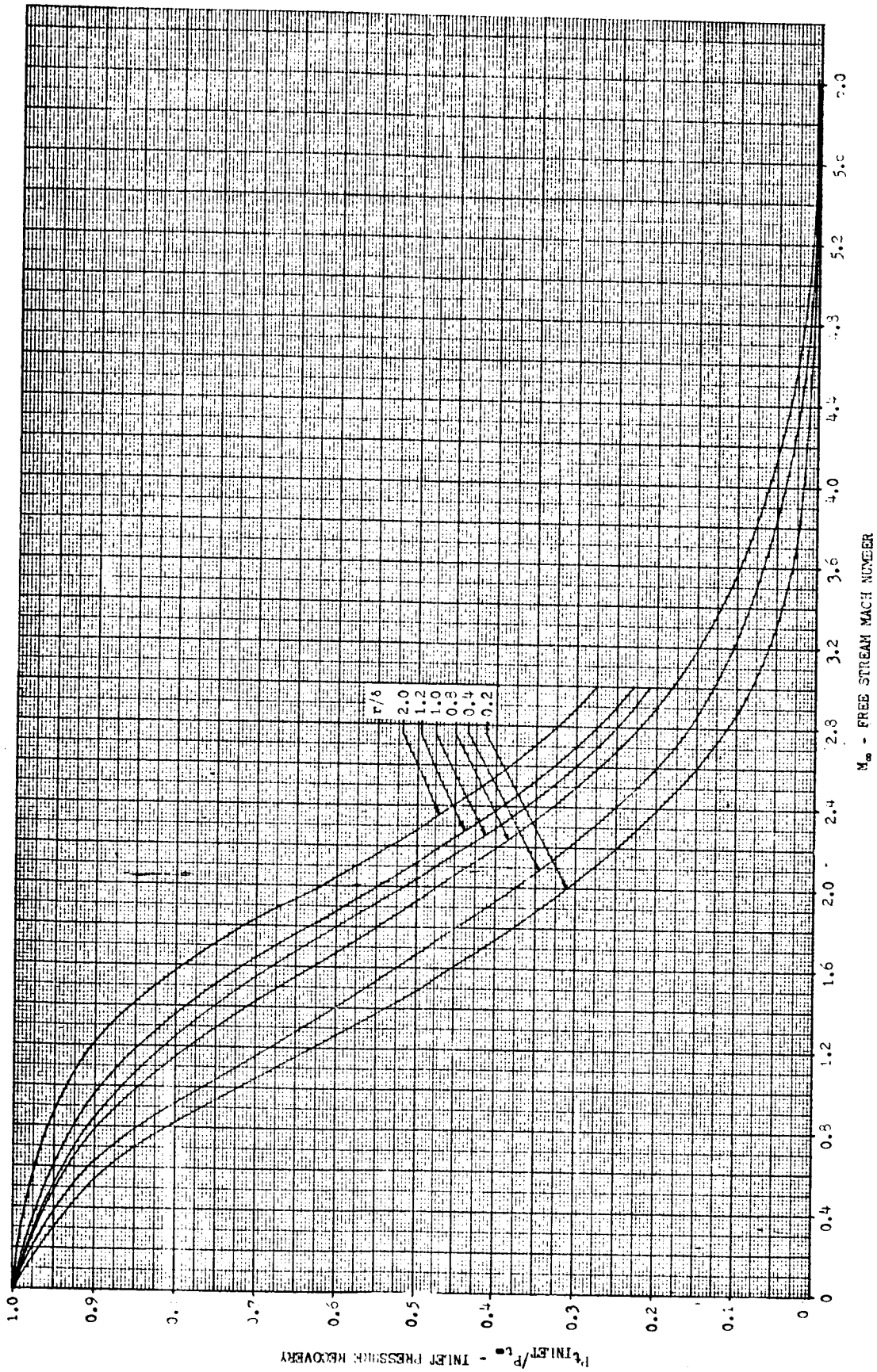


FIGURE 3C Average Inlet Total Pressure

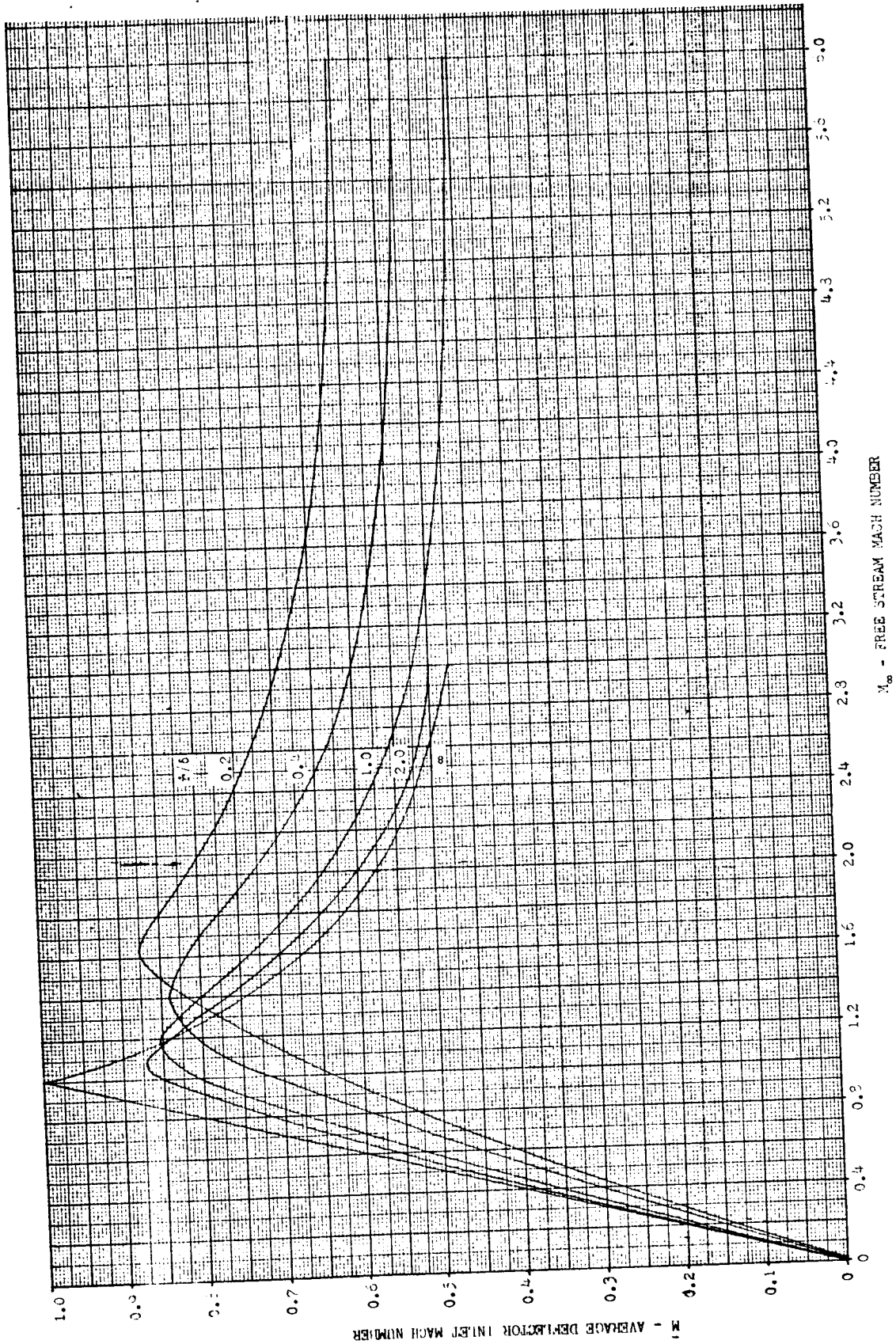


FIGURE 4C Average Deflector Inlet Mach Number

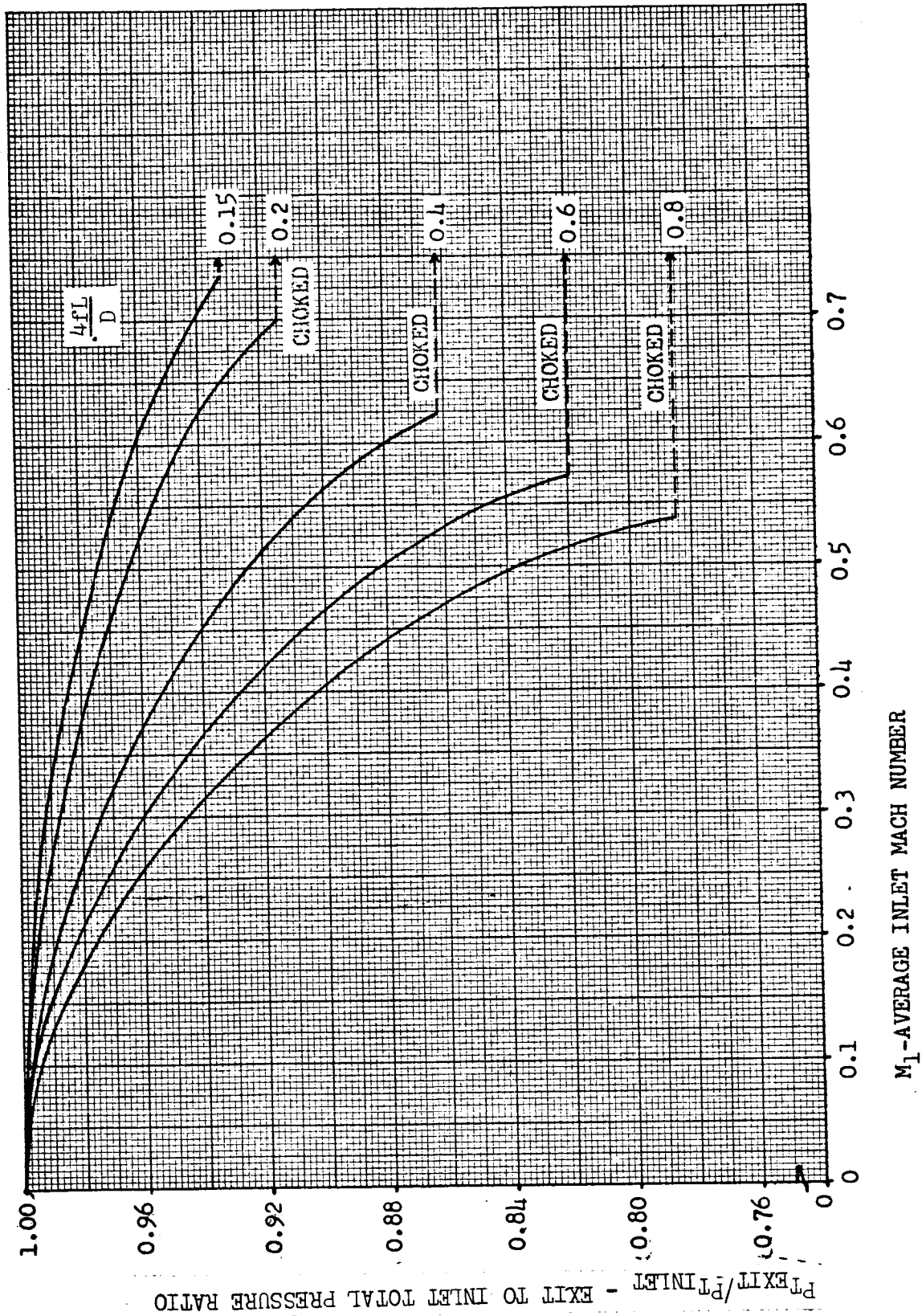


FIGURE 5C Flow Deflector Total Pressure Ratio

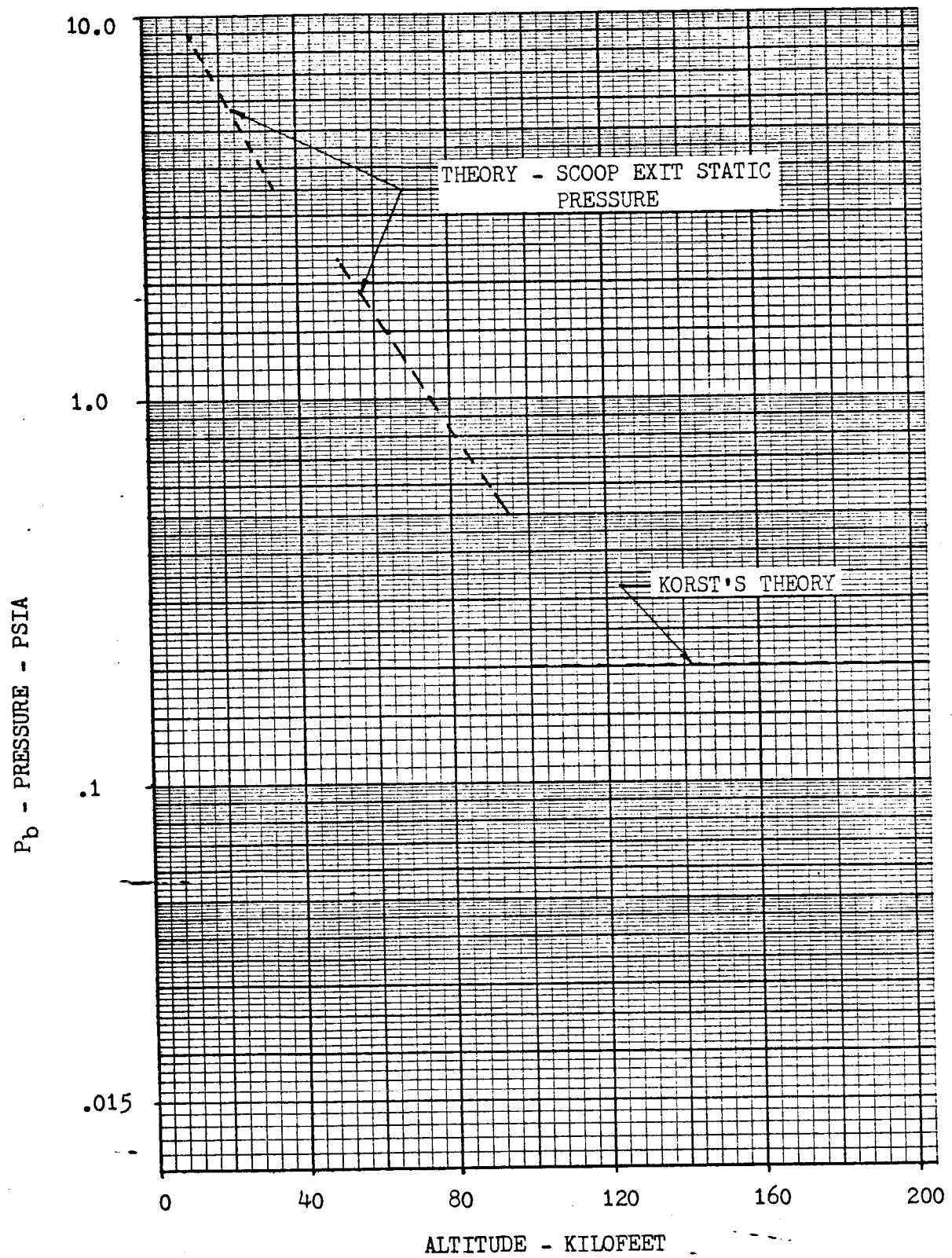


FIGURE 6C Theory Base Pressure

3.2 Korst Theory

In Korst's theory a two-dimensional back step model is used. In analyzing supersonic flow past the back step, the following assumptions are made:

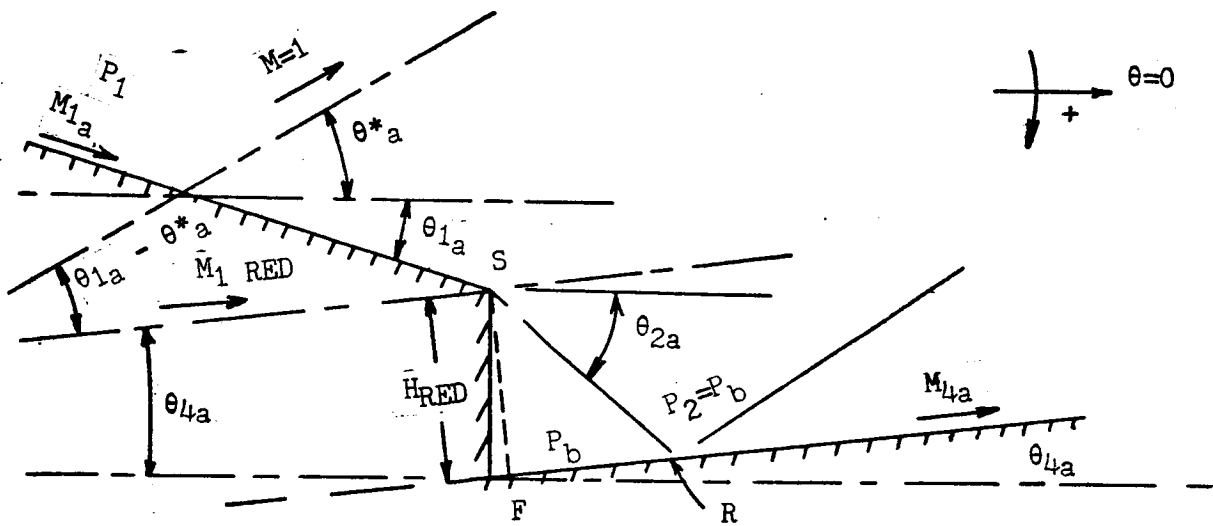
- a) The inviscid flow configuration near the wake is produced without external interference. The expansion around the corner is then represented by the Prandtl-Meyer solution and the boundary of the corresponding inviscid jet will be straight.
- b) The exact configuration of the rear facing wall within reasonable limits, is of no consequence to the inviscid flow solution.

Under these assumptions it is possible to formulate a generalized approach to the back-step problem by the reduced Mach number concept. This is not only possible for application of the restricted theory, but also for initially disturbed mixing regions if the latter are given or determined behind the corner expansion.

The generalization of the single supersonic back-step problem by means of the reduced Mach number concept is illustrated in Figure 7C. This theory has been programmed and is known as the 3D Base Heating Computer Program.

To calculate the recirculated mass flow using Korst theory, the step height and the mixing width must be known. The step height and mixing width are calculated using a mean interference method suggested by Goethert (Reference 22). This average impingement point is equal to $4/\pi$ times the distance at which impingement first occurs. The mixing width is then also calculated using this value. This method applied to the S-IC configuration is shown in Figure 8C. The resultant base pressure is shown in Figure 6C.

The base pressures calculated are considered stagnation pressure, and therefore, are the maximum pressures that occur in the base region. The base pressure is assumed constant over the entire base. These theoretical calculations are only valid after jet impingement has sealed the area between three engine plumes, which is estimated at 76 seconds of S-IC flight time. Either experimental data or another theoretical method is necessary to complete the analysis from sea level to the point of recirculation.



WHERE:

$$M_{1 \text{ RED}} = f \left[M_{1a}, \left[(\theta_{1a} - \theta^*_a) - (\theta_{1a} - \theta_{4a}) \right] \right]$$

$$P_2/P_1 = (P_2/P_1 \text{ RED})(P_1 \text{ RED}/P_{Oa})/(P_1/P_{Oa})$$

$$P_1 \text{ RED}/P_{Oa} = f \left[M_{1 \text{ RED}}, P_1/P_{Oa} \right]$$

$$P_b/P_1 \text{ RED} = P_2/P_1 \text{ RED} = f \left[M_{1 \text{ RED}} \right]$$

FIGURE 7C Reduced Mach Number Concept for Flow Past a Generalized Back Step

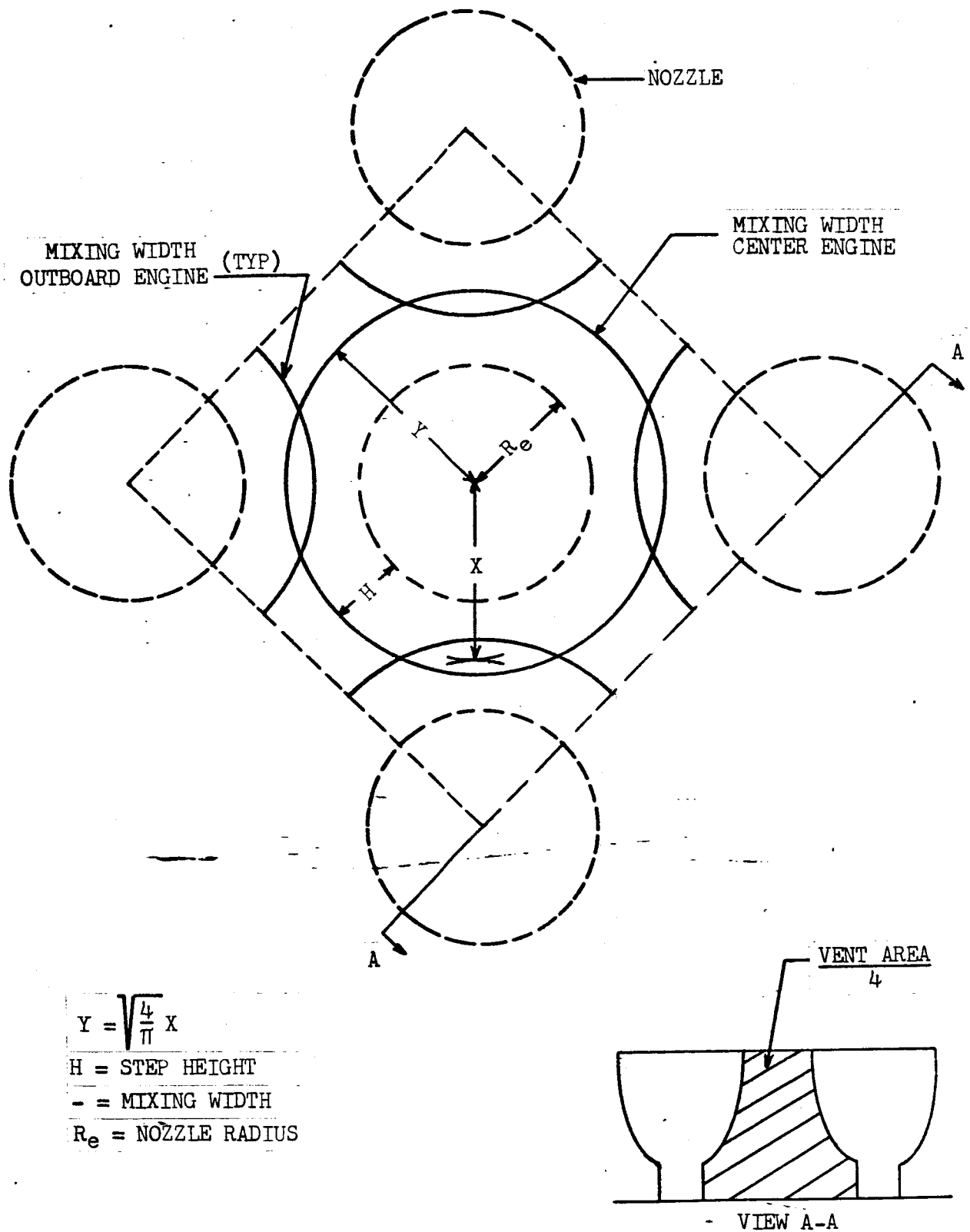


FIGURE 8C Mixing Width and Step Height for the Theoretical Pressure Calculation

REFERENCES

1. Czeck, E. A., "An Investigation of the Base Environment of the Saturn S-IC Booster at Low Altitudes Using Short Duration Experimental Techniques," CAL Technical Report No. HM-2045-Y-2, February 1966.
2. "The Application of Short Duration Techniques to the Experimental Study of Base Heating," CAL Technical Report No. HM-1510-Y-1(I), April, 1962.
3. Hendershot, K., Llinas, J., "S-IC Model Combustor Development," CAL Internal Memo No. AHRD-PS-64-11, August, 1964.
4. Vidal, R. J., "Transient Surface Temperature Measurements," CAL Report No. 114, March 1962.
5. Skinner, G. T., "Analog Network to Convert Surface Temperature to Heat Flux," CAL Report No. 100, February 1960.
6. Bogdan, L., "Measurement of Radiative Heat Transfer with Thin-Film Resistance Thermometers," CAL Report No. HM-1510-Y-9, July 1963.
7. Bogdan, L., "Heat Transfer Instrumentation," CAL Report WTH-021, March 1963.
8. Bogdan, L., "High-Temperature, Thin-Film, Resistance Thermometers for Heat Transfer Measurements," CAL Report No. HM-1510-Y-6, February 1963.
9. "Preliminary Data Release, Saturn S-IC Stage Model Base Heating Test, Cornell 8-by 8-foot Transonic Wind Tunnel (Phase II, Part I, Project X-8)," Boeing Coordination Sheet AERO-H-127, March 13, 1963.
10. "Preliminary Data Release, Saturn S-IC Stage Model Base Heating Test, Lewis 10-by 10-foot Supersonic Wind Tunnel (Phase II, Part II, Project X-8)," Boeing Coordination Sheet AERO-H-391, December 16, 1963.
11. "Preliminary Data Release Saturn S-IC Stage Model Base Heating Test, Cornell High Altitude Chamber (Phase I, Project X-8)," Boeing Coordination Sheet AERO-H-249, July 24, 1963.
12. "Data Report - Saturn V/S-IC Wind Tunnel Base Heating Test, Project AT-11," Boeing Document T5-6619, April 11, 1966.
13. Eastman, D. W., and Radtke, L. P., "Two Dimensional or Axially Symmetric Real Gas Flows by the Method of Characteristics, Part III: A Summary of Results from the IBM 7090 Program for Calculating the Flow Fields of Supersonic Jet," Boeing Document D2-10599.

REFERENCES (Continued)

14. Jakob, M., Heat Transfer, Volume II, John Wiley and Sons, Inc., February 1963, pps. 65-66.
15. McAdams, W. H., Heat Transmission, Third Edition, McGraw-Hill Book Company, Inc., 1954.
16. Mullen, C. R., "Saturn S-IC Stage Model Base Heating Test Program," Boeing Document D5-11238, December 1962.
17. Korst, H. H., et. al., "Research on Transonic and Supersonic Flow of a Real Fluid at Abrupt Increase in Cross Section," University of Illinois ME Technical Report 392-5, December 1959.
18. Van Driest, E. R., "The Problem of Aerodynamic Heating," Aeronautical Engineering Review, October 1956, pp. 26.
19. Chapman, D. R., "An Analysis of Base Pressure at Supersonic Velocities and Comparison with Experiment," NACA Report 1051, 1951.
20. "Deflector Inlet and Exit Total Pressure Study," Boeing Coordination Sheet AERO-H-264, August, 1963.
21. Simon, P. L. and Kowalsk, K. L., "Charts of Boundary Layer Mass Flow and Momentum for Inlet Performance Analysis Mach Number Range, 0.2 to 5.0," NACA TN 3583, November 1955.
22. Goethert, B. H., "Base Flow Characteristics of Missiles with Cluster-Rocket Exhausts," IAS Paper 60-89.

NOMENCLATURE

(UNLESS OTHERWISE DEFINED)

B ₁	Basic stage (CAL 8 by 8)
B ₃	Basic stage with 6-inch combustor extension (LRC 10 by 10)
B ₄	B ₃ with 16-inch nose extension (LRC 8 by 6)
C _p	Pressure coefficient, $\frac{P_N - P_\infty}{q}$
C*	Characteristic exhaust velocity - ft/sec
D ₁	Basic flow deflector (See Figure 8.)
D ₂	Design No. 2 flow deflector (See Figure 8.)
D ₃	Design No. 3 flow deflector (See Figure 8.)
F	F _{in} Also radiation form factor
H _N	Heat-transfer gage (Subscript "N" designates gage or orifice number)
M	Mach number
N ₁₋₅	Basic five nozzles
N ₇	Instrumented and plugged nozzle at Engine No. 5 position
N ₈	Instrumented and plugged nozzle at Engine No. 3 position
N ₉	Instrumented and plugged nozzle at Engine No. 4 position
N ₁₀	Instrumented and plugged nozzle at Engine No. 2 position
N _{G3} N _{G4}	Gimbal pattern No. 1 (See Figure 3.)
N _{G5} N _{G6}	Gimbal pattern No. 2 (See Figure 3.)

NOMENCLATURE (Continued)

$N_{G7}N_{G8}$	Gimbal pattern No. 3 (See Figure 4.)
$N_{G9}N_{G10}$	Gimbal pattern No. 4 (See Figure 4.)
$N_{G11}N_{G12}N_{G13}$	Gimbal pattern No. 5 (See Figure 5.)
O/F	Oxygen-to-fuel ratio
P	Pressure - psia
PL ₁	Cold base plate - heat transfer and pressure
PL ₂	Cold base plate - pressure
PL ₃	Hot base plate - heat transfer
P _N	Pressure gage (Subscript "N" designates gage or orifice number)
ΔP	Base pressure change during runs - psia
q	Dynamic pressure, $\frac{1}{2}\rho V^2$, psia
q _c	Convective heat transfer - BTU/FT ² SEC
q _r	Radiative heat transfer - BTU/FT ² SEC
q _T	Total heat transfer - BTU/FT ² SEC
r	Normal distance from model axis
R	Radius of model (R = 4.4 inches) Also specific gas constant
S ₁	Basic engine fairing (See Figure 6.)
S ₂	Engine fairing design No. 1 (See Figure 6.)
S ₄	Engine fairing design No. 2 (See Figure 6.)

NOMENCLATURE (Continued)

SC_1	Basic engine fairing scoop (See Figure 7.)
SC_2	No. 2 design engine fairing scoop (See Figure 7.)
T	Temperature - $^{\circ}R$
V	Velocity - ft/sec
X/D	Ratio of distance of heat-transfer gage from nozzle exit plane to diameter of nozzle at exit plane
y	Distance from surface to a point in the boundary layer
α	Angle of attack
γ	Ratio of specific heat
δ	Boundary layer thickness - inches
ϵ	Emissivity
η	Combustion efficiency
θ	Angle - clockwise rotation
ρ	Density - slugs/ft ³
τ	Stefan-Boltzmann Constant
\dot{w}	Mass flow - lbs/sec

Subscripts

c	Combustion chamber
o	Total
∞	Tunnel free stream
w	Wall or surface

REVISIONS

REVISIONS

117